Matrix Porewater in Crystalline Rocks: Extraction and Analysis

NWMO TR-2013-23 December 2013

Florian Eichinger[1] and H.Niklaus Waber[2]

[1] Hydroisotop GmbH, Schweitenkirchen, Germany
[2] Rock-Water Interaction, Institute of Geological Sciences, University of Bern, Switzerland

nwmo
NUCLEAR WASTE MANAGEMENT ORGANIZATION
SOCIÉTÉ DE GESTION DES DÉCHETS NUCLÉAIRES

Nuclear Waste Management Organization
22 St. Clair Avenue East, 6th Floor
Toronto, Ontario
M4T 2S3
Canada

Tel: 416-934-9814
Web: www.nwmo.ca

Matrix Porewater in Crystalline Rocks: Extraction and Analysis

NWMO TR-2013-23

December 2013

Florian Eichinger[1] and H. Niklaus Waber[2]

[1] Hydroisotop GmbH, Schweitenkirchen, Germany
[2] Rock-Water Interaction, Institute of Geological Sciences, University of Bern, Switzerland

This report has been prepared under contract to NWMO. The report has been reviewed by NWMO, but the views and conclusions are those of the authors and do not necessarily represent those of the NWMO.

All copyright and intellectual property rights belong to NWMO.

Document History

Title:	Matrix Porewater in Crystalline Rocks: Extraction and Analysis		
Report Number:	NWMO TR-2013-23		
Revision:	R000	Date:	December 2013
HYDROISOTOP GmbH			
Authored by:	Florian Eichinger		
Rock-Water Interaction, Institute of Geological Sciences, University of Bern			
Authored by:	H. Niklaus Waber		
Nuclear Waste Management Organization			
Reviewed by:	Laura Kennell, Sarah Hirschorn and Monique Hobbs		
Accepted by:	Mark Jensen		

ABSTRACT

Title: **Matrix Porewater in Crystalline Rocks: Extraction and Analysis**
Report No.: **NWMO TR-2013-23**
Author(s): Florian Eichinger[1] and H.Niklaus Waber[2]
Company: [1]Hydroisotop GmbH, Schweitenkirchen, Germany
[2]Rock-Water Interaction, Institute of Geological Sciences, University of Bern, Switzerland
Date: December 2013

Abstract
The chemical and isotopic characterization of porewater residing in the inter- and intragranular pore space of the low-permeability rock matrix is an important component with respect to the site characterization and safety assessment of potential host rocks for a radioactive waste disposal.

The chemical and isotopic composition of porewater in such low permeability rocks has to be derived by indirect extraction techniques applied to naturally saturated rock material. In most of such indirect extraction techniques – especially in case of rocks of a porosity below about 2 vol.% – the original porewater concentrations are diluted and need to be back-calculated to in-situ concentrations. This requires a well-defined value for the connected porosity – accessible to different solutes under in-situ conditions. The derivation of such porosity values, as well as solute concentrations, is subject to various perturbations during drilling, core sampling, storage and experiments in the laboratory.

The present study aims to demonstrate the feasibility of a variety of these techniques to characterize porewater in crystalline rocks. The methods, which have been developed during multiple porewater studies in crystalline environments, were applied on four core samples from the deep borehole DH-GAP04, drilled in the Kangerlussuaq area, Southwest Greenland, as part of the joint NWMO–Posiva–SKB Greenland Analogue Project (GAP).

Potential artefacts that can influence the estimation of in situ porewater chemistry and isotopes, as well as their controls, are described in detail in this report, using specific examples from borehole DH-GAP04.

TABLE OF CONTENTS

Page

ABSTRACT ..... **iii**

1. INTRODUCTION **1**

2. HYDROGEOLOGICAL BACKGROUND **4**

3. MATERIALS AND METHODS **6**

3.1 SAMPLING **6**
3.2 SAMPLE PREPARATION **7**
3.3 EXPERIMENTAL SETUP AND ANALYTICAL METHODS **7**
3.3.1 Petrological and Mineralogical Investigations 8
3.3.2 Visualization of Pore Space 8
3.3.3 Density Measurements 8
3.3.4 Water Content and Water-loss (Connected) Porosity 9
3.3.5 Porewater Extraction Methods 10
3.3.5.1 Diffusive Isotope Exchange Technique 10
3.3.5.2 Out-diffusion Experiments 13

4. PETROGRAPHY AND MINERALOGY **15**

4.1 SAMPLE GAP04-1 (INTERMEDIATE GNEISS, 501.5 M BHL) **16**
4.2 SAMPLE GAP04-2 (INTERMEDIATE GNEISS, 651.9 M BHL) **19**
4.3 SAMPLE GAP04-3 (INTERMEDIATE GNEISS, 557.7 M BHL) **22**
4.4 SAMPLE GAP04-4 (FELSIC GNEISS, 607.7 M BHL) **25**

5. WATER CONTENT AND WATER-LOSS POROSITY **28**

5.1 BACKGROUND OF WATER CONTENT DETERMINATION **28**
5.2 WATER CONTENT OF DH-GAP04 SAMPLES **28**
5.3 UNCERTAINTIES IN WATER CONTENT DETERMINATION AND THEIR CONTROL **33**
5.3.1 Potential Experimental Artefacts 33
5.3.2 Potential Artefacts Induced by the Drilling Process 35
5.4 BACKGROUND AND METHODOLOGY OF BULK DENSITY DETERMINATION **37**
5.5 DENSITY OF DH-GAP04 SAMPLES **37**
5.6 UNCERTAINTIES IN BULK DENSITY DETERMINATION **37**
5.7 BACKGROUND METHODOLOGY OF WATER-LOSS (CONNECTED) POROSITY DETERMINATION **38**
5.8 WATER-LOSS POROSITY OF DH-GAP04 SAMPLES **38**
5.9 UNCERTAINTIES IN THE WATER-LOSS POROSITY DETERMINATION **39**
5.10 CHARACTERIZATION OF PORE SPACE **39**

6. CHEMICAL TIME-SERIES FROM OUT-DIFFUSION EXPERIMENTS **44**

6.1 MONITORING OF OUT-DIFFUSION EXPERIMENTS: SOLUTE TIME SERIES **45**
6.1.1 Sampling and Analytical Strategy 45
6.1.2 Chemical Composition of Time-series Sub-samples 45
6.1.3 Chemistry of Time-series Sub-samples as Function of Time 48

6.1.4 Interpretation of Solute Time-series 50
6.2 CHEMICAL COMPOSITION OF FINAL OUT-DIFFUSION SOLUTION 61

7. CHLORINE, BROMINE AND CHLORINE ISOTOPES IN POREWATERS 65

7.1 BACKGROUND – CONSERVATIVE TRACER INVESTIGATIONS 65
7.2 CHLORINE, BROMINE AND CHLORINE ISOTOPES IN POREWATER FROM DH-GAP04 65
7.3 UNCERTAINTIES IN THE POREWATER Cl, Br AND CHLORINE ISOTOPE DETERMINATION AND THEIR CONTROL 66

8. DETERMINATION OF $\delta^{18}O$ AND $\delta^{2}H$ OF POREWATER 68

8.1 BACKGROUND AND AIM OF $\delta^{18}O$ AND $\delta^{2}H$ DETERMINATION IN POREWATER 68
8.2 ^{18}O AND $\delta^{2}H$ OF POREWATER OF DH-GAP04 CORE SAMPLES 68
8.3 UNCERTAINTIES IN THE DETERMIATION OF POREWATER STABLE ISOTOPE COMPOSITIONS AND THEIR CONTROL 72

9. SUMMARY AND CONCLUSIONS 75

ACKNOWLEDGEMENTS 81

REFERENCES 82

APPENDIX A: TABULAR PRESENTATION OF ION CONCENTRATIONS OF ELUATE TIME SERIES 87

LIST OF TABLES

Page

Table 3.1: Borehole DH-GAP04 – List of Samples Used for Porewater Extraction Technique Investigations 6
Table 3.2: Borehole DH-GAP04 – Porewater Extraction Experiments and Analyses Performed on Drillcore Samples and Experimental Solutions 7
Table 4.1: Borehole DH-GAP04 – Lithology, Structure, Texture and Observed Hydrothermal Alteration of Core Samples Used for Matrix Porewater Investigations (IGN = intermediate gneiss, FGN = felsic gneiss, NS = neosomatic parts) 15
Table 4.2: Borehole DH-GAP04 – Mineralogy of Core Samples Used for Porewater Experiments Obtained from Transmitted Light and Scanning Electron Microscopy 27
Table 5.1: Mass and Mass Differences of Wet Cores Before and After the Out-diffusion Experiments in DH-GAP04 Drill Core Samples 30
Table 5.2: Mass of Dissolved Gypsum Replacing Water and Final Mass of Evaporated Porewater in DH-GAP04 Drill Core Samples 32
Table 5.3: Mass of Water Removed by Drying at 40°C and 105°C from DH-GAP04 Drill Core Samples 32
Table 5.4: Water Contents Determined Gravimetrically by Drying at 40°C of DH-GAP04 Drill Core Samples 33
Table 5.5: Water Contents Neglecting the Different Observed Artefacts; Water Contents are Calculated Based on the Mass of Water Removed at the Different Drying Temperatures and Different Wet Core Masses; Values do not Consider Dissolution of Gypsum 33
Table 5.6: Bulk Wet and Bulk Dry Density of Core Samples from Borehole DH-GAP04 37
Table 5.7: Water-loss Porosity of Core Samples from Borehole DH-GAP04 39
Table 6.1: Chemical Composition of Final Eluate Solutions from Out-diffusion Experiments 63
Table 6.2: Mineral Saturation Indices of Final Eluate Solutions from Out-diffusion Experiments 64
Table 7.1: Chloride and Bromide Concentrations, Br*1000/Cl Mass Ratios and δ37Cl Signatures of Porewater Extracted from Core Samples of Borehole DH-GAP04 66
Table 8.1: Chloride Control Weight Measurements on Isotope Diffusive Exchange Experiments Conducted with LAB and N-GRIP Test Water Solutions 69
Table 8.2: Chloride – Measured Isotope Ratios (δ^{18}O, δ^{2}H) on Initial (standard) and Reacted Test Water Solutions (LAB and N-GRIP) 70
Table 8.3: Hypothetical Water Contents of the Sample Subjected to Isotope Diffusive Exchange as Calculated from the Isotope Composition of the Reacted Test Water Solutions (LAB and N-GRIP) in Comparison with the Gravimetric Water Content Determined by Drying of the Rock Material after the Experiment 70
Table 9.1: Summary of Artefacts Influencing Porewater Characterization Methods and Their Possible Control, Prevention and Evaluation 75
Table 9.2: Recommendation for Porewater Investigations in Crystalline Rocks 78

LIST OF FIGURES

Page

Figure 2.1: Location and Course of Borehole DH-GAP04 (modified after Pöllänen et al. 2012) .. 5
Figure 2.2: Transmissivity of Water-conducting Fractures Encountered in Borehole DH-GAP04 as a Function of Depth (data from Pöllänen et al. 2012); Positions of the Porewater Samples are Marked in Red 5

Figure 4.1: Intermediate Gneiss Sample GAP04-1 (501.5 m BHL): (a) Macroscopic Appearance; (b) Overview of the Mineral Assemblage Under Transmitted, Cross-polarized Light; (c) Plagioclase and Quartz Under Transmitted, Plane-polarized Light; (d) Quartz, Slightly Chloritized Biotite and Amphibole Under Transmitted, Cross-polarized Light, Quartz Shows Sericite-filled Microfractures; (e) Biotite, Amphibole, Opaque Ore Minerals, Plagioclase and Quartz Assemblage Under Transmitted Cross-polarized Light; (f) Amphibole Associated with Opaque Ore Mineral 17
Figure 4.2: SEM Images of Intermediate Gneiss Sample GAP04-1 (501.5 m BHL); (a) Microfracture Filled with Gypsum; (b)-(f) Dispersed Gypsum in Rock Matrix Associated with Different Minerals; Gyp = gypsum, Plg = plagioclase, Amph = amphibole, Cel = Celestine, Qtz = quartz, Apa = apatite, Smec = smectite 18
Figure 4.3: Foliated Intermediate Gneiss Sample GAP04-2 (651.9 m BHL); (a) Macroscopic Appearance; (b) Overview of the Mineral Assemblage Under Transmitted, Cross-polarized Light; (c) Moderately Saussuritized Plagioclase and Quartz Under Transmitted, Plane-polarized Light; (d) and (e) Amphibole Pervaded by Smectite-filled Microfissures and Intergrown with Fine-grained Quartz and Opaque Minerals Under Transmitted, Cross-polarized Light (f); Biotite Intergrown with Fine-grained Quartz 20
Figure 4.4: SEM Images of Intermediate Gneiss Sample GAP04-2 (651.9 m BHL); (a), (b) Gypsum Surrounded by Fe-oxide, Plagioclase, Quartz and Amphibole; (c) Alteration Products of Amphibole (smectite) Surrounded by Plagioclase; (d) Apatite Surrounded by Amphibole and Plagioclase; Gyp = gypsum, Plg = plagioclase, Amph = amphibole, Qtz = quartz, Apa = apatite, Smec = smectite 21
Figure 4.5: Intermediate Gneiss Sample GAP04-3 (557.7 m BHL); (a) Macroscopic Appearance; (b) Overview of the Mineral Assemblage Under Transmitted, Cross-polarized Light; (c) Plagioclase and Quartz Under Transmitted, Plane-polarized Light; (d) Amphibole with Quartz and Opaque Minerals Under Transmitted, Cross-polarized Light (e); Fine-grained Quartz with Medium-grained Plagioclase; (f) Medium-grained Amphibole Pervaded by Smectite-filled) Microfissures, Very Fine-grained Quartz and Fine-grained Plagioclase..... 23
Figure 4.6: SEM Images of Intermediate Gneiss Sample GAP04-3 (557.7 m BHL); (a)-(c) Gypsum-filled Fractures with Surrounding Minerals in Different Scales; (d)-(f) Gypsum Dispersed in Rock Matrix with Coexisting Pyrite, Chalcopyrite and Celestine; Gyp = gypsum, Plg = plagioclase, Amph = amphibole, Qtz = quartz, Apa = apatite, Kfs = K-feldspar, Py = pyrite, Cc = Calcite, Chalcopy = chalcopyrite 24
Figure 4.7: Intermediate Gneiss Sample GAP04-4 (607.7 m BHL); (a) Macroscopic Appearance; (b) Overview of the Mineral Assemblage Under Transmitted, Cross-polarized Light; (c) Quartz and Plagioclase Under Transmitted, Plane-polarized Light; (d) Amphibole with Quartz and Opaque Minerals Under Transmitted, Cross-polarized Light (e); Fine- to Medium-grained Quartz with Medium-grained Plagioclase; (f) Quartz with Fluid Inclusion Tracks 26
Figure 4.8: SEM Images of Intermediate Gneiss Sample GAP04-4 (607.7 m BHL); gypsum dispersed in rock matrix with coexisting celestine (a) and pyrite (b); Gyp = gypsum, Plg = plagioclase, Qtz = quartz, Apa = apatite, Py = pyrite, Cel = celestine, Lat = lanthanite... 27
Figure 5.1: Examples of Drying Time-series at 105°C of Core Pieces Used for Diffusive Isotope Exchange Experiments (left) and Step-wise Drying at 40°C and 105°C for Large-sized Core Used for Out-diffusion Experiments (right). Analytical Error of the Weight Measurements is the Analytical Uncertainty of the Balance at ± 0.001 g 29
Figure 5.2: Comparison of the Core Wet Mass Before and After Immersion into the Test Water of the Out-diffusion Experiments. Uncertainty of the Determination of Wet Weight is Approximately ± 0.01 g, Caused by the Drying of the Core Surface 30

Figure 5.3: Microfracture Penetrating Through the Rock Matrix of the Intermediate Gneiss Sample GAP04-3 Under Crossed-polarized Transmitted Light (a) and Under UV Light (b). Thin Sections were Prepared with Water and Impregnated with Water-based Resin, Explaining the Dissolution of the Majority of the Gypsum in the Microfissure. Sections for SEM Investigations were Prepared without Water and Show Fully Preserved Gypsum in the Microfractures (c) 31
Figure 5.4: Intermediate Gneiss Sample GAP04-1; Visualization of the Connected Pore Space by Impregnation and UV-fluorescence Microscopy. (a), (c) Intergranular Connected Porosity Between Rock-forming Feldspar, Quartz and Amphibole Minerals Under UV and Transmitted Crossed-polarized Light; (b), (d) Intergranular Connected Porosity Between Biotite and Feldspar Minerals and Intragranular Porosity of Microfractures in Plagioclase Under UV and Transmitted Crossed-polarized Light 40
Figure 5.5: Intermediate Gneiss Sample GAP04-2; Visualization of the Connected Pore Space by Impregnation and UV-fluorescence Microscopy. (a), (b) Intergranular Connected Porosity Between Rock-forming Minerals and Intragranular Porosity in Moderately Altered Plagioclase Under UV and Transmitted Crossed-polarized Light; (c), (d) Intergranular Connected Porosity Between Feldspar and Quartz Minerals Under UV and Transmitted Crossed-polarized Light; (e), (f) Inter- and Intragranular Porosity in Amphibole Under UV and Transmitted Crossed-polarized Light 41
Figure 5.6: Intermediate Gneiss Sample GAP04-3; Visualization of the Connected Pore Space by Impregnation and UV-fluorescence Microscopy. (a), (b) Intergranular Connected Porosity Between Rock-forming Minerals and Intragranular Porosity in a Smectite-filled Microfissure in Amphibole Under UV and Transmitted Crossed-polarized Light; (c), (d) Intergranular Connected Porosity Between Feldspar and Quartz Minerals and Intragranular Connected Porosity Along Cleavages of Plagioclase Under UV and Transmitted Crossed-polarized Light; (e), (f) Impregnated Microfracture (originally gypsum-filled) Under UV and Transmitted Crossed-polarized Light 42
Figure 5.7: Felsic Gneiss Sample GAP04-4; Visualization of the Connected Pore Space by Impregnation and UV-fluorescence Microscopy. (a), (b) Intergranular Connected Porosity Between Rock-forming Minerals Under UV and Transmitted Crossed-polarized Light; (c), (d) Intergranular Connected Porosity Between Feldspar and Quartz Minerals and Intragranular Connected Porosity Along Cleavages of Plagioclase Under UV and Transmitted Crossed-polarized Light 43
Figure 6.1: Behaviour of SO_4^{-2} and Alkaline and Earth-alkaline Cations as a Function of Cl^- Concentrations, Which Serve as a Proxy for the Elution Time, in Out-diffusion Experiments of the Intermediate Gneiss Sample GAP04-1 (left) and the Felsic Gneiss Sample GAP04-4 (right). Also Given are Correlation Coefficients of the Linear and Exponential Fits, Respectively. Note the Different Concentration Scales for the Two Samples. Error Bars Indicate the Analytical Error of ± 5% 47
Figure 6.2: Behaviour of the Alkaline and Earth-alkaline Cations as a Function of SO_4^{-2}, Which Serves as a Proxy for the Elution Time, in Out-diffusion Experiments of the Intermediate Gneiss Sample GAP04-1 (left) and the Felsic Gneiss Sample GAP04-4 (right). Note the Differences in Cation Concentrations and Elution Behaviour (except for Mg^{+2}) Between the Two Samples 48
Figure 6.3: Intermediate Gneiss Sample GAP04-1; Concentrations of Cl^- and SO_4^{-2} (top) and SO_4^{-2}, Ca^{+2} and Mg^{+2} (bottom) in Time-series Eluate Solutions as a Function of Out-diffusion Time. Note that the Cl^- and Mg^{+2} Concentrations are Multiplied by Factors of 20 and 10, Respectively. Error Bars Indicate an Analytical Error of ±5% 53
Figure 6.4: Intermediate Gneiss Sample GAP04-1; Concentrations of SO_4^{-2}, Ca^{+2} and Mg^{+2} (top) and Cl^-, Na^+ and K^+ (bottom) in Time-series Eluate Solutions as a Function of Out-

diffusion Time. Note That the Sr^{+2}, Cl^- and K^+ Concentrations are Multiplied by Factors of 100, 20 and 10, Respectively. Error Bars Indicate the Analytical error of ±5% 54
Figure 6.5: Intermediate Gneiss Sample GAP04-2; Concentrations of Cl^- and SO_4^{-2} (top) and Cl^-, Na^+ and K^+ (bottom) in Time-series Eluate Solutions as a Function of Out-diffusion Time. Note That the Cl^- Concentrations are Multiplied by Factors of 20 and 10, and K^+ by a Factor of 10. Arrows in the Lower Plot Indicate Sub-samples That Underwent Evaporation During Storage. Error Bars Indicate the Analytical Error of ±5% 55
Figure 6.6: Intermediate Gneiss Sample GAP04-2; Concentrations of SO_4^{-2}, Ca^{+2} and Mg^{+2} (top) and SO_4^{-2}, Ca^{+2} and Sr^{+2} (bottom) in Time-series Eluate Solutions as a Function of Out-diffusion Time. Note That the Mg^{+2} and Sr^{+2} Concentrations are Multiplied by Factors of 10 and 100, Respectively. Error Bars Indicate the Analytical Error of ±5% 56
Figure 6.7: Intermediate Gneiss Sample GAP04-3; Concentrations of Cl^- and SO_4^{-2} (top) and Cl^-, Na^+ and K^+ (bottom) in Time-series Eluate Solutions as a Function of Out-diffusion Time. Note That the Cl^- Concentrations are Multiplied by Factors of 20 and 10, and K^+ by a Factor of 10. Arrows Indicate Sub-samples That Underwent Evaporation During Storage. Error Bars Indicate the Analytical Error of ±5% 57
Figure 6.8: Intermediate Gneiss Sample GAP04-3; Concentrations of SO_4^{-2}, Ca^{+2} and Mg^{+2} (top) and SO_4^{-2}, Ca^{+2} and Sr^{+2} (bottom) in Time-series Eluate Solutions as a Function of Out-diffusion Time. Note That the Mg^{+2} and Sr^{+2} Concentrations are Multiplied by Factors of 10 and 100, Respectively. Arrows Indicate Sub-samples That Underwent Evaporation During Storage. Error Bars Indicate the Analytical Error of ±5% 58
Figure 6.9: Felsic Gneiss Sample GAP04-4; Concentrations of Cl^-, Br^- and SO_4^{-2} (top) and Cl^-, Na^+ and K^+ (bottom) in Time-series Eluate Solutions as a Function of Out-diffusion Time. Note That the K^+ and Br^- Concentrations are Multiplied by Factors of 10 and 100, Respectively. Error Bars Indicate the Analytical Error of ±5% 59
Figure 6.10: Felsic Gneiss Sample GAP04-4; Concentrations of SO_4^{-2}, Ca^{+2} and Mg^{+2} (top) and SO_4^{-2}, Ca^{+2} and Sr^{+2} (bottom) in Time-series Eluate Solutions as a Function of Out-diffusion Time. Note That the Mg^{+2} and Sr^{+2} Concentrations are Multiplied by Factors of 10 and 100, Respectively. Error Bars Indicate the Analytical Error of ±5% 60
Figure 6.11: Schoeller Diagram of Final Eluate Solutions from Out-diffusion Experiments Conducted with Intermediate Gneiss (samples GAP04-1 to -3, blue) and Felsic Gneiss (sample GAP04-4, red) Drillcore Samples. Note the Large Differences in Composition and Chemical Type for the Solutions from Different Rock Types 62
Figure 8.1: Measured Isotope Ratios ($\delta^{18}O$, δ^2H) of Initial (Standard) and Reacted Test Water Solutions (LAB and N-GRIP). Note the Different Deviations from the Global Meteoric Water Line (GMWL; Craig 1961) for the Isotope Composition of Reacted Test Water Solutions from the Same Sample; Analytical Uncertainties are ±0.25‰ for $\delta^{18}O$ and 1.5‰ for δ^2H 71

1. INTRODUCTION

Porewater in low-permeability crystalline bedrock resides in the connected inter- and intragranular pore space of the rock matrix. In this pore space, solute transport is dominated by diffusion. The *intergranular pore space* consists of the grain boundary porosity between different mineral grains. In turn, the *intragranular pore space* comprises the porosity within mineral grains. This porosity is associated with mineral alteration processes, such as mineral transformations during hydrothermal and/or weathering events (e.g., the sericitization and saussuritization of feldspars), partial dissolution along cleavage and twinning planes, and tectonically induced microfractures in individual mineral grains.

Porewater in the crystalline rock matrix, and fracture groundwater that circulates in regional and local fracture networks, are connected systems that tend to attain chemical and isotopic equilibrium. The degree of interaction between matrix porewater and fracture groundwater in the water-conducting zones depends on the chemical gradient(s) established between the two reservoirs. Such interaction can be quantified as a function of time and space by comparing chemical and isotopic signatures of the two reservoirs, combined with knowledge of the time periods of constant boundary conditions (i.e., constant groundwater composition in the water-conducting zones and the initial conditions in the rock matrix).

The characterization of the porewater composition and the solute transport processes in the rock matrix contribute important information for the long-term safety assessment of deep geological repositories for radioactive waste. Thus, knowledge of the porewater composition will allow better constraints on the processes affecting the near-field of a repository. In designs where repository construction is restricted to bedrock of low permeability, the first water to interact with the repository barrier materials (e.g., bentonite, Cu-canister) will be the porewater. This interaction could result in changes of the physical and chemical properties of the various barrier materials. Knowledge of the porewater composition and its evolution over recent geological time – particularly during the last thousands to hundreds of thousands of years in accordance with the expected lifespan of a geologic repository – is considered to be of high importance.

In combination with the knowledge gained about solute transport in the rock matrix, the characterization of porewater also contributes to a better understanding of processes related to the far-field environment of a repository. Thus, it provides valuable information about matrix diffusion as a potential retardation factor for radionuclides, and allows better constraints to be placed on the palaeohydrogeolocial history of a repository site. Due to the exchange by diffusion between fracture groundwater and matrix porewater, released radionuclides may be temporally immobilized by matrix diffusion, and possible subsequent sorption on mineral surfaces. For radionuclides susceptible to sorption, the accessible surface areas are greatly enhanced by matrix diffusion when compared to the accessible surface area on fracture surfaces alone. Matrix diffusion has the potential to increase solute transport times to the biosphere from the repository, possibly to timeframes as long as the half-life of the radionuclide under consideration.

Matrix porewater can serve as an archive of past changes in fracture groundwater compositions, allowing for the palaeohydrological history of a site to be assessed (Waber et al., 2012). A chemical and isotopic signal established in the porewater at a certain time in its hydrogeological evolution might be preserved over long, geological time periods (e.g. Eichinger

et al. 2006, 2008, 2010, 2013,; Waber et al. 2005, 2008, 2009 a, b). For chemically conservative tracers, the preservation of such signatures depends on: 1) the distance of the porewater sample to the nearest water-conducting fracture in three dimensions, 2) the solute transport properties of the rock (diffusion coefficient, solute-accessible porosity), and 3) the boundary conditions (i.e., the fracture groundwater composition as a function of time). The interpretation of an observed porewater signature is greatly facilitated if the porewater signature has been transmitted from constant boundary conditions. In reality, however, superimposed signatures, as a result of changing boundary conditions with time, are more realistic. Unravelling complex, superimposed signatures can be achieved by comparing data sets from various tracers that yield different information about the conditions present during infiltration of a fracture groundwater. The porewater Cl concentration gives indication about the salinity, whereas the Br/Cl ratio and the Cl-isotope composition provide information about the salinity source. The stable water isotopes ($\delta^{18}O$, $\delta^{2}H$) provide information about the climatic conditions and/or origin of the water.

The interpretation of observed porewater signatures needs to be consistent for all tracers to allow the reconstruction of palaeohydrogeological history. The time resolution of such reconstruction depends on the degree of detail in the spatial variation of porewater composition and independent knowledge about changes in fracture groundwater composition. At present, the time resolution may be in the range of just a few hundreds of years to a time period since the last glaciation, if a continuous porewater profile, extending from the water-conducting fracture into the rock matrix, can be generated (Waber et al. 2012). In the case of lower porewater sample frequency, the resolution may be limited only to major events going back as far as the Tertiary (e.g., Waber and Smellie 2008; Eichinger 2009; Waber et al. 2009 a, b).

In contrast to fracture groundwater, porewater cannot be sampled by conventional groundwater sampling techniques. The chemical and isotopic composition of porewater has, therefore, to be derived by indirect extraction techniques based on rock material. In most of such indirect extraction techniques – especially in case of rocks of a porosity below about 2 vol.% – the original porewater concentrations are diluted and need to be back-calculated to in-situ concentrations. This requires a well-defined value for the connected porosity – accessible to different solutes under in-situ conditions. The derivation of such porosity values, as well as solute concentrations, is prone to various perturbations during drilling, core sampling, storage and experiments in the laboratory. The obtained data have to be carefully evaluated for potential perturbations induced by drilling activities, rock stress release and sample treatment in the laboratory in order to derive values that are representative of in-situ conditions. This requires detailed knowledge about the rock composition, the rock texture, and the local stress field, because porewater composition is dependent on these factors as well. The effects of the drilling activities and rock stress release on the derived porewater composition and rock petrophysical properties have been explored for isotropic crystalline rocks by Waber et al. (2011) and for anisotropic crystalline rocks by Eichinger et al. (2013).

In the past decade, matrix porewater studies were successfully conducted in several crystalline rock environments. Investigations were pioneered within the Swedish Site Investigation Programs of SKB at Laxemar and Forsmark, starting in 2004 (e.g. summary reports by Waber and Smellie 2009 a, b and references therein). At these sites, porewater was mainly extracted from isotropic, equigranular, low-metamorphic quartz-monzodioritic and granodioritic rocks. These investigations were followed by benchmarking tests in the well-defined environment of the Grimsel underground rock laboratory, GTS, Switzerland (Eichinger et al. 2008; Eichinger 2009; Möri 2009), again in low-metamorphic granodioritic rock. In parallel, porewater extraction techniques were also adapted and applied to anisotropic, heterogeneous, high-metamorphic

gneiss within the Site Characterization Program of Posiva at Olkiluoto, Finland (Eichinger et al. 2006, 2010, 2013). At all of these locations, the obtained porewater data contribute important information regarding the interpretation of solute transport processes in the crystalline rock matrix and the palaeohydrogeological evolution over the Quaternary and Tertiary periods.
The present study aims to demonstrate the feasibility of a variety of individual techniques to characterize porewater composition and solute transport in crystalline rocks. Specifically, this study describes: 1) the necessary methods for porewater characterization in crystalline rocks; and 2) potential disturbing artefacts – control, prevention and evaluation. The study has been conducted on core from the joint NWMO–Posiva–SKB Greenland Analogue Project (GAP), which focuses on processes associated with glaciation and permafrost, and the impact of such processes on the long-term performance of a deep geological repository for nuclear waste. From a deep borehole (DH-GAP04) drilled in the Kangerlussuaq area, Southwest Greenland, four drillcore samples, comprising high-grade metamorphic gneiss, were subjected to the various porewater characterization techniques. The applied methods are described and evaluated in detail in the following sections, including potential disturbing effects, derived results, and the representativeness of the methods in the context of in-situ conditions.

2. HYDROGEOLOGICAL BACKGROUND

Borehole DH-GAP04 is located in the Kangerlussuaq area (Southwest Greenland), approximately 200 m south of the ice margin of the Russell glacier (Figure 2.1).

The Kangerlussuaq area is situated within the Nagssugtoqidian fold belt, which is a part of the West Greenland Precambrian shield, and consists mainly of Archean and Proterozoic rocks (Aaltonen et al. 2010). The rocks of the Nagssugtoqidian Orogen are predominately Archean ortho gneisses that were reworked under high grade metamorphism during the Palaeoproterozoic (Van Gool et al. 2002). The primary structures are of ductile to semi-ductile nature, containing folded or sheared zones of various types of gneiss (Harper et al. 2012).

The earliest glaciation of Greenland likely took place approximately 2.4 Ma BP (Wallroth et al. 2010). It is very likely that there have been numerous glaciation/deglaciation cycles since then; however, due to the erosive nature of the last two glaciations, little evidence of prior glaciation remains in-situ on the ice free Greenland mainland (Wallroth et al. 2010). At the beginning of the Holocene, the ice margin was presumably in a position close to the current outer coast of Southwest Greenland (Engels et al. 2010). Radiocarbon dating of basal lake sediments indicates that deglaciation in the Kangerlussuaq area started about 8900-6000 years ago (Bennicke & Björck 2002; Weidicke & Bennicke 2007). It is assumed that the ice margin was 5-20 km behind the present-day position during the Holocene climate optimum (~7000-5000 years ago; Aaltonen et al. 2010). The ice sheet advanced to the position of prominent moraines, located less than 2 km from the present-day ice margin, during the Neoglaciation (about 4000 years BP). The position of the ice margin during the Little Ice Age (15th to 19th century) was only several tens to a few hundreds of meters from the present-day ice margin in the investigation area (Forman et al. 2007).

At present, the Kanglerussuaq area has an arid, continental, low-arctic climate, with a mean annual air temperature of about -4°C and an average annual precipitation of 149 mm (Jörgensen & Andreasen 2007; Aaltonen et al. 2010).

The Kangerlussuaq area is located within the zone of continuous permafrost, approximately 50-60 km east of the boundary of discontinuous permafrost (Christiansen & Humlum 2000). Investigations in borehole DH-GAP03, which is located some 500 m SW of DH-GAP04, indicate a recent permafrost depth of 335 m below surface (b.s.) (Harper et al. 2012).

Borehole DH-GAP04 was drilled at an inclination of 70° in a NNE direction (azimuth = 10-39°) to a borehole length (BHL) of 687 m, corresponding to a maximum vertical depth of 632.5 m (Pöllänen et al. 2012).

According to temperature logging for the first 320 m length of the borehole, the system appears to be influenced by permafrost (Pöllänen et al. 2012). Between 415 and 682 m along the borehole (392-644 m b.s.), a total of 9 water-conducting fractures were detected by downhole differential flow logging. The transmissivity of these water-conducting fractures varies between 1.6×10^{-9} and 3.3×10^{-6} m^2/s (Figures 2.2). The distance along the borehole between porewater samples and the nearest water-conducting fracture ranges between 2.6 and 24 m.

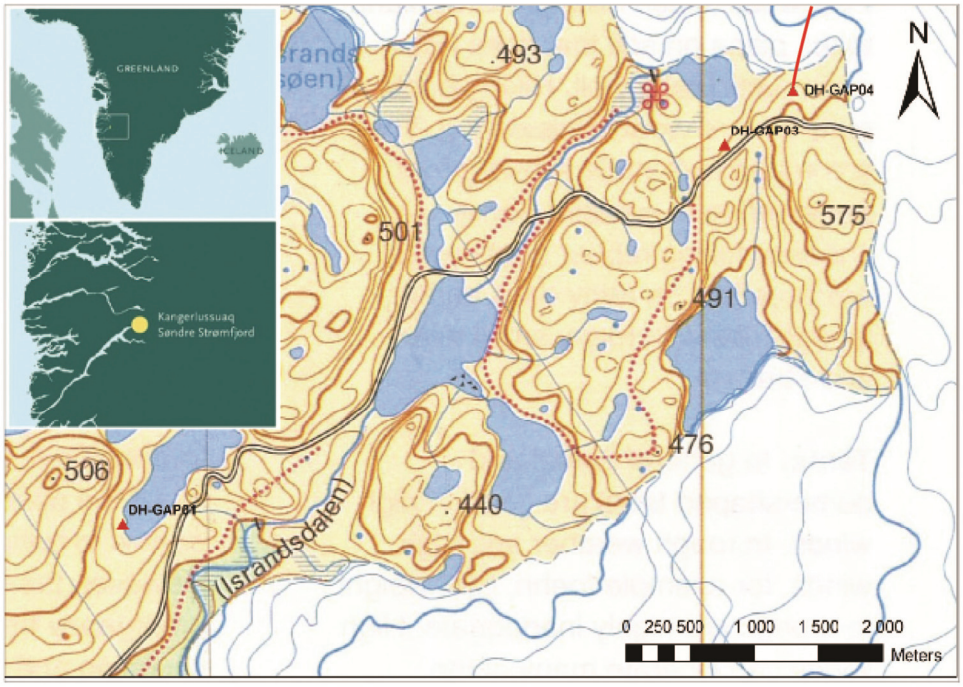

Figure 2.1: Location and Course of Borehole DH-GAP04 (modified after Pöllänen et al. 2012)

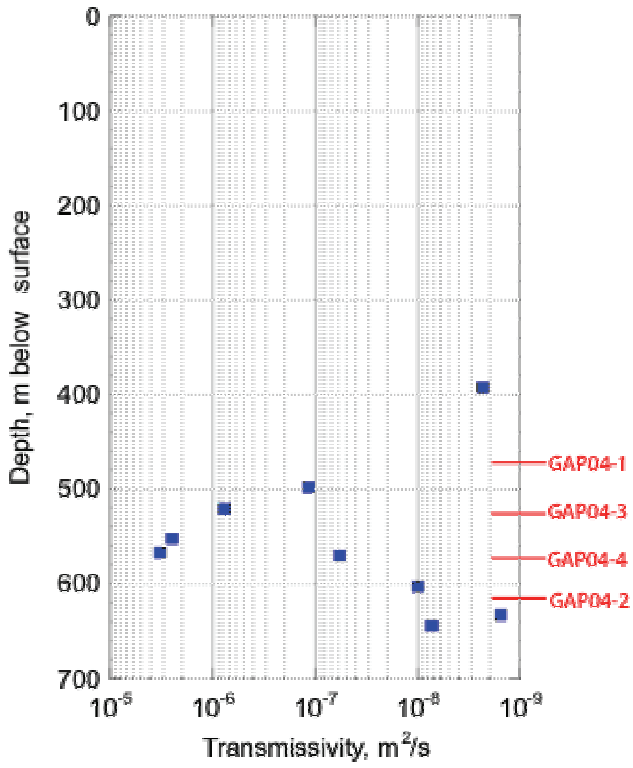

Figure 2.2: Transmissivity of Water-conducting Fractures Encountered in Borehole DH-GAP04 as a Function of Depth (data from Pöllänen et al. 2012); Positions of the Porewater Samples are Marked in Red

3. MATERIALS AND METHODS

Indirect methods have to be used to obtain information about the chemical and isotopic composition of porewater in crystalline rocks. In the following sub-sections, the sampling and methods used to characterise rock properties, to extract porewater, and to evaluate the influence of different artefacts are described in detail.

3.1 SAMPLING

Four drillcore samples from depths between 500 and 652 m borehole length (BHL; i.e., 473-616 m b.s.) were collected from borehole DH-GAP04, which was drilled in June 2011. The samples were received at the University of Bern on December 12th and 13th, 2011.

An important requirement for porewater samples is the preservation of the in-situ saturated state of the drilled rock material during sampling, storage and transportation from the drill site to the laboratory in order to allow the most accurate measurements of the water content and the derivation of the in-situ water-loss porosity. The packing of the samples was conducted on site by field personnel following the instructions given by the Rock-Water Interaction Group (RWI) at the University of Bern. Following drilling, the samples were wiped clean immediately after recovery, packed into a PVC bag, which was flushed with nitrogen and subsequently evacuated and heat-sealed. The same procedure was repeated for a second PVC bag, and finally for a plastic coated Al-foil bag. This triple sealing approach minimizes the evaporation of porewater, as evaporation would result in reduced measured water contents and, thus, a deviation of the calculated porewater tracer concentrations and isotope signatures from those present under in-situ conditions.

Table 3.1: Borehole DH-GAP04 – List of Samples Used for Porewater Extraction Technique Investigations

Lab Sample Nr.	Posiva sample Nr.	Interval along borehole		Av. Borehole Length	Av. Vertical Depth	Core Length	Date sampled	Date received & prepared
		From	To					
		m	m	m BHL[1)]	m b.s.[2)]	m		
GAP04-1	DH-GAP04 501.35-501.61	501.35	501.61	501.48	473.4	0.26	June 2011	12.12.11
GAP04-2	DH-GAP04 651.80-652.02	651.80	652.02	651.91	526.5	0.22	June 2011	12.12.11
GAP04-3	DH-GAP04 557.59-557.78	557.59	557.78	557.69	572.8	0.19	June 2011	13.12.11
GAP04-4	DH-GAP04 606.63-606.83	606.63	606.83	606.73	615.5	0.20	June 2011	13.12.11

[1)] BHL. = borehole length (i.e. along borehole), [2)] b.s. = below surface

Following arrival at the RWI laboratory at the University of Bern, the sealed cores were stored immediately in a cooling room at 4°C and subsequently prepared for the different experiments.

Already at this time it became obvious that the packing of the cores was not tight and the bags were slightly inflated. All samples prepared for porewater investigations are listed in Table 3.1, together with their depth along borehole, their vertical depth and the sample length.

3.2 SAMPLE PREPARATION

In the laboratory, the samples were unpacked and immediately wrapped in parafilm to prevent evaporation of porewater during dry sawing, which was performed to cut the cores into full-diameter cylinders of variable length. After sawing, the surfaces of the obtained pieces were cleaned with paper towels and wrapped in parafilm. The sample preparation was conducted as rapidly as possible (within 20 minutes) after opening of the sealed bags, in order to minimize evaporation.

The different experiments conducted, together with the analytical programme performed on each rock sample and its experimental solutions, are listed in Table 3.2.

Table 3.2: Borehole DH-GAP04 – Porewater Extraction Experiments and Analyses Performed on Drillcore Samples and Experimental Solutions

Lab Sample	Petrophysical and Petrological Investigations			Diffusive Isotope Exchange Technique	
	Gravimetric Water Content & Porosity	Mineralogy	Impregnation of pore space	Experimental set-up	$\delta^{18}O$, $\delta^{2}H$
GAP04-1	X	X	X	X	X
GAP04-2	X	X	X	X	X
GAP04-3	X	X	X		
GAP04-4	X	X	X	X	X
	Out-diffusion Experiments				
	Experimental set-up	pH & Alkalinity	Anions and Cations	$\delta^{37}Cl$	Time Series
GAP04-1	X	X	X	X	X
GAP04-2	X	X	X	X	X
GAP04-3	X	X	X	X	X
GAP04-4	X	X	X	X	X

3.3 EXPERIMENTAL SETUP AND ANALYTICAL METHODS

Unless otherwise specified, the experimental and analytical work has been conducted at the laboratories of the Institute of Geological Sciences, University of Bern, Switzerland.

3.3.1 Petrological and Mineralogical Investigations

Mineralogical investigations were performed on all four core samples. The investigations included transmitted and reflected light microscopy of thin sections, and scanning electron microscope (SEM) investigations of separately prepared thin sections. The latter were prepared without water and using oil as sawing and polishing media to prevent dissolution of easily dissolvable mineral phases, such as sulphates. SEM images and mineral phase identification were performed on a Zeiss EVO50 scanning electron microscope using the secondary electron and EDS spectra mode, respectively.

3.3.2 Visualization of Pore Space

For the visualization of pore space, core fragments were impregnated in the laboratory by fluorescence resin, NHC-9, which was developed by NAGRA and Sika AG (Frieg et al. 1998) . This resin has been previously applied in projects focusing on the characterization of pore space in crystalline rocks under in-situ conditions (Grimsel Test Site, Switzerland; Frieg et al. 1998; Schild et al. 2001; Möri 2009) and under laboratory conditions (Olkiluoto, Finland; Eichinger et al. 2012, 2013). NHC-9 is an acrylic and fluorescing resin that has a viscosity similar to that of water and is completely miscible with water. The size of the molecule is similar to that of water, allowing the resin to enter all water-saturated pores.

The pore space was visualized and characterized on the four core samples. Semicircular core sections, including the rim zone of the cores with a thickness of 1.5 cm and a length of 3 cm, were sawed from the core samples and oven dried (105°C) for at least one week. After cooling, the samples were submerged into the resin under vacuum for about 24 h. Subsequently, the impregnated rock samples were oven dried at 70°C for 12 h, allowing the resin to polymerise. Finally, thin sections were produced from the impregnated rock section for optical inspection of the pore space using an UV-microscope with an attached digital camera.

3.3.3 Density Measurements

The calculation of water-loss (i.e., connected) porosity from the gravimetric water content requires a measure of the grain density. In rocks of low porosity, the bulk density can be used as a proxy for the grain density because the differences between bulk and grain density are within or just outside the range of analytical uncertainty. A measure for the bulk wet density of the rocks investigated was obtained from the volume and saturated mass of the core samples used for out-diffusion experiments. The volume was calculated from measurements of the height and diameter of the core samples using a Vernier calliper, with an error of ± 0.01 mm. Variations in the core diameter over the lengths of the samples were found to be less than 0.05 mm for most samples and a constant diameter was used in the calculation of the volume.

Measurement of the exact core length can be difficult if the surfaces of the upper and lower end of the cores are uneven. Care should be taken during dry sawing to obtain planar top and bottom surfaces on the cylindrical core samples. In case of uneven surfaces, the volume of the cores was alternatively determined according to Archimede's principle by immersion of the core into water. The volume is then obtained by:

$$V_{rock} = \frac{m_{rock,air} - m_{rock,water}}{\rho_{water}} \quad (1)$$

where V_{rock} is the volume of the core sample, $m_{rock,air}$ the mass of the core sample under atmospheric conditions, $m_{rock,water}$ the mass of the core sample emerged in deionized water, and ρ_{water} the density of the water at a certain temperature (e.g., 0.998 g/cm^3 at 21°C).

From sample volume and wet or dry mass, the bulk wet or dry density follows from:

$$\rho_{bulk,wet} = \frac{m_{wet}}{V_{rock}} \quad \text{and} \quad \rho_{bulk,dry} = \frac{m_{dry}}{V_{rock}} \; . \quad (2)$$

The errors for the bulk wet and dry density are determined by Gaussian error propagation according to:

$$\sigma(\rho) = \sqrt{\left(d\rho dm_{core} \times \sigma(m_{core})\right)^2 + \left(d\rho dr \times \sigma(r)\right)^2 + \left(d\rho dh \times \sigma(h)\right)^2} \; , \quad (3)$$

where
$\sigma(m_{wet})$ = $m_{core,wet}$ calculated – $m_{core,wet}$ measured after emerging into test solution (cf. Chapter 5),
$\sigma(m_{dry})$ = ±0.002 g (uncertainty of dry weight determination),
$\sigma(r)$ = ± 0.05 cm (uncertainty in the radius determination), and
$\sigma(h)$ = ± 0.2 cm (uncertainty in the height determination).

3.3.4 Water Content and Water-loss (Connected) Porosity

The water content was determined on core material used for the diffusive isotope exchange technique and on the large-sized cores used in out-diffusion experiments. The sample material used in the isotope exchange and out-diffusion experiments remained saturated throughout these experiments (see Section 3.3.5). The degree of sample saturation upon arrival of the samples in the laboratory was estimated by comparing the weights of the large sized samples (533 to 644 g) used in the out-diffusion experiments before and after the experiment.

The drillcore pieces were placed in a crystallization dish, weighed, and subsequently dried until constant weight conditions were attained. Core pieces used for the diffusive isotope exchange experiments were dried at 105°C. However, changes observed in the chemical composition of the out-diffusion experiment solutions as a function of time suggested the presence of gypsum, and possibly other hydrated sulphate phases, in the rock samples. Therefore, when these experiments were terminated, the core segments used for the out-diffusion experiments were first dried at 40°C and subsequently at 105°C until constant weight conditions were attained. This sequential drying was deemed necessary because drying at 105°C removes structural water of hydrated sulphate phases and results in an overestimation of the water content.

Before taking the initial wet weight of the large-sized core pieces, the surface was allowed to dry until stable weight was achieved for ~10 sec. Subsequently, weighing was carried out weekly until the sample weight remained constant (±0.002 g) for at least 14 days. Drying times varied between 21 and 49 days for the core sections used for the diffusive isotope exchange experiments (with masses of 146–227 g), and between 70 and 84 days at 40°C and an

additional 36 to 50 days at 105°C for the large-sized samples used in the out-diffusion experiments (with masses of 533–644 g).

The water-loss (connected porosity), ϕ_{WL}, is calculated according to:

$$\phi_{WL} = WC_{wet} * \frac{\rho_{bulk,wet}}{\rho_{water}} \quad = \quad \phi_{WL} = \frac{m_{pw} \times 100}{r^2 \times h \times \pi \times \rho_{water}} \quad , \qquad (4)$$

where WC_{wet} is the water content based on the wet weight of the rock sample and $\rho_{bulk,wet}$ the bulk wet density of the rock. In a first approximation, the density of water, ρ_{water}, is assumed to be 1 g/cm^3, because the highest Cl concentrations in the porewater are far below that of ocean seawater (cf. Chapter 7).

The error of the water-loss porosity was determined according to:

$$\sigma(\phi_{WL}) = \sqrt{\begin{array}{l}\left(d\phi_{WL} dm_{PW} \times \sigma(m_{PW})\right)^2 + \left(d\phi_{WL} dr \times \sigma(r)\right)^2 + \\ \left(d\phi_{WL} dh \times \sigma(h)\right)^2 + \left(d\phi_{WL} d\rho_{water} \times \sigma(\rho_{water})\right)^2\end{array}} \quad , \qquad (5)$$

where
$\sigma(m_{pw})$ = difference between $m_{core,dry\ surface}$ before and after drying (including evaporation and gypsum dissolution) + 0.1 g,
$\sigma(r)$ = 0.05 cm,
$\sigma(h)$ = 0.2 cm, and
$\sigma(\rho_{water})$ = 0.03 g/cm^3.

As shown by the Gaussian error propagation, the error of the water content and the water-loss porosity depends predominately on the accuracy of the determination of the mass of porewater (i.e., on the measured initial wet weight and final dry weight of the cores). Observed differences in the core weights before and after the experiment are taken into account in the error calculation.

3.3.5 Porewater Extraction Methods

3.3.5.1 Diffusive Isotope Exchange Technique

The diffusive isotope exchange technique used to determine the isotopic composition, $\delta^{18}O$ and $\delta^{2}H$, of the porewater, and the mass of porewater, was originally developed by Rogge (1997) and Rübel et al. (2002) for sedimentary rocks. The technique was later adapted for crystalline rocks by Waber and Smellie (2005) and Eichinger et al. (2006). In this method, originally saturated rock material is placed into two vapour-tight containers together with different test waters of known isotopic composition. The porewater and test water are then allowed to isotopically equilibrate via the vapour phase without any direct contact between the core material and the test water. The porewater isotope composition and the water content of the

rock sample can then be derived by isotope mass balance relationships. It has been shown that the uncertainty of the derived isotope composition largely depends on the ratio of porewater to test water used in the experiments (e.g., Rübel et al. 2002).

For the GAP core samples, 1.5 to 2.0 mL of test water was placed in a Petri dish in the centre of a glass vessel and surrounded by hand crushed core pieces (2-4 cm^3), with a total mass of 146 to 227 g. To minimize condensation, about 0.6 mol of NaCl was dissolved in the test water to lower its vapour pressure. For every sample, two experiments were performed, one using test water with an isotopic composition close to that expected in the porewater ("LAB"-sample) and test water with an isotopic composition far from that expected for the porewater ("TEW"-sample). Test water and core material were weighed before and after the experiment to test for loss of test water on the container walls and/or rock material due to evaporation and/or condensation.

The test water used for the LAB sample was normal laboratory tap water ($\delta^{18}O$ = -11.99‰ V-SMOW; $\delta^{2}H$=-87.30‰ V-SMOW), while that for the TEW-sample was water from an ice core drilled in Greenland ($\delta^{18}O$ = -26.8‰ V-SMOW; $\delta^{2}H$=-207.7‰ V-SMOW). The equilibration time in the three reservoirs – rock porewater, test water and the air inside the container as a diaphragm – depends on the volume of the container, the size of the rock pieces, and the distance of the rock pieces from the test water (see Rogge 1997).

The minimum time period required for complete isotopic equilibration can be calculated according to Rogge (1997). Thereby, the response time, τ, which corresponds to the equilibration time, is calculated according to:

$$\tau = \frac{\mu}{R_{total}} \tag{6}$$

where μ = the characteristic mass derived from the ratio of the mass of test water to that of porewater, and R_{total} = total exchange rate. The total exchange rate, R_{total}, is calculated according to:

$$R_{total} = \frac{d_{test}^2}{D_{water} * m_{TW}} + \frac{d_{PW}^2}{D_{water} * m_{PW}} + \frac{1_{air}}{D_{air} * \rho_{air} * A_{air}} \tag{7}$$

where d_{test} = distance between the surface of the test water and the surface of the most distant rock piece; d_{PW} = diffusion distance for water in the pore space of the rock piece (i.e., generally the maximum radius of the largest piece of rock); D_{water} = diffusion coefficient in water; A = cross section area of the container; *tw* = test water; and *pw* = porewater.

After an equilibration time of 60 days, the two test waters were removed and analysed by cavity ring down spectroscopy using a Picarro L 2130 at Hydroisotop GmbH, Germany. The results for the test waters are reported relative to the V-SMOW standard, with a precision of ± 0.15‰ for $\delta^{18}O$ and ± 1.5‰ for $\delta^{2}H$.

The diffusive isotope exchange technique delivers the $\delta^{18}O$ and $\delta^{2}H$ ratios and the mass of the porewater present in the connected pore space of the rock sample. These parameters are

calculated from the analytical results obtained for the two test water solutions, using mass-balance relationships according to:

$$m_{pw} * C_{pw}\Big|_{t=0} + m_{tw} * C_{tw}\Big|_{t=0} = (m_{pw} + m_{tw}) * C_{tw}\Big|_{t=\infty} \quad , \tag{8}$$

where *m* = mass, *C* = isotope concentration, *pw* = porewater, *tw* = test water; *t = 0* means the isotope concentrations at the beginning and *t* = ∞ at the end of the experiment.
The water content (WC_{IsoEx}) of the samples is calculated by transformation of Equation (8) to:

$$WC_{IsoEx} = \left[\frac{m_{TW(Std2)} \times m_{Rock(Std1)} \times (C_{TW^0(Std2)} - C_{TW\infty(Std2)}) + m_{TW(Std1)} \times m_{Rock(Std2)} \times (C_{TW\infty(Std1)} - C_{TW^0(Std1)})}{m_{Rock(Std1)} \times m_{Rock(Std2)} \times (C_{TW\infty(Std2)} - C_{TW\infty(Std1)})} \right] \times 100 \tag{9}$$

where m_{Rock} = mass of rock, *Std 1* = test solution 1, and *Std 2* = test solution 2.
The stable isotope ratios are calculated by transformation of Equation (8) to:

$$C_{PW} = \frac{C_{TW\infty(Std1)} \times m_{TW(Std2)} \times m_{Rock(Std1)} \times (C_{TW\infty(Std2)} - C_{TW^0(Std2)}) - C_{TW\infty(Std2)} \times m_{TW(Std1)} \times m_{Rock(Std2)} \times (C_{TW\infty(Std1)} - C_{TW^0(Std1)})}{m_{TW(Std2)} \times m_{Rock(Std1)} \times (C_{TW\infty(Std2)} - C_{TW^0(Std2)}) - m_{TW(Std1)} \times m_{Rock(Std2)} \times (C_{TW\infty(Std1)} - C_{TW^0(Std1)})} \tag{10}$$

The errors of the calculated $\delta^{18}O$, $\delta^{2}H$ and mass of the porewater are calculated by Gaussian error propagation according to:

$$\sigma(C_{PW}) = \sqrt{\begin{aligned} &\left(dC_{PW} dm_{TW(Std1)} \times \sigma(m_{TW(Std1)})\right)^2 + \left(dC_{PW} dm_{TW(Std2)} \times \sigma(m_{TW(Std2)})\right)^2 + \\ &+\left(dC_{PW} dC_{TW(Std1)} \times \sigma(C_{TW(Std1)})\right)^2 + \left(dC_{PW} dC_{TW(Std2)} \times \sigma(C_{TW(Std2)})\right)^2 + \\ &+\left(dC_{PW} dC_{TW\infty(Std1)} \times \sigma(C_{TW\infty(Std1)})\right)^2 + \left(dC_{PW} dC_{TW\infty(Std2)} \times \sigma(C_{TW\infty(Std2)})\right)^2 \end{aligned}} \tag{11}$$

$$\sigma(m_{PW}) = \sqrt{\begin{aligned} &\left(dm_{PW} dm_{TW(Std1)} \times \sigma(m_{TW(Std1)})\right)^2 + \left(dm_{PW} dm_{TW(Std2)} \times \sigma(m_{TW(Std2)})\right)^2 + \\ &+\left(dm_{PW} dC_{TW(Std1)} \times \sigma(C_{TW(Std1)})\right)^2 + \left(dm_{PW} dC_{TW(Std2)} \times \sigma(C_{TW(Std2)})\right)^2 + \\ &+\left(dm_{PW} dC_{TW\infty(Std1)} \times \sigma(C_{TW\infty(Std1)})\right)^2 + \left(dm_{PW} dC_{TW\infty(Std2)} \times \sigma(C_{TW\infty(Std2)})\right)^2 \end{aligned}} \quad \text{and} \tag{12}$$

where
$\sigma(m_{TW(Std1)})$ = 0.002 g,
$\sigma(m_{TW(Std2)})$ = 0.002 g,
$\sigma(C_{TW(Std1)})$ = 0.15 ‰ for $\delta^{18}O$ and 1.5‰ for $\delta^{2}H$,
$\sigma(C_{TW(Std2)})$ = 0.15 ‰ for $\delta^{18}O$ and δ1.5‰ for ^{2}H,
$\sigma(C_{TW\infty(Std1)})$ = 0.15 ‰ for $\delta^{18}O$ and δ1.5‰ for ^{2}H, and
$\sigma(C_{TW\infty(Std2)})$ = 0.15 ‰ for $\delta^{18}O$ and δ1.5‰ for ^{2}H.

3.3.5.2 Out-diffusion Experiments

Out-diffusion experiments were performed on intact core samples of about 10 to 12 cm length and about 5 cm in diameter by immersion in ultrapure water. The volume of test water varied between 77 and 88 mL. During the experiments, the two water reservoirs (i.e., porewater and test water) were allowed to exchange until equilibrium with respect to the Cl concentration. This equilibrium is reached when the Cl concentration reaches a plateau and remains constant within the analytical error range (± 5%) for at least 21 days. Based on the experience from previous drillings, the two reservoirs were allowed to equilibrate for 283 days.

After placing the core sample in the polyethylene (PE) vessel, the vessel was sealed and put in a shaking water bath (40 rpm) at a constant temperature of 45°C to accelerate the diffusion process. The PE-vessels were covered by a vapour-tight lid, which is equipped with two swagelock™ valves and PEEK™ sampling lines. To avoid undesired bacterial activity during the experiments, 1 mL of chloroform was added. The rock sample, experiment container, and test water were weighed before and after the experiment to ensure that no loss of test water occurred during the experiment. At specific time intervals of initially a few days, and later a few weeks, 0.5 mL of test water solution was sampled using a PVC-syringe to determine the chloride concentration as a function of time. After equilibrium with respect to chloride was attained, the vessels were removed from the water bath and cooled to room temperature. The weights were recorded and the final solution was analysed immediately for pH and total alkalinity. Following that, the final solution and time-series samples were analysed for major cation and anion concentrations.

Alkalinity titration and pH measurements were performed using a Metrohm Titrino DMP 785 instrument. Chemical analyses of the final and time-series solutions were performed by ion chromatography using a Metrohm ProfIC AnCat MCS IC system with automated 5 μL and 50 μL injection loops. The relative analytical error of these analyses is ± 5% based on multiple measurements of external check standard solutions (1σ).

The $^{37}Cl/^{35}Cl$ isotopic ratio, expressed as $\delta^{37}Cl$ relative to SMOC, was measured at the University of Waterloo Environmental Isotope Laboratory (EIL) in Canada using a VG SIRA 9 mass spectrometer. Measurements were made with a precision of ± 0.15 (1σ) based on repeat analyses of SMOC.

For the chemically conservative elements, Cl and Br, the concentrations of the experiment solution can be converted to porewater concentrations by applying mass balance calculations after equilibrium between test water and porewater is achieved. Using knowledge of the mass of porewater in the rock sample, the Cl and Br concentrations of the porewater can be calculated according to:

$$C_{pw} = \frac{(m_{pw} + m_{TWi} - \sum^{n} m_s) * C_{TW\infty} - (m_{TWi} * C_{TWi}) + \sum^{n} m_s * C_s}{m_{pw}} \qquad (13)$$

where C_{pw} = porewater concentration; m_{pw} = mass of porewater; m_{TWi} = initial mass of test water; C_{TWi} = initial Cl-concentration of test water; m_s = mass of sub sample used for time series; and C_s = Cl and Br concentration of sub sample used for time series.

The term $\sum^{n} m_s * C_s$ in Equation (13) describes the amount of Cl and Br removed from the initial experimental solution for the Cl and Br time-series samples. A correction for chloride and bromide in the initial experiment solution (m_{TWi}*C_{TWi}) is necessary if this solution is not entirely free of Cl and Br.

The errors for the conservative element concentrations (Cl, Br) are calculated according to:

$$\sigma(C_{PW}) = \sqrt{\begin{array}{l}\left(dC_{PW}dm_{PW} \times \sigma(m_{PW})\right)^2 + \left(dC_{PW}dm_{TWi} \times \sigma(m_{TWi})\right)^2 + \\ +\left(dC_{PW}dC_{TW\infty} \times \sigma(C_{TW\infty})\right)^2 + \left(dC_{PW}dC_{TWi} \times \sigma(C_{TWi})\right)^2 + \\ (\sigma(\sum m_S))^2 + (\sigma(\sum m_S \times c_S))^2\end{array}} \qquad (14)$$

where
$\sigma(m_{pw})$ = difference between $m_{core,dry\ surface}$ before and after drying (including evaporation and gypsum dissolution) + 0.1 g,
$\sigma(m_{TWi})$ = difference between $m_{TWi} - m_S - m_{TW\infty}$ -2mL (2 mL = remaining water in the cylinder),
$\sigma(C_{TWi})$ = 5% (Cl) and 10 % (Br) of the analysed concentration,
$\sigma(C_{TW\infty})$ = 5% (Cl) and 10 % (Br) of the analysed concentration,
$\sigma(m_S)$ = 0.05 mL, and
$\sigma(C_S)$ = 5% (Cl) and 10% (Br) of the analysed concentration.

The unit for the porewater concentration is given as mg/kg_{H2O} (and not mg/L) because it is derived on a mass basis rather than a volumetric basis. By using the porewater mass instead of the volumetric water content or porosity, uncertainties related to the rock density measurements are avoided. Furthermore, uncertainty related to the density of the porewater, which is not known beforehand, is avoided. The error attached to the calculated porewater concentrations reduces to the cumulative error of two weight measurements and the analytical error of the chemical analyses.

4. PETROGRAPHY AND MINERALOGY

The evaluation of experimental porewater results, and the interpretation of porewater concentrations derived by indirect methods using rock material, requires knowledge about the composition and physical properties of the rock. Knowledge of the physical properties of the rock mass provides information that can assist in interpretations of porewater chemistry (as measured in the laboratory), geochemical evolution and solute transport. Analysis of both the porewaters and the core sample(s) will provide information on the following:

- Modification of the test water chemistry by significant mineral dissolution (e.g., sulphates);
- Modification of the test water isotopic composition by different minerals, such as clay minerals or gypsum;
- The structure, texture and grain size of the rock are important in the context of solute diffusion (geometry factor);
- The type(s) of pore space where porewater resides (intergranular vs intragranular); and
- Cross-check of the experimentally determined petrophysical properties of the rock with its observed mineralogy (e.g., density).

According to the drillcore logs (pers comm. Ismo Aaltonen, Posiva, 2012), the 687 m long borehole DH-GAP04 consists of intermediate gneiss (46.6%), mafic gneiss (41.1%), minor felsic gneiss (10.5%), and subordinate pegmatitic granite (1.4%) and diatexitic gneiss (0.4%; pers. comm. Ismo Aaltonen, Posiva, 2012). The first 290 m BHL of the drillcore consists only of mafic gneiss, intercalated by 1.0 to 2.4 m thick intermediate gneiss sections. In the lower section of the borehole (290-687 m BHL), the drillcore consists predominately of intermediate gneiss and felsic gneiss, intercalated by 1.3 to 4.6 m thick pegmatitic granite and diatexitic gneiss sections.

The rocks encountered in borehole DH-GAP04 consist predominately of macroscopically unaltered bedrock. Alteration of rock forming minerals was observed around a few closed fractures (pers. comm. Ismo Aaltonen, Posiva, 2012).

The four core samples from borehole DH-GAP04 obtained for porewater extraction method investigations consist of intermediate gneiss (3 samples) and felsic gneiss (1 sample, Table 4.1). No fractures were observable macroscopically on the surface of these cores.

Table 4.1: Borehole DH-GAP04 – Lithology, Structure, Texture and Observed Hydrothermal Alteration of Core Samples Used for Matrix Porewater Investigations (IGN = intermediate gneiss, FGN = felsic gneiss, NS = neosomatic parts)

Lab Sample	Depth along borehole [m]	Vertical depth [m]	Lithology	Structure	Texture*
GAP04-1	501.5	473.4	IGN	80% NS	GNE 1
GAP04-2	651.9	572.8	IGN	60% NS	GNE 2
GAP04-3	557.7	526.5	IGN	70% NS	GNE 1
GAP04-4	606.7	615.5	FGN	90% NS	GNE 1

* Classification of foliation according to Posiva nomenclature; GNE = gneissic; Foliation intensity: 1 = weakly foliated, 2 = moderately foliated (pers. comm. Ismo Aaltonen, Posiva, 2012)

4.1 SAMPLE GAP04-1 (INTERMEDIATE GNEISS, 501.5 M BHL)

Core sample GAP04-1 consists of a weakly foliated, equigranular, macroscopically unaltered intermediate gneiss (Figure 4a). It is mainly composed of plagioclase, quartz, amphibole, biotite, opaque ore minerals and gypsum, with minor smectite and apatite. Rutile, zircon, celestine, lanthanite and apatite are present as accessory minerals (Table 4.2, Figure 4.1b-f). The core sample is intercalated by filled micro veins, which could be observed under microscope (Figure 4.1a, b).

Plagioclase occurs as xenomorphic-hypidiomorphic, fine-grained (0.1-0.3 mm) to medium grained (1.0-3.3 mm) crystals (Figure 4.1c). Plagioclase displays no alteration (Figure 4.1b, c).

Quartz is present as xenomorphic-hypidiomorphic, very fine-grained (0.01-0.1 mm) to fine-grained crystals (Figure 4.1b-f). Several fine-grained quartz grains contain microfissures with sericite infill. These are limited to the individual grains and do not penetrate into adjacent ones (Figure 4.1e).

Amphibole occurs in bundles as xenomorphic, fine-grained to very fine-grained crystals, mainly associated with biotite, fine-grained quartz, plagioclase and opaque ore minerals (Figure 4.1a, e, f).

Biotite is present as xenomorphic-hypidiomorphic, fine-grained to medium-grained crystals, in association with opaque ore minerals and amphibole (Figure 4.1d, e). Biotite is weakly chloritized and does not seem to be oriented in one particular direction in the investigated thin section.

Opaque ore minerals consist predominately of iron oxides and iron sulfides and are present as very fine-grained to coarse-grained (3.3-10 mm) xenomorphic crystals. They are mostly associated with biotite and amphibole (Figure 4.1e, f, 4.2c).

Gypsum occurs as xenomorphic, very fine-grained to fine-grained rounded crystals, dispersed in the rock matrix (Figure 4.2c-f) and as fracture infill (Figure 4.2a). Gypsum occurs together with celestine (Figure 4.2f). The gypsum appears to be of hydrothermal origin.

Alteration products of amphiboles, probably smectite and chlorite, are present as xenomorphic fine-grained aggregates, mostly associated with amphiboles, opaque ore minerals and as rim zones around amphiboles and gypsum (Figure 4.2b).

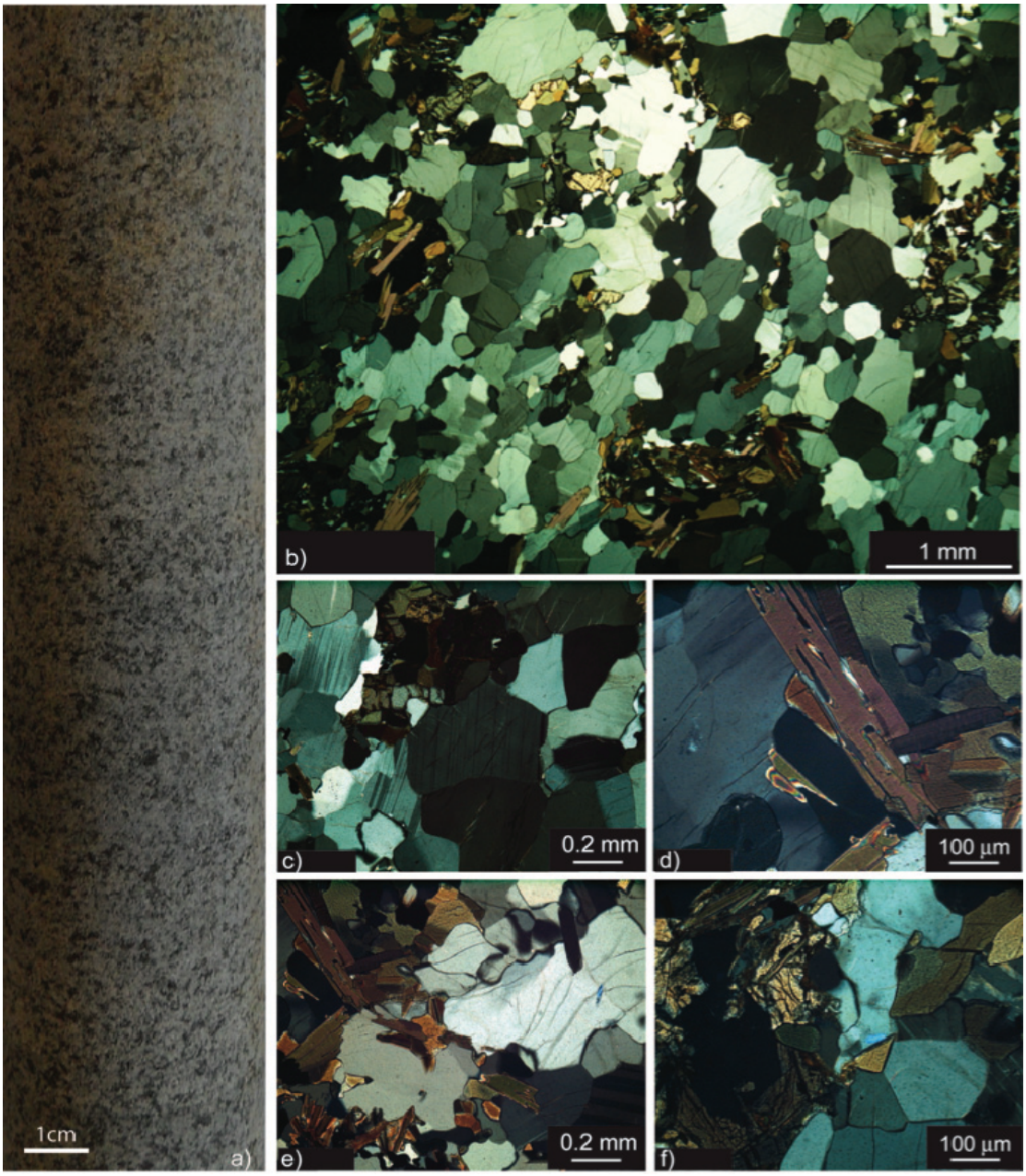

Figure 4.1: Intermediate Gneiss Sample GAP04-1 (501.5 m BHL): (a) Macroscopic Appearance; (b) Overview of the Mineral Assemblage Under Transmitted, Cross-polarized Light; (c) Plagioclase and Quartz Under Transmitted, Plane-polarized Light; (d) Quartz, Slightly Chloritized Biotite and Amphibole Under Transmitted, Cross-polarized Light, Quartz Shows Sericite-filled Microfractures; (e) Biotite, Amphibole, Opaque Ore Minerals, Plagioclase and Quartz Assemblage Under Transmitted Cross-polarized Light; (f) Amphibole Associated with Opaque Ore Mineral

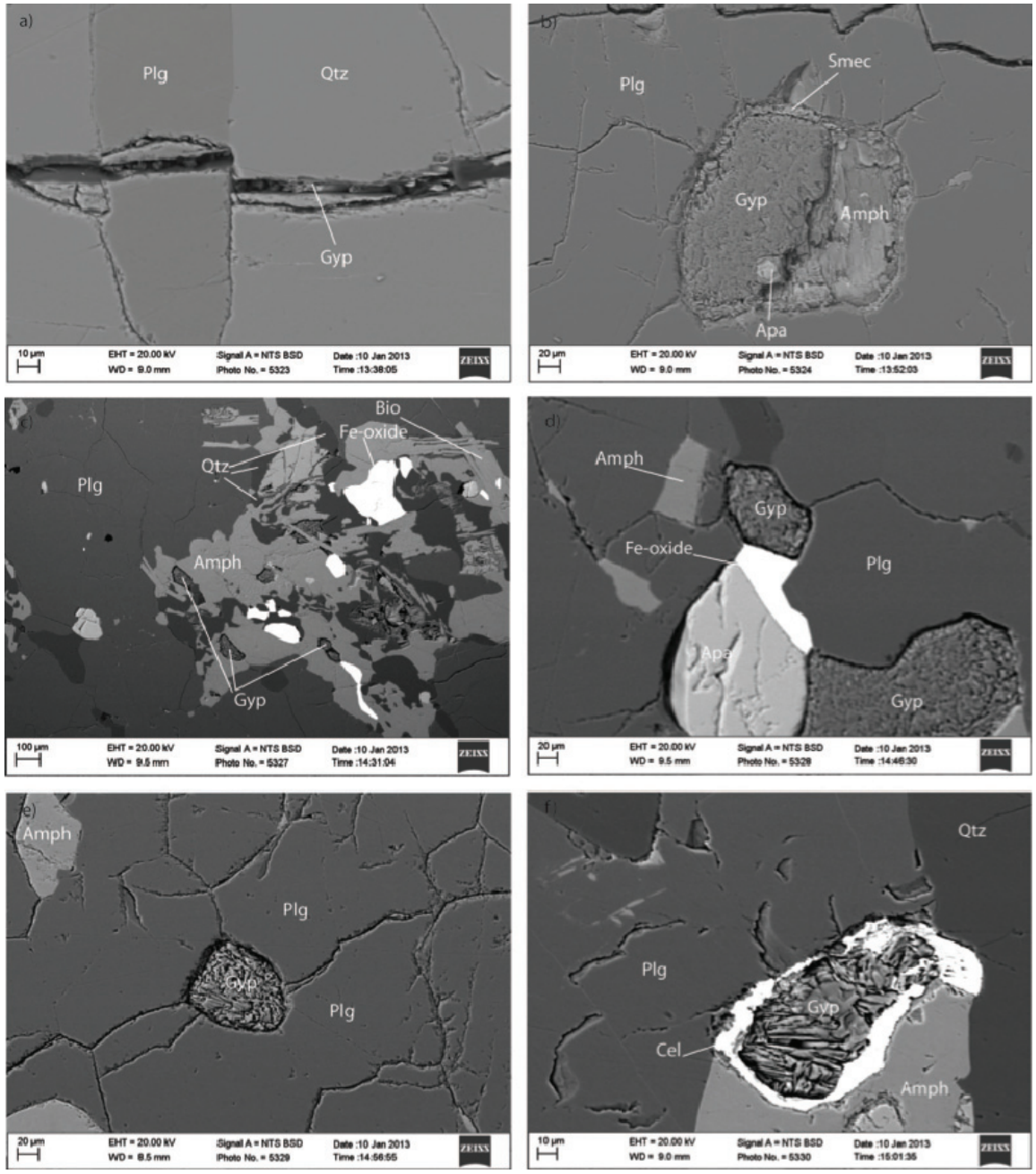

Figure 4.2: SEM Images of Intermediate Gneiss Sample GAP04-1 (501.5 m BHL); (a) Microfracture Filled with Gypsum; (b)-(f) Dispersed Gypsum in Rock Matrix Associated with Different Minerals; Gyp = gypsum, Plg = plagioclase, Amph = amphibole, Cel = Celestine, Qtz = quartz, Apa = apatite, Smec = smectite

4.2 SAMPLE GAP04-2 (INTERMEDIATE GNEISS, 651.9 M BHL)

Core sample GAP04-2 consists of a foliated, equigranular, macroscopically unaltered intermediate gneiss (Figure 4.3a). The foliation manifests itself in the palaeosomatic bands. The intermediate gneiss is mainly composed of plagioclase, quartz, amphibole and biotite, with minor opaque minerals, alteration products (smectite, chlorite) and gypsum (Table 4.2, Figure 4.3b-f, Figure 4.4). Muscovite, calcite, apatite, lanthanite and florencite are present as accessory minerals. Microveins are not observable in the investigated thin sections. The red spots on the core surface (Figure 4.3a) are caused by oxidation of pyrite or magnetite during drilling and sample transport.

Plagioclase occurs as xenomorphic to hypidiomorphic, fine- to coarse-grained minerals (Figure 4.3b). Plagioclase crystals are moderately saussuritized and, sometimes, show microfissures filled with sericite (Figure 4.3c).

Quartz is present as xenomorphic to hypidiomorphic, very fine- to medium-grained crystals (Figure 4.3b). Several medium-grained quartz grains contain microfissures with sericite infills, which partly penetrate into adjacent grains. Very fine-grained quartz grains are present in medium- to coarse-grained plagioclase and are intergrown with amphiboles (Figure 4.3d).

Amphibole is present in orientated bands as xenomorphic to hypidiomorphic, fine- to medium-grained crystals, which are associated with fine-grained quartz and opaque minerals (Figures 4.3d, e and 4.4a, d). Amphiboles are pervaded by filled microfissures and by alteration products, such as smectite (Figure 4.4a).

Biotite is present as xenomorphic-hypidiomorphic, fine- to medium-grained crystals, which can be associated with opaque ore minerals and amphibole (Figure 4.3a, f). Biotite is weakly chloritized and orientated in the investigated thin section.

Opaque ore minerals consist predominately of iron oxides and iron sulphides, and are present as very fine- to fine-grained xenomorphic crystals. They are often associated with amphibole (Figure 4.3d).

Hydrothermally formed gypsum occurs as xenomorphic, very fine-grained to fine-grained rounded crystals dispersed in the rock fabric (Figure 4.4a, b).

Alteration products of amphibole (smectite and/or chlorite) are present as xenomorphic, fine-grained aggregates in the rock matrix and as microfissure infill (Figure 4.4c).

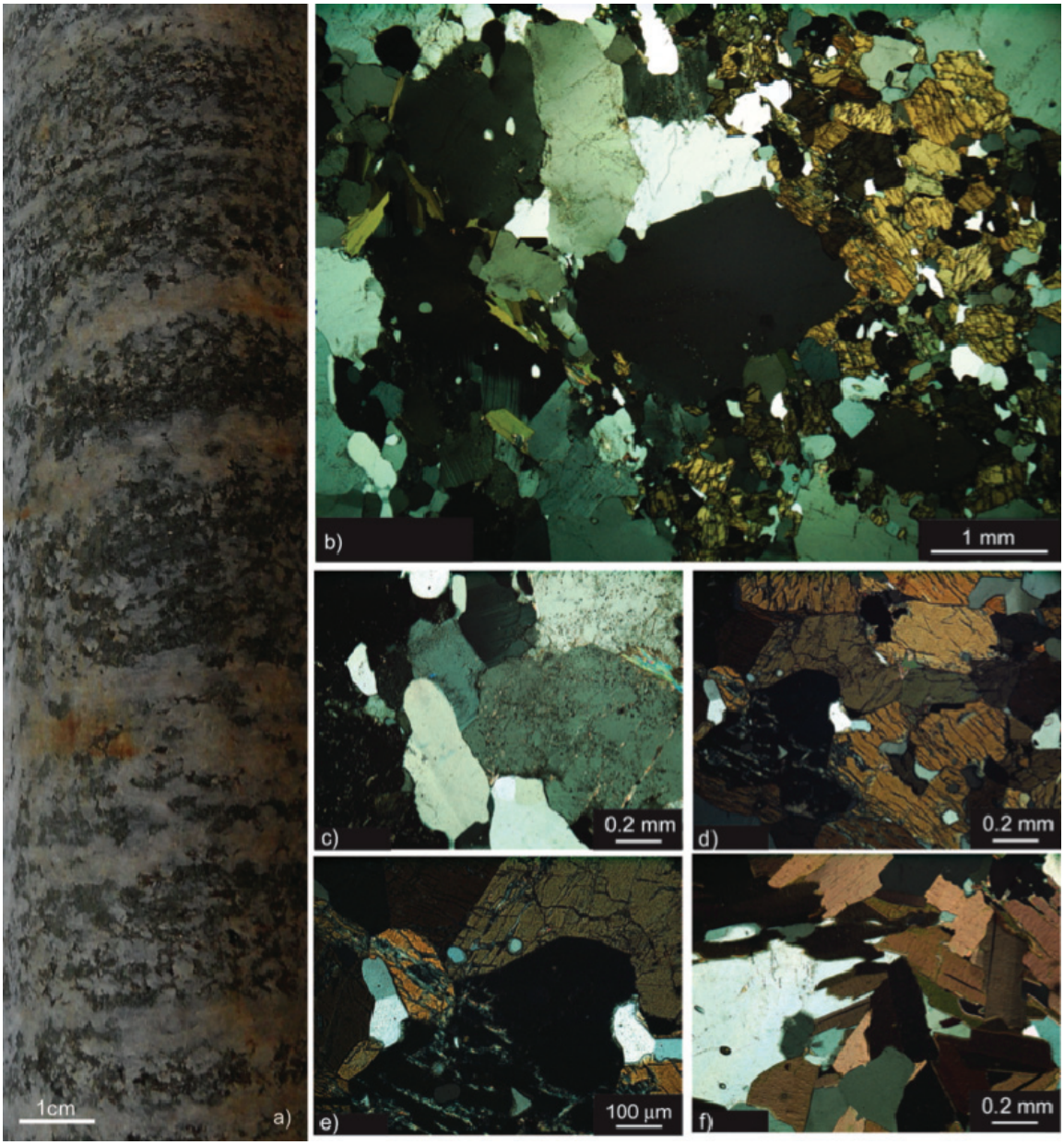

Figure 4.3: Foliated Intermediate Gneiss Sample GAP04-2 (651.9 m BHL); (a) Macroscopic Appearance; (b) Overview of the Mineral Assemblage Under Transmitted, Cross-polarized Light; (c) Moderately Saussuritized Plagioclase and Quartz Under Transmitted, Plane-polarized Light; (d) and (e) Amphibole Pervaded by Smectite-filled Microfissures and Intergrown with Fine-grained Quartz and Opaque Minerals Under Transmitted, Cross-polarized Light (f); Biotite Intergrown with Fine-grained Quartz

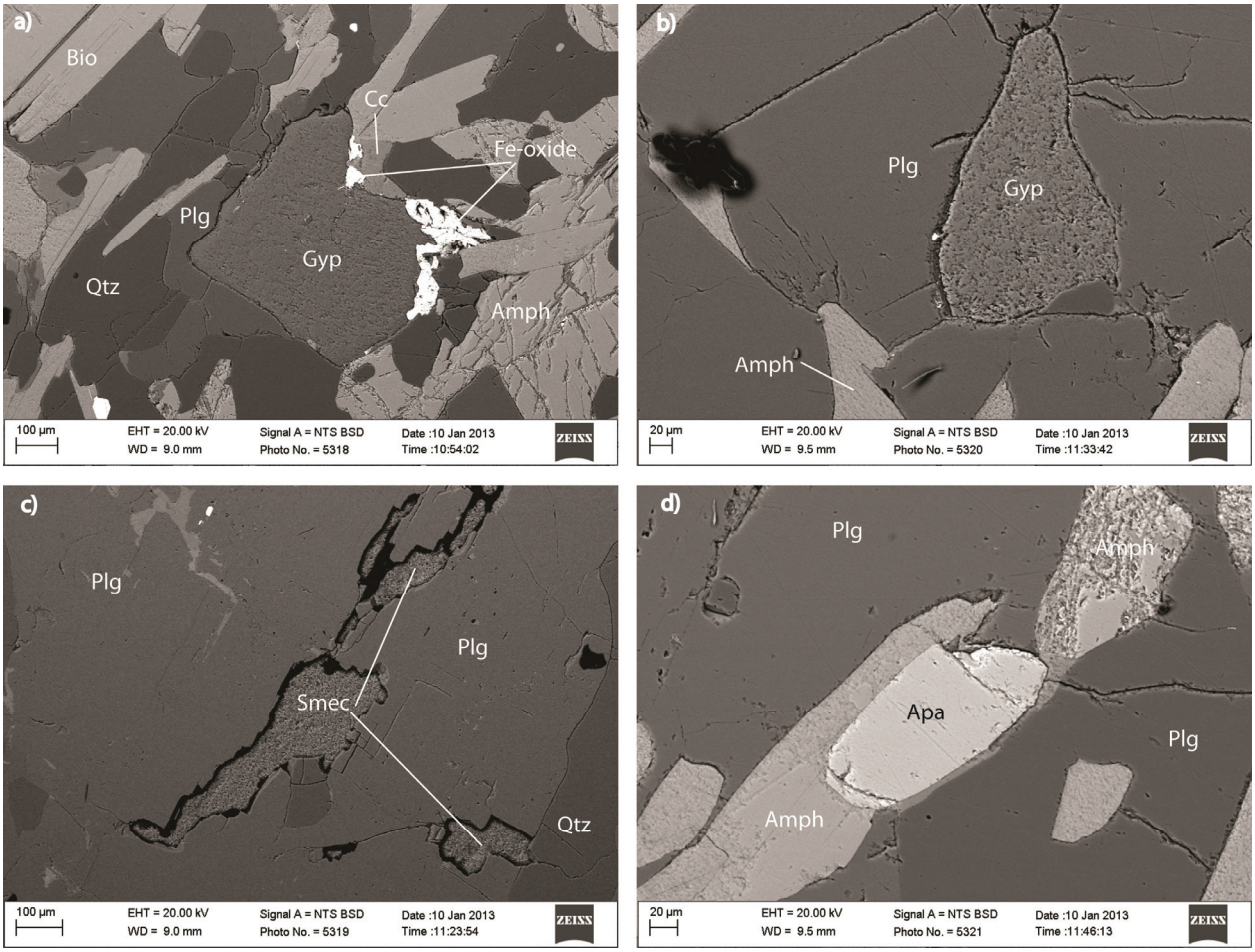

Figure 4.4: SEM Images of Intermediate Gneiss Sample GAP04-2 (651.9 m BHL); (a), (b) Gypsum Surrounded by Fe-oxide, Plagioclase, Quartz and Amphibole; (c) Alteration Products of Amphibole (smectite) Surrounded by Plagioclase; (d) Apatite Surrounded by Amphibole and Plagioclase; Gyp = gypsum, Plg = plagioclase, Amph = amphibole, Qtz = quartz, Apa = apatite, Smec = smectite

4.3 SAMPLE GAP04-3 (INTERMEDIATE GNEISS, 557.7 M BHL)

Core sample GAP04-3 is a slightly foliated, equigranular and macroscopically unaltered intermediate gneiss (Figure 4.5a). It is mainly composed of plagioclase, quartz, amphibole, opaque ore minerals and biotite, with minor gypsum and amphibole alteration products (smectite and/or chlorite, Figures 4.5b-f and 4.6, Table 4.2). Celestine, zircon, florencite, synchysite, allanite, lanthanite, calcite, rutile, apatite and muscovite are present as accessory minerals.

Plagioclase occurs as xenomorphic to hypidiomorphic, fine- to medium-grained minerals (Figure 4.5b, c). Plagioclase is mostly unaltered and shows sericite-filled microfissures. A few fine-grained plagioclase grains show a weak to moderate saussuritization.

Quartz is present as xenomorphic to hypidiomorphic, very fine- to medium-grained crystals (Figure 4.5b, c, e). Fine- and medium-grained quartz often contains sericite-filled microfissures, which are limited to the individual grains. Very fine- and fine-grained quartz occurs mainly associated with amphibole minerals (Figure 4.5f).

Amphibole occurs as xenomorphic fine- to medium grained crystals, intergrown with opaque ore minerals (Figure 4.5b, d, f). Amphibole is pervaded by clay mineral filled fissures.

Opaque ore minerals, which consist, according to the SEM investigations, of pyrite, chalcopyrite and Fe-oxides are present as fine- to medium grained xenomorphic crystals, mostly associated with amphiboles (Figure 4.5d). Very-fine grained pyrites were also detected along gypsum filled veins and associated with gypsum minerals dispersed in the rock matrix (Figure 4.6b, d, f).

Biotite is present as xenomorphic-hypidiomorphic, fine- to medium-grained crystals. Biotite is weakly chloritized and does not appear to be orientated in the investigated thin section.

Gypsum occurs as xenomorphic, very fine- to fine-grained rounded crystals dispersed in the rock matrix and as fracture fillings in 5-20 µm thick veins (Figure 4.6). Gypsum occurs together with very-fine grained pyrite and celestine.

Alteration products of amphibole (smectite, chlorite) are present as xenomorphic fine-grained aggregates in the rock matrix and as microfissure infill.

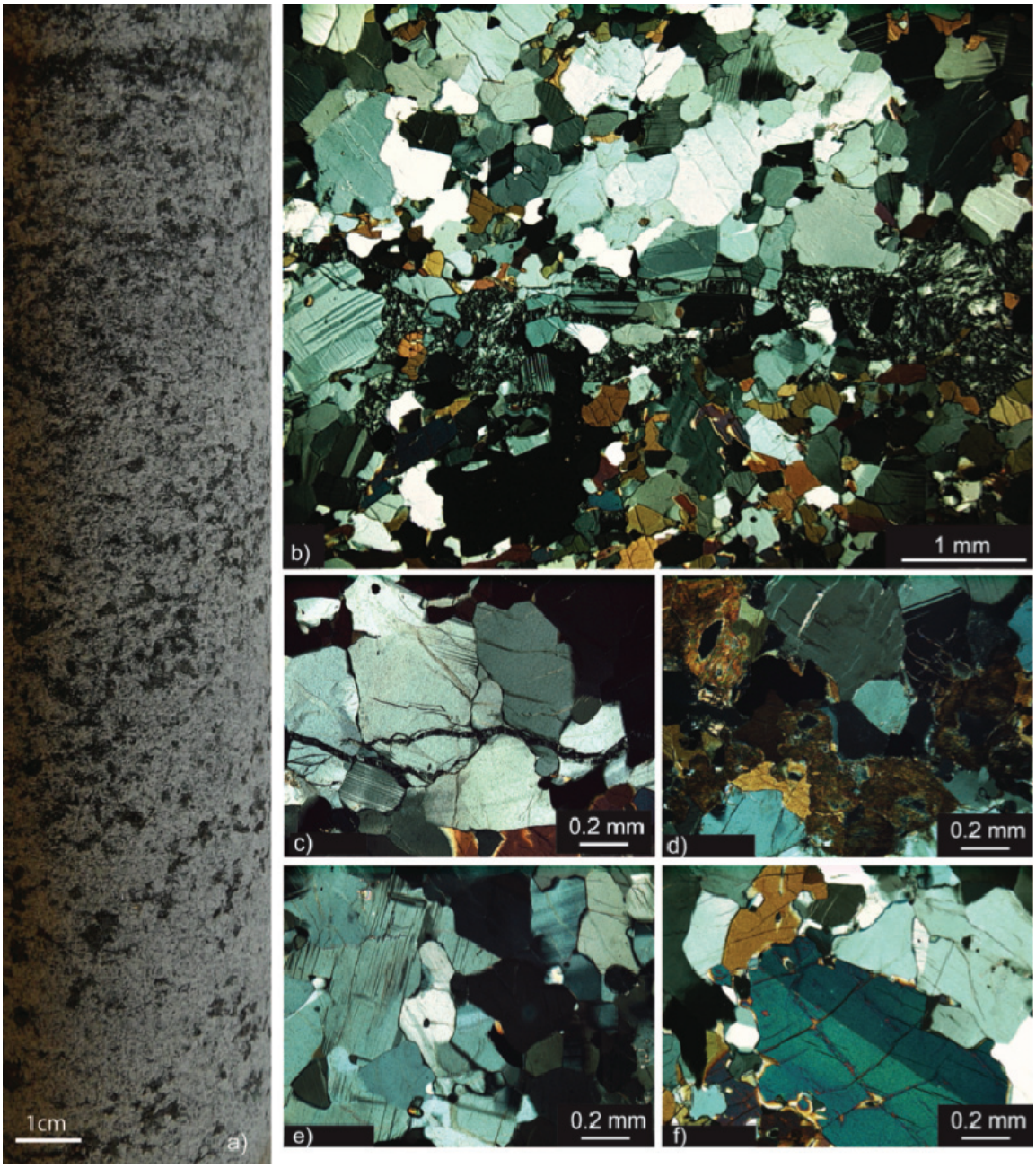

Figure 4.5: Intermediate Gneiss Sample GAP04-3 (557.7 m BHL); (a) Macroscopic Appearance; (b) Overview of the Mineral Assemblage Under Transmitted, Cross-polarized Light; (c) Plagioclase and Quartz Under Transmitted, Plane-polarized Light; (d) Amphibole with Quartz and Opaque Minerals Under Transmitted, Cross-polarized Light (e); Fine-grained Quartz with Medium-grained Plagioclase; (f) Medium-grained Amphibole Pervaded by Smectite-filled) Microfissures, Very Fine-grained Quartz and Fine-grained Plagioclase

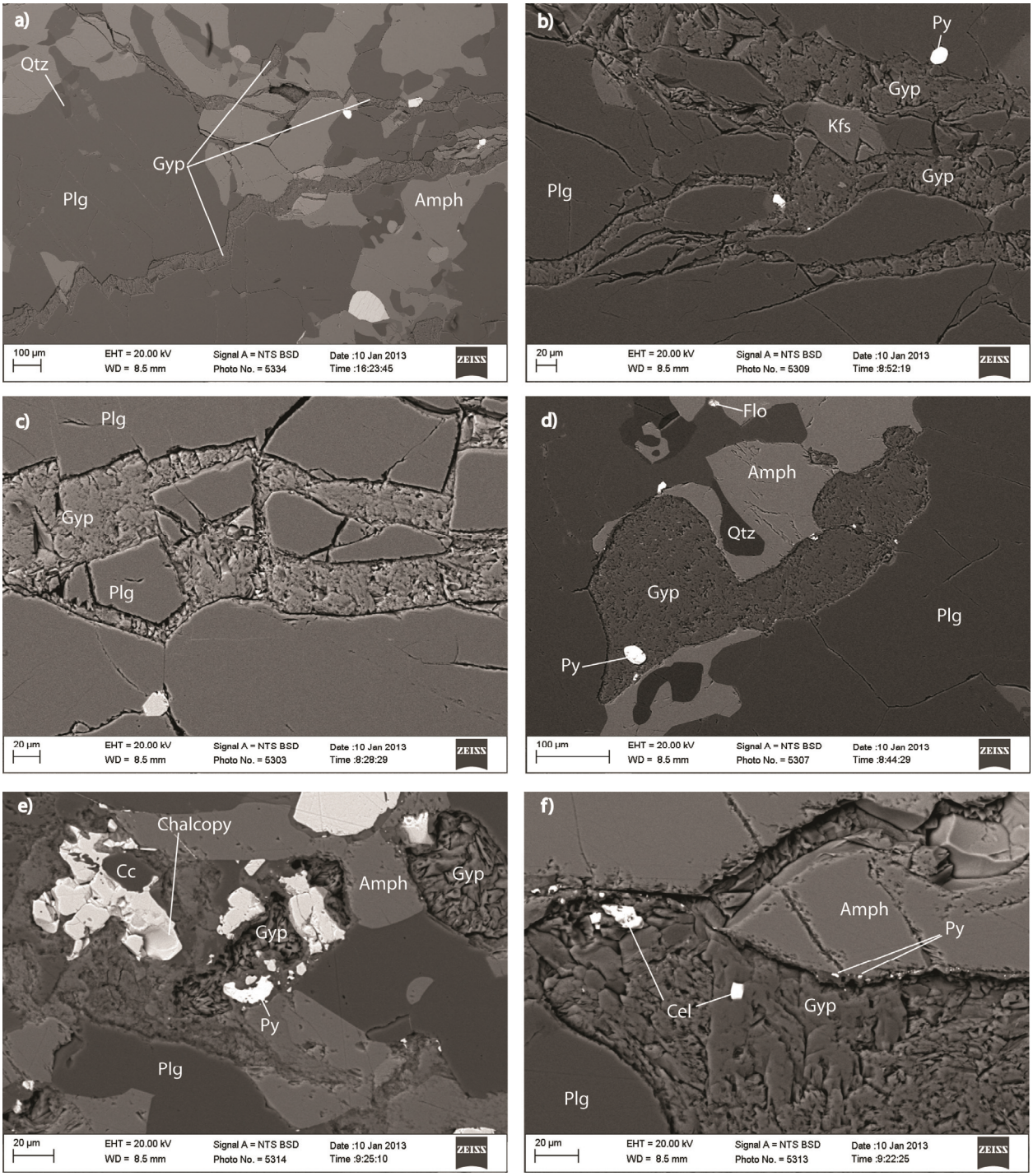

Figure 4.6: SEM Images of Intermediate Gneiss Sample GAP04-3 (557.7 m BHL); (a)-(c) Gypsum-filled Fractures with Surrounding Minerals in Different Scales; (d)-(f) Gypsum Dispersed in Rock Matrix with Coexisting Pyrite, Chalcopyrite and Celestine; Gyp = gypsum, Plg = plagioclase, Amph = amphibole, Qtz = quartz, Apa = apatite, Kfs = K-feldspar, Py = pyrite, Cc = Calcite, Chalcopy = chalcopyrite

4.4 SAMPLE GAP04-4 (FELSIC GNEISS, 607.7 M BHL)

Core sample GAP04-4 consists of a slightly foliated, equigranular and macroscopically unaltered felsic gneiss with palaeosomatic bands (Figure 4.7a). It consists mainly of quartz, plagioclase and K-feldspar, with minor opaque ore minerals, biotite, amphibole, gypsum, muscovite and apatite. Zircon, lanthanite, rutile and celestine are present as accessory minerals (Figures 4.7b-f and 4.8, Table 4.2).

Quartz occurs as xenomorphic to hypidiomorphic, very fine- to fine-grained crystals, and as xenomorphic to hypidiomorphic, coarse-grained grains (Figure 4.7b, c, e). Medium- to coarse-grained quartz sometimes contains sericite-filled microfissures (Figure 4.7e). Very fine- to fine-grained quartz is associated with fine-grained plagioclase and K-feldspar (Figure 4.7c). Quartz grains contain fluid inclusions (possibly of different generations) (Figure 4.7f). Their occurrence supports the necessity of the application of non-destructive pore-water extraction methods.

Plagioclase and K-feldspar occur as xenomorphic to hypidiomorphic, fine-grained and unaltered minerals (Figure 4.7a, b, e), and as xenomorphic, strongly saussuritized and sericitized minerals in clusters, intergrown with muscovite and opaque ore minerals. Fine-grained unaltered plagioclase and K-feldspar is associated with fine-grained quartz.

Opaque ore mineral consist, according to the SEM investigations, of pyrite and Fe-oxides, which occur as xenomorphic, fine- to coarse grained crystals, predominately intergrown with strongly altered feldspar and muscovite. Very fine-grained pyrite is present around gypsum crystals (Figure 4.8b).

Amphibole occurs as xenomorphic, fine- to medium grained crystals (Figure 4.7d).

Biotite is present as xenomorphic-hypidiomorphic, fine-grained to medium-grained crystals.

The presence of soluble gypsum and pyrite, and the alteration products of main rock forming minerals – such as sericite, smectite, chlorite and saussurite, in the core samples may have an influence on the test water chemistry and, in the case of mineral dissolution (which is probable for gypsum) an influence on the water content determination for the core samples. The occurrence of hydrated minerals, like gypsum and clay minerals, might have an influence on the isotopic determination of porewater, because crystal water (gypsum) and interlayer water (clay minerals) are believed to exchange isotopically with the porewater and applied test water. The rock textures, structures and grain size distributions of the core samples, which vary from sample to sample (cf. Table 4.1), will influence the transport properties of dissolved solutes in the pore space and have to be taken into consideration during the evaluation and interpretation of experimentally determined pore diffusion coefficients.

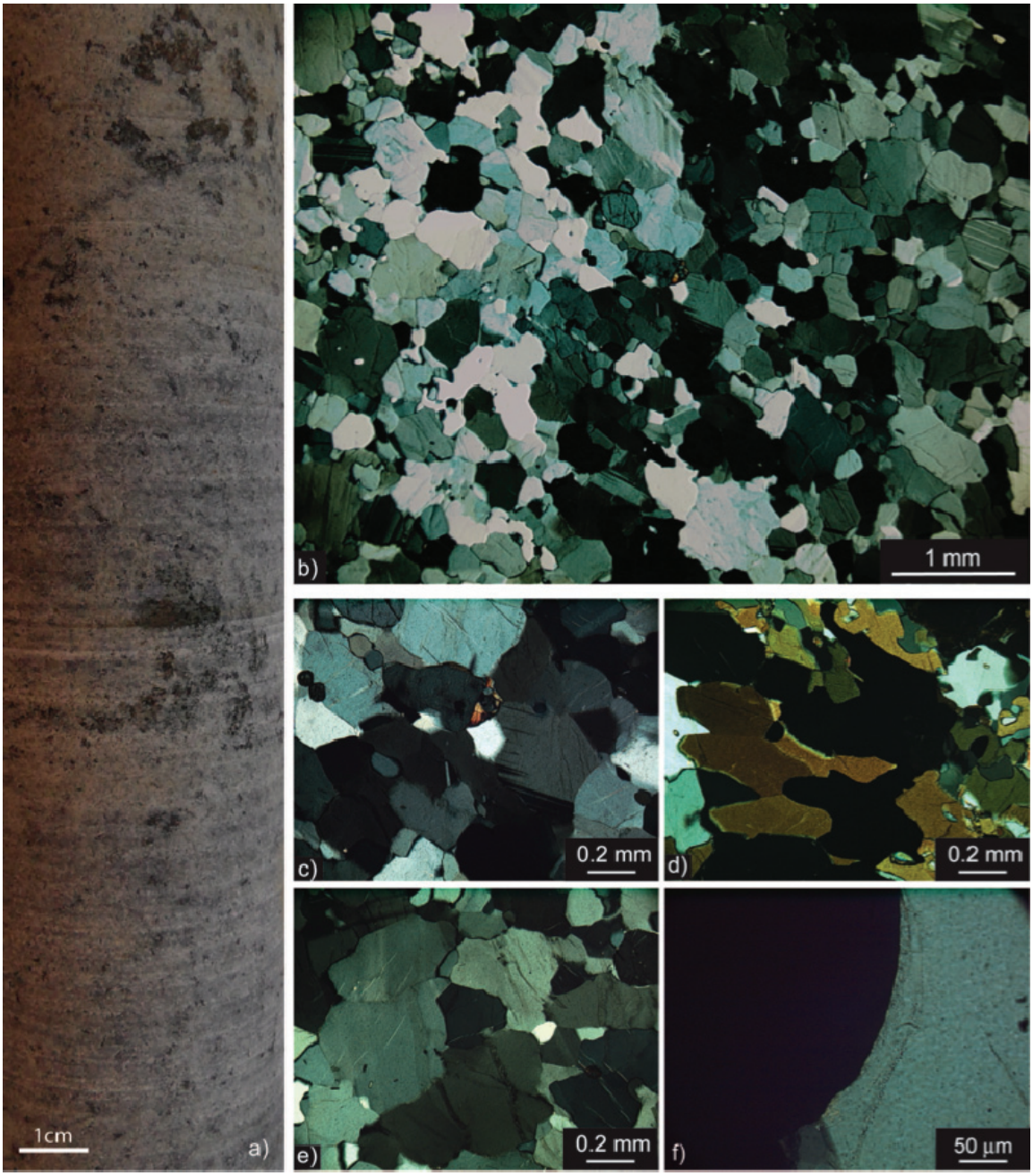

Figure 4.7: Intermediate Gneiss Sample GAP04-4 (607.7 m BHL); (a) Macroscopic Appearance; (b) Overview of the Mineral Assemblage Under Transmitted, Cross-polarized Light; (c) Quartz and Plagioclase Under Transmitted, Plane-polarized Light; (d) Amphibole with Quartz and Opaque Minerals Under Transmitted, Cross-polarized Light (e); Fine- to Medium-grained Quartz with Medium-grained Plagioclase; (f) Quartz with Fluid Inclusion Tracks

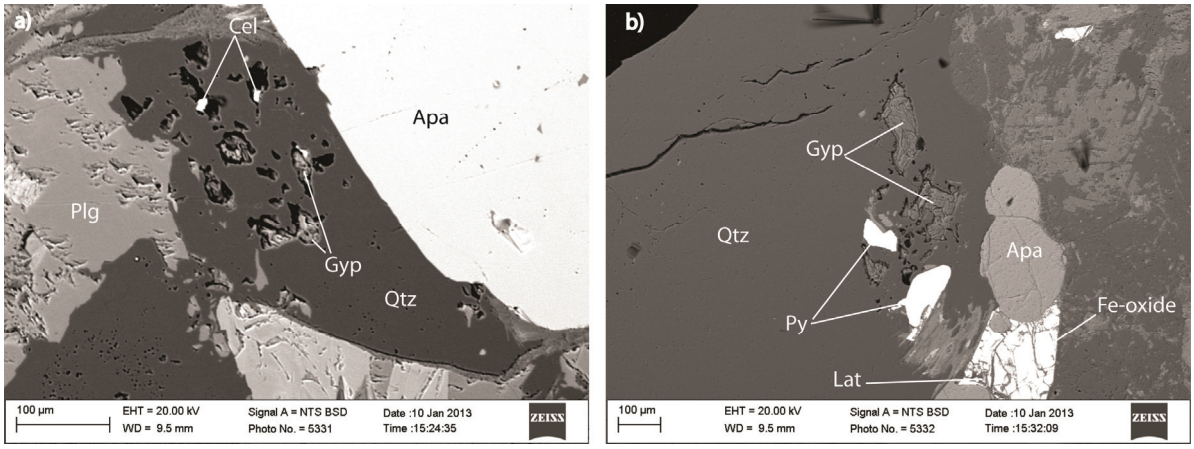

Figure 4.8: SEM Images of Intermediate Gneiss Sample GAP04-4 (607.7 m BHL); gypsum dispersed in rock matrix with coexisting celestine (a) and pyrite (b); Gyp = gypsum, Plg = plagioclase, Qtz = quartz, Apa = apatite, Py = pyrite, Cel = celestine, Lat = lanthanite.

Table 4.2: Borehole DH-GAP04 – Mineralogy of Core Samples Used for Porewater Experiments Obtained from Transmitted Light and Scanning Electron Microscopy

Mineral (vol.%)	GAP04-1 IGM	GAP04-2 IGM	GAP04-3 IGM	GAP04-4 FGM
Quartz	25	25	25	50
K-feldspar	-	Acc.	Acc.	5
Plagioclase	40	40	35	35
Biotite	10	10	5	2
Amphibole	16	20	25	1
Opaque minerals*	6	3	7	3
Gypsum	2	1	2	1
Alteration products (smectite, chlorite)**	Acc.	Acc.	Acc.	-
Rutile	Acc.	-	Acc.	Acc.
Muscovite	-	Acc.	Acc.	1
Zircon	Acc.	-	Acc.	Acc.
Celestine	Acc.	-	Acc.	Acc.
Apatite	Acc.	Acc.	Acc.	1
Florencite [$CeAl_3(PO_4)_2(OH)_6$]	-	Acc.	Acc.	-
Synchysite [$CaCe(CO_3)_2F$]	-	-	Acc.	-
Allanite [$(Ce,Ca,Y,La)_2(Al,Fe^{+3})_3(SiO_4)_3(OH)$]	-	-	Acc.	-
Lanthanite [$(Ce,La,Nd)_2(CO_3)_3$]	Acc.	Acc.	Acc.	Acc.
Calcite	-	Acc.	Acc.	-

* Opaque minerals consist predominately of pyrite, chalcopyrite and Fe-oxides (see text).
** Alteration of amphibole.

5. WATER CONTENT AND WATER-LOSS POROSITY

5.1 BACKGROUND OF WATER CONTENT DETERMINATION

The determination of in-situ porewater tracer concentrations in low-permeability crystalline rock samples is based on the knowledge of the in-situ mass of porewater (cf. Equation 13). Additionally, the water content is the basis for the calculation of the connected porosity of a rock sample (cf. Section 5.7 and 5.8).

In this study, the water content is determined gravimetrically by drying the naturally saturated core samples until stable weight conditions, and also by the diffusive isotope exchange technique. The experience of multiple porewater studies in crystalline rocks showed that water-content data cannot be extrapolated to other samples of the same lithology because of macroscopically unobservable textural and mineralogical heterogeneities. Therefore, the water content was determined on every sub-sample. The large size of the core pieces, especially those used for the out-diffusion experiments, guarantees that such heterogeneities are taken into account in the estimates of water content. The drying times of large-sized cores can last up to several months.

Conventionally, the water content of low-permeability crystalline rocks is determined by resaturation of previously dried and sawed core aliquots with a volume of 2-3 cm^3 (ISRM 1979). These methods are not qualified for porewater studies, as presented here, because:

- textural and mineralogical heterogeneities in the large-sized cores are not taken into account in the analyses of only a small aliquot, and
- full resaturation of low-permeability crystalline core samples is difficult and cannot be sufficiently controlled (Möri 2009).

5.2 WATER CONTENT OF DH-GAP04 SAMPLES

Water contents were determined on 4 originally saturated drillcore samples from borehole DH-GAP04. The water content was determined by two independent methods (i.e., gravimetrically by drying at 40°C and 105°C to stable weight conditions, and by the diffusive isotope exchange technique; cf. Chapter 3).

The gravimetric water content (WC_{WL}) was determined on core pieces used prior to the out-diffusion experiments ($WC_{WL,core}$) and on core pieces used for the diffusive isotope exchange technique ($WC_{WL,IsoEx}$). During out-diffusion, as well as isotope exchange experiments, the core samples remained saturated.

Core pieces used prior to out-diffusion experiments were dried at 40°C until stable weight was achieved and again at 105°C until stable weight. In contrast, the core pieces used for the diffusive isotope exchange technique were dried at 105°C only until stable weight. The step-wise drying of the large size out-diffusion cores was applied because the chemistry of the test solutions (cf. Chapter 6) and the mineralogical investigations (cf. Chapter 4), both done after drying of the pieces used for the diffusive isotope exchange experiments, gave evidence of the occurrence of gypsum in microfractures and dispersed in the rock matrix.

Drying times (at 105°C) for the small sized pieces, used for the diffusive isotope exchange experiments, varied between 21 and 49 days (Figure 5.1). For the large-sized out-diffusion cores, stable weight conditions were attained after a drying time of 70 to 84 days at 40°C, and after an additional 36 to 50 days of drying at 105°C (Figure 5.1).

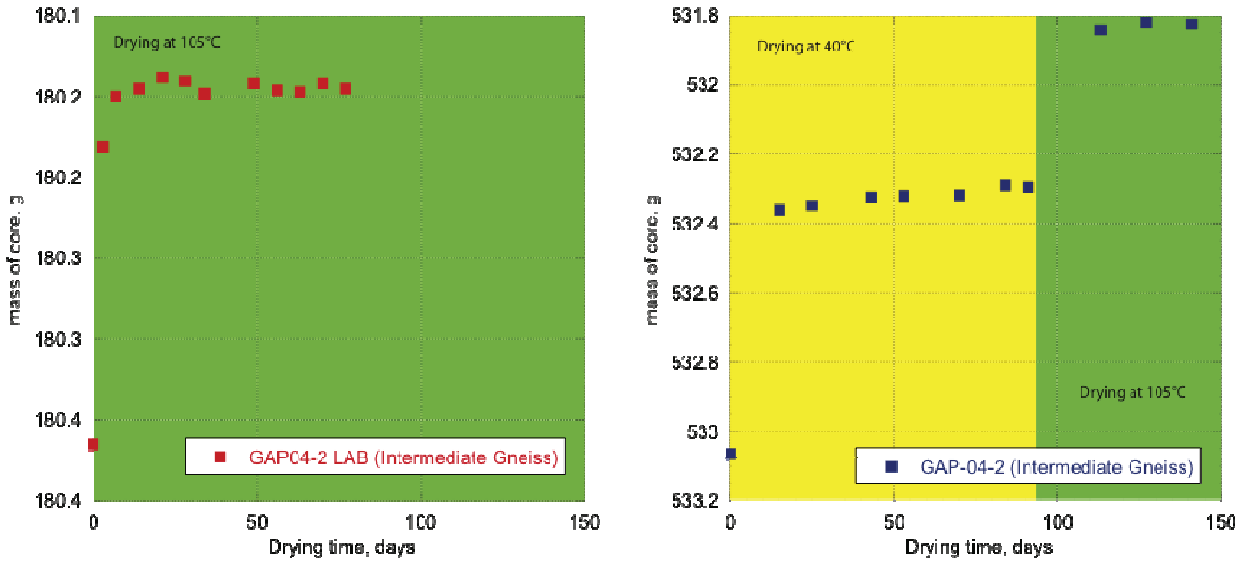

Figure 5.1: Examples of Drying Time-series at 105°C of Core Pieces Used for Diffusive Isotope Exchange Experiments (left) and Step-wise Drying at 40°C and 105°C for Large-sized Core Used for Out-diffusion Experiments (right). Analytical Error of the Weight Measurements is the Analytical Uncertainty of the Balance at ± 0.001 g

The large-sized cores showed a mass increase during the out-diffusion experiments of 0.22 to 0.34 g (Table 5.1, Figure 5.2). This is attributed to evaporation effects during transport and a subsequent re-saturation during the nine month long out-diffusion experiments. Unfortunately, no initial weights of the wet cores were taken on-site. The interpretation that evaporation occurred is supported by the observation of air within the sample bags and the fact that the core surfaces were completely dry upon arrival at the lab. It is noted that the time between the core recovery and arrival at the lab was six months.

Water uptake during the experiments is possible within the cores due to the creation of new pore space as a result of stress release effects during the drilling process; this process cannot be monitored because the evaporation effects cannot be quantified and tend to mask any other possible artefacts. Water uptake could lead to an increase in the mass of porewater during the experiments. The experience from previous porewater studies in crystalline environments, however, indicates only a minor influence of stress release during out-diffusion experiments with respect to water content determinations (Waber et al. 2011, Meier 2012, Eichinger et al. 2013). Such observations may also apply to the cores obtained from borehole DH-GAP04.

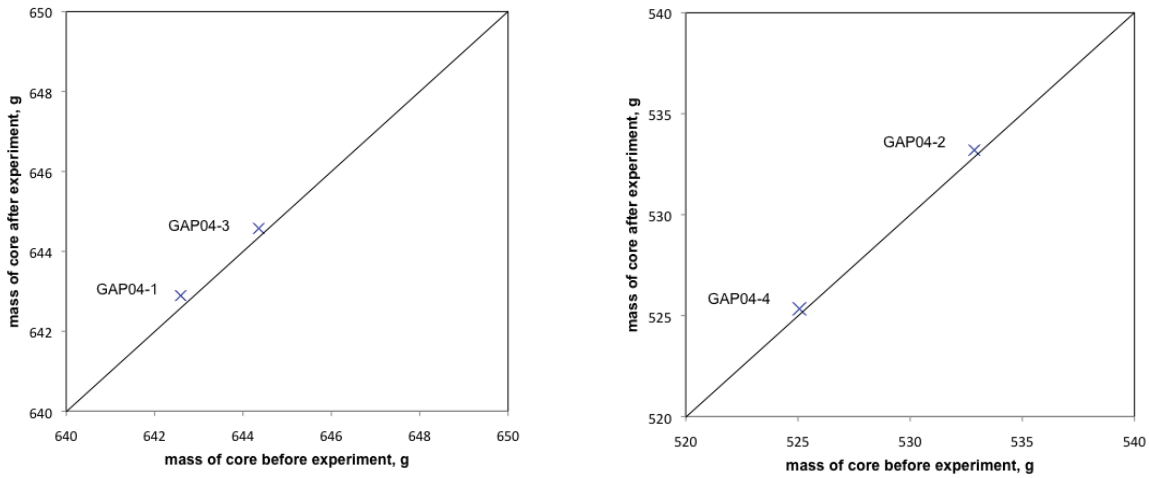

Figure 5.2: Comparison of the Core Wet Mass Before and After Immersion into the Test Water of the Out-diffusion Experiments. Uncertainty of the Determination of Wet Weight is Approximately ± 0.01 g, Caused by the Drying of the Core Surface

Table 5.1: Mass and Mass Differences of Wet Cores Before and After the Out-diffusion Experiments in DH-GAP04 Drill Core Samples

Lab Sample	Lith.	$m_{core,wet}$ before exp.	$m_{core,wet}$ after exp.	Diff $m_{core,wet}$
		(g)	(g)	(g)
GAP04-1	IGN	642.592	642.892	0.300
GAP04-2	IGN	532.859	533.197	0.338
GAP04-3	IGN	644.359	644.575	0.216
GAP04-4	FGN	525.067	525.299	0.269

The exact determination of the naturally saturated in-situ mass of the cores is additionally hindered by the dissolution of gypsum during the out-diffusion experiments. Gypsum, which occurs dispersed in the rock matrix and as microfracture infill (cf. Chapter 4), is dissolved and replaced by test water (Figure 5.3). The measured decrease in core mass before and after the experiment overestimates the new pore volume created by mineral dissolution because of the density difference between the dissolved mineral and the test water that re-saturates the new pore volume. Thus, the actual effect of re-saturation due to evaporative loss of water during storage is higher than indicated by the comparison of the core masses before and after the experiment. The mass of dissolved gypsum, and of the water filling the newly created pore volume, can be estimated for the individual core sections using the sulphate concentrations in the final out-diffusion test water solutions (cf. Table 5.7). Assuming that essentially all sulphate in the final test water originates from gypsum dissolution, the mass and volume of dissolved gypsum can be estimated. This assumption is supported by the large dilution of the porewater SO_4 concentration because of the high test water to porewater ratio (V_{TW}:V_{PW} ≈ 50 – 100).

The solubility of $CaSO_4 \cdot 2H_2O$ depends on the ionic strength and temperature of the solution. At 45°C, it is about 0.016 mol/L (≈2.2 g/L) in pure water and increases about 0.02 mol/L (≈2.7 g/L) in a 0.05 M NaCl solution, the latter corresponding roughly to the average of Cl and Na

concentrations in the porewater of the different samples (cf. Chapter 6). In the same solutions at 0°C, the solubility will be about 0.013 mol/L (≈1.7 g/L) and 0.017 mol/L (≈2.3 g/L). As gypsum is present in the rock, it is reasonable to assume that the porewater is in equilibrium with gypsum under in-situ conditions. Porewater SO_4 concentrations will, thus, vary between 0.013 mol/L and 0.017 mol/L. With the above mentioned test water to porewater ratio, this suggests a contribution of SO_4 from the porewater to the final test water solution in the range of about 1.3-3.4×10^{-3} mol/L (12-46 mg/L). Measured SO_4 concentrations in the final test solutions, however, vary by 0.016 and 0.020 mol/L for samples GAP04-1 to -3 and by 14×10^{-3} mol/L for sample GAP04-4. For samples GAP04-1 to -3, this suggests that most of the SO_4 in these final solutions results from gypsum dissolution, whereas this is less pronounced in sample GAP04-4.

Accepting the assumption that most of the SO_4 in the final solutions stems from gypsum dissolution, the mass of gypsum dissolved from the cores would range between 19.3 to 276 mg. This corresponds to a volume of 0.008-0.12 cm^3 and converts to 0.008-0.12 g of water, assuming a density (ρ_{H_2O}) of 1 g/cm^3 (Table 5.2). Based on gypsum dissolution alone (i.e., without any effects of evaporation during transport), the mass of the cores should thus be 0.01-0.17 g lighter after the experiments than before the experiments. This suggests that the mass of porewater evaporated during transport needs to be increased by 0.01-0.17 g, depending on the core sample. Therefore, the mass of porewater evaporated during transport varies between 0.28 g and 0.47 g (Table 5.2), corresponding to 30-45% of the total porewater of the individual samples.

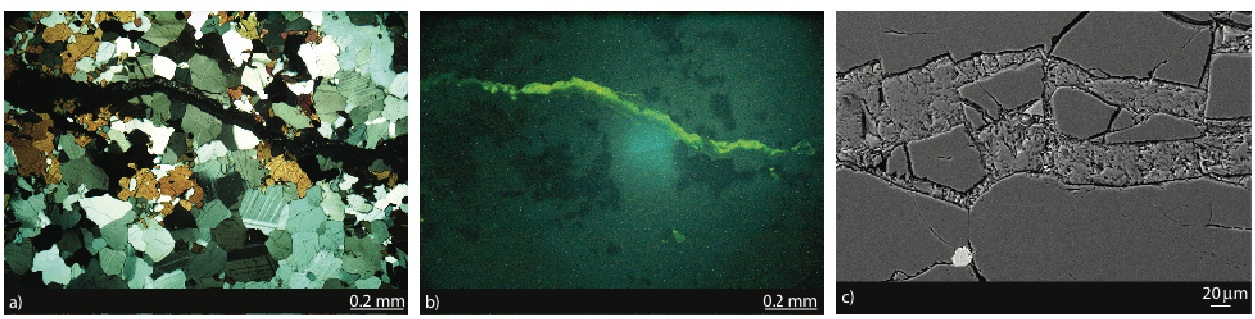

Figure 5.3: Microfracture Penetrating Through the Rock Matrix of the Intermediate Gneiss Sample GAP04-3 Under Crossed-polarized Transmitted Light (a) and Under UV Light (b). Thin Sections were Prepared with Water and Impregnated with Water-based Resin, Explaining the Dissolution of the Majority of the Gypsum in the Microfissure. Sections for SEM Investigations were Prepared without Water and Show Fully Preserved Gypsum in the Microfractures (c)

The determination of the final dry weight by drying of the cores – and hence the mass of porewater – is also influenced by the presence of gypsum in the rock matrix and as microfracture infill. Under ambient conditions, gypsum is stable up to about 42°C and then begins to dehydrate over intermediate phases (bassanite) to anhydrite. Drying at 105°C over extended time, and until stable weight conditions, will remove all crystal water from gypsum. The difference in core mass between the samples dried at 40°C and 105°C can be associated with water lost from gypsum (and possible other hydrated sulphate phases). The mass of gypsum crystal water then calculates to be 0.17-1.27 g. This corresponds to about 28-61% of the total water removed (Table 5.3) and, thus, has a significant impact on the calculated mass of porewater and water content of the samples (as shown in Table 5.5).

Table 5.2: Mass of Dissolved Gypsum Replacing Water and Final Mass of Evaporated Porewater in DH-GAP04 Drill Core Samples

Lab Sample	m_{SO_4} in test water*	$m_{gypsum,dissolved}$	$V_{gypsum,dissolved}$	$m_{H_2O,replaced}$	Diff $m_{gypsum-H_2O}$	$m_{pw,evaporated}$
	(g)	(g)	(cm^3)	(g)	(g)	(g)
GAP04-1	154	0.28	0.12	0.12	0.16	0.46
GAP04-2	127	0.23	0.10	0.10	0.13	0.47
GAP04-3	148	0.27	0.11	0.11	0.16	0.39
GAP04-4	10.8	0.019	0.008	0.008	0.011	0.28

* the total mass of sulphate dissolved in the test solution is determined by the SO_4 concentration and volume of the test solution (cf. Table 6.1).

Table 5.3: Mass of Water Removed by Drying at 40°C and 105°C from DH-GAP04 Drill Core Samples

Lab Sample	$m_{core,dry}$ 40°C	$m_{core,dry}$ 105°C	m_{PW} at 40°C*	m_{water} at 105°C*	$m_{w@105°C}$ - $m_{w@40°C}$ = crystal water
			(g)	(g)	(g)
GAP04-1	642.592	642.892	0.917	2.183	1.266
GAP04-2	532.859	533.197	0.569	1.039	0.470
GAP04-3	644.359	644.575	0.909	2.315	1.406
GAP04-4	525.067	525.299	0.435	0.604	0.169

* calculated based on the wet weight before the experiment

Taking all these artefacts into account, the gravimetric water contents calculated for the large-sized out-diffusion cores of the intermediate gneiss samples are almost constant and vary between 0.19±0.04 and 0.21±0.04 wt.% (Table 5.4). The gravimetric water content of the felsic gneiss sample is 0.14±0.03 wt.% (Table 5.4).

The calculation of the water contents, without taking into account the observed artefacts (i.e., evaporation, dissolution of gypsum, removing of gypsum crystal water), show that the water contents can deviate up to 90% from the final calculated values (see Table 5.5). The gravimetric water content values of the core pieces used for diffusive isotope exchange experiments do not represent in-situ conditions because these samples were only dried at 105°C and the values cannot be corrected for gypsum dehydration. Similarly, the water contents determined by the diffusive isotope exchange technique are not reliable because evaporation during transport precludes a derivation of the water content by isotope mass balance (cf. Chapter 8).

Table 5.4: Water Contents Determined Gravimetrically by Drying at 40°C of DH-GAP04 Drill Core Samples

Lab Sample	Depth	Lithology	Water content ($WC_{WL,core}$)	Error WC
	m b.s.		(wt.%)	(wt.%)
GAP04-1	473.4	IGN	0.21	0.04
GAP04-2	572.8	IGN	0.19	0.04
GAP04-3	526.5	IGN	0.20	0.04
GAP04-4	615.5	FGN	0.14	0.03

Table 5.5: Water Contents Neglecting the Different Observed Artefacts; Water Contents are Calculated Based on the Mass of Water Removed at the Different Drying Temperatures and Different Wet Core Masses; Values do not Consider Dissolution of Gypsum

Lab Sample	Depth	Lithology	WC($m_{corewet}$ before exp.) 40°C	WC($m_{corewet}$ before exp.) 105°C	WC($m_{corewet}$ after exp.) 40°C	WC($m_{corewet}$ after exp.) 105°C
	(m b.s.)		(wt.%)	(wt.%)	(wt.%)	(wt.%)
GAP04-1	473.4	IGN	0.14	0.34	0.17	0.37
GAP04-2	572.8	IGN	0.11	0.19	0.15	0.23
GAP04-3	526.5	IGN	0.14	0.36	0.17	0.38
GAP04-4	615.5	FGN	0.08	0.12	0.12	0.15

5.3 UNCERTAINTIES IN WATER CONTENT DETERMINATION AND THEIR CONTROL

The determination of the water content can be disturbed by several processes and artefacts, which can be divided into drilling induced and experimental artefacts.

5.3.1 Potential Experimental Artefacts

For the exact determination of the water content, it is necessary to determine the initial wet weight of the core samples immediately after recovery from the borehole and the final dry mass of core after the experiments. Potential experimentally induced artefacts that can modify the water content of a rock sample from that of in-situ conditions include:

- evaporation during the packing and transport,
- creation of artificial pore space and entrance of water during preparation of core samples,
- overestimation of the amount of porewater due to a dehydration of hydrated minerals during drying,
- incomplete drying of the core pieces, and
- overestimation of the amount of porewater due to water sorbed on the core surfaces.

These artefacts can be controlled by well-defined logistics in the field and a well-defined analytical laboratory protocol.

Control of evaporation during packing and transport

Non-destructive porewater studies, as they have to be applied for crystalline rocks, are based on naturally saturated core samples. Therefore, it is necessary to preserve the natural saturation state and to prevent/minimize any evaporation effects during packing and transport. Such effects can be minimized by the specially developed packing procedure described in Section 3.1, which guarantees a short atmospheric exposure time and a complete barrier against evaporation during transport. The time between packing and preparation of the samples in the laboratory should not be longer than one week.

Potential evaporation during transport can be controlled by comparing the weights of the core samples before wrapping and after unwrapping in the lab. Intact vacuum in the single bags and wet core surfaces upon arrival at the lab are good indications of the preservation of the saturated state between the time of core recovery and sample preparation.

Creation of artificial pore space and entrance of water during the preparation of core pieces

Additional pore space can be created during sawing of samples, resulting in the ingress of water into the newly created pore space. The magnitude of artefacts induced by preparation (i.e., sawing) depends on the sample size. Based on gravimetric water loss of resaturated samples of different thicknesses, Tullborg and Larson (2006) found that porosity values (which are proportional to the water contents at equal density) of thin slices of medium-grained granite samples (0.3 and 20 mm) are up to 50% higher than porosity values of thicker (60 mm) core pieces. They attribute the increase of porosity – and hence the water content – to the artificial connection of unconnected pores, which are not accessible to water in the 60 mm pieces, and to the generation of newly created pores and microcracks, which penetrate through the thinly sliced core pieces.

The influence of preparation artefacts due to sawing can be minimized by using large-sized full diameter core samples. The length of the naturally saturated core pieces used in the present study for the determination of the gravimetric water content were between 8 and 20 cm and exceeded the sample thicknesses used by Tullborg and Larson (2006).

Control of potential dehydration of hydrated minerals

For the determination of the gravimetric water content, naturally saturated crystalline rock samples are commonly dried at 105°C until stable weight conditions are reached. This temperature is adequate to vaporize the accessible inter- and intragranular porewater, but not the crystal and interlayer water of rock forming minerals. The temperature used, however, is sufficient to remove crystal water from hydrated salts like gypsum ($CaSO_4 \cdot 2H_2O$), which can be present dispersed in the rock matrix of crystalline rocks or as microfracture infillings. Assuming gypsum contents between 0.1 and 1 vol.% in a 1 kg crystalline core sample ($\rho_{core,ave}$ = 2.7 g/cm^3), 0.17 to 1.7 g of H_2O are bound in $CaSO_4 \cdot 2H_2O$. This water will be removed from gypsum by drying at 105°C until stable weight conditions. In a rock sample with a free accessible porewater content of 0.3 wt.% (= 3 g porewater per kg rock), the gypsum bound water exceeds the inter- and intragranular water by anywhere from 6 to 57%.

If such hydrated salts are present in the investigated rocks, the samples have to be dried at 40°C until stable weight conditions. The drying at 40°C takes longer to achieve stable weight conditions than simply drying at 105°C. A prerequisite to detect such hydrated phases, which can influence the gravimetric water content and also the water content determined by the

isotope diffusive exchange technique (cf. Chapter 8), are fundamental mineralogical and petrographical investigations using X-ray diffraction (not applied in this study), transmitted light microscopy and scanning electron microscopy.

Control of complete drying of crystalline core samples

The completeness of the drying process is controlled by regular monitoring of the core weights. The final dry weight is recorded when the weight differences for any given sample are ≤0.002 g over a time period of at least two weeks.

Control of the influence of surface-sorbed water

Due to the use of drilling fluid, all core samples prepared for water content measurements have wetted surfaces. The water sorbed on the core surface (here referred as surface water), which is used as an indicator for possible evaporation, is not part of the matrix porewater and leads to an overestimation of the water content. Drillcore samples are cut out of the bedrock. The area around the core, which is moistened by drilling fluid, is not present in-situ and, hence, this artificially created water volume cannot be taken into account as part of the natural mass of porewater.

With respect to the exact determination of the water content, the ideal procedure is to dry the surface water from the cores before the initial weight of the saturated sample is taken. Experience from multiple sample preparations showed that the surfaces of the cores are dried after 2 minutes without evaporation of porewater under normal room conditions (Eichinger 2009). During drying of the surface of the cores under the atmosphere, the weights should be monitored and recorded.

5.3.2 Potential Artefacts Induced by the Drilling Process

Influence of stress release

Rock samples recovered from deep boreholes are affected by the release of the stresses that they are subject to under in-situ conditions. This results in a decrease of the elastic moduli of rock building minerals. Due to anisotropy in the mechanical properties of mineral grains, this process leads to the generation of microcracks and an increase of pore apertures. Thus, the physical porosity of rock samples may be increased. As a consequence, drilling fluid may penetrate into the newly created pore space, which could lead to an increase in the measured water content of the samples.

Perturbations related to stress release are commonly identified in drill core samples. The microcracks, which are caused by stress release, are open and are tensile in nature, with closing pressures approximately equal to the in-situ vertical stress. Microcracking induced by stress release depends on a variety of parameters. The magnitude of stress release is controlled by the sampling depth; increasing load (with depth) results in higher vertical stresses and effect the magnitude of shear stresses, which depend primarily on the local and regional horizontal and sub-horizontal stress distributions within the bedrock. Microcracking induced by stress release has been described in samples between 200 and 11'000 m b.s. (e.g., Kowallis and Wang 1983, Meglis et al. 1991, Morrow et al. 1994, Jacobsson et al. 2007). The effects of stress release also depend on the sample lithology and texture. Morrow et al. (1994) found a correlation between the degree of microcracking induced by stress release and the quartz

content of samples from the KTB borehole and the Kola superdeep borehole. The results of Meglis et al. (1991), from scientific boreholes in New York and Connecticut, suggest that the orientation of stress-release microcracks is controlled by the foliation of the drill core samples. The magnitude of stress release also strongly depends on the local stress field. This could explain the discrepancy between stress release induced microcracks observed at shallow depths (e.g., Kowallis and Wang 1983, Meglis et al. 1991) when compared to studies from the Kola superdeep borehole, which suggest that microcracking induced by stress release is negligible down to a depth of 800 to 1'000 m b.s. (Gorbatsevich 2003).

Quantitative information about the influence of stress release and the penetration of drilling fluid in drillcore samples can only be gained by applying traced drilling fluid during the drilling process, and such investigations have been conducted at both the Swedish Forsmark site (Waber et al. 2011) and the Finnish Olkiluoto site (Meier 2012, Eichinger et al. 2013). At both sites, sections of deep boreholes were drilled with NaI traced drilling fluid of known composition. The volume of penetrated drilling fluid in the investigated core samples was obtained by out-diffusion experiments (cf. Chapter 3.3.4). Modelling of the elution behaviour of the artificial tracer iodide and the natural tracer chloride revealed that the relative increase in water content caused by stress release approximates 2.4% for isotropic granodiorite from the Forsmark site (Waber et al. 2011) and between 0.8 and 2.5%, and 5.0 and 8.9%, for anisotropic veined gneisses and isotropic TGG-gneiss, respectively, from the Olkiluoto site (Meier 2012, Eichinger et al. 2013). The penetration of drilling fluid into the newly created pore space depends on the rock type, and may impact estimates of solute concentrations in the porewater – values may lie outside of the bounds of analytical uncertainty for the experimental procedure(s). The potential impact of stress release on determinations of water content is discussed further in the context of this study in Chapter 7.

Influence of the drilling disturbed zone

In addition to stress release, the drilling process can disrupt the drill core samples due to the mechanical impact of the drill bit. The disruption induced by drilling is limited to the outermost rim of the drill core, termed the “drilling disturbed zone” (DDZ). It causes an enlargement of the existing pores and the creation of new pores and microcracks along the rim zone. The quantification of the drilling disturbed zone is assessed utilising the tracer elution behaviour of out-diffusion experiments and 2-D transport modelling, similar to what is done to assess the magnitude of stress-release induced artefacts.

The DDZ was identified in crystalline drillcores from the Äspö underground laboratory and from the Forsmark and Olkiluoto investigation sites. For quartz-monzodiorite samples from the Äspö Hard Rock Laboratory (HRL) in Sweden, Waber et al. (2011) found a DDZ of about 0.1 mm. These samples were stress released as they were collected from a short borehole close to a 20-year-old tunnel wall. All induced enlargement of the pore space was associated with mechanical disruption during the drilling process. In granodioritic core samples from about 550 m b.s. in a deep borehole drilled at the Forsmark site, Waber et al. (2011) characterized the disrupted zone to be up to 6 mm into the core. For veined gneiss and TGG-gneiss samples from Olkiluoto, Meier (2012, reported in Eichinger et al. 2013) found a disrupted zone of 0.4 to 2.2 mm and 1.0 to 1.8 mm, respectively. New pore space, created by the drilling process, appears to be related only to a small outer-rim portion of the drill core. Considering the large volume used in porewater out-diffusion experiments, it is interpreted that the perturbation of the pore space (and water-content measurements) in crystalline drillcore samples is predominantly caused by stress release rather than mechanical drilling damage.

5.4 BACKGROUND AND METHODOLOGY OF BULK DENSITY DETERMINATION

A measure for the bulk wet and bulk dry density of the DH-GAP04 rock samples was obtained from the volume and the saturated mass of the core sections used for out-diffusion experiments. The volume was calculated from measurements of the height and diameter of the core samples used for the out-diffusion experiments using a Vernier Calliper.

Density measurements can often not account precisely enough for mineralogical heterogeneities because, commonly, samples of only a few g (or few cm^3) are used. The saturated mass of rock samples used here is between 530 and 600 g and, thus, the calculated bulk wet and dry density accounts for the heterogeneity in the mineralogy. Uncertainties affecting these determinations were described in Section 5.3.

5.5 DENSITY OF DH-GAP04 SAMPLES

The bulk wet and dry densities were determined on the core sections used for the out-diffusion experiments based on the measured volume, as well as the wet and dry masses, respectively. The top and bottom surfaces of the cores were all even, so that the geometric measurements have a small uncertainty and so does the calculated volume. The wet and dry masses of the cores were determined according to the procedure described in Chapter 3.

Bulk wet densities of the intermediate gneiss samples vary between 2.73±0.12 and 2.76±0.12g/cm^3 (Table 5.6). The bulk wet density of the felsic gneiss sample is 2.70±0.12 g/cm^3 (Table 5.6). Within analytical error, the bulk dry density of the samples is almost identical to the bulk wet density (Table 5.6), which indicates that the dissolution of gypsum during the experiments had almost no influence on the density of the rocks.

Table 5.6: Bulk Wet and Bulk Dry Density of Core Samples from Borehole DH-GAP04

Lab Sample	Lithology	Diameter	Length	V (core)	$m_{core,wet}$ *	$m_{core,dry}$	$\rho_{bulk,wet}$	Error $\rho_{bulk,wet}$	$\rho_{bulk,dry}$	Error $\rho_{bulk,dry}$
		Cm	cm	cm^3	g	G	g/cm^3	g/cm^3	g/cm^3	g/cm^3
GAP04-1	IGN	5.06	11.61	233.47	643.052	641.675	2.75	0.12	2.75	0.12
GAP04-2	IGN	5.05	9.66	193.49	533.329	532.29	2.76	0.12	2.75	0.12
GAP04-3	IGN	5.06	11.74	236.08	644.749	643.45	2.73	0.12	2.73	0.12
GAP04-4	FGN	5.05	9.72	194.69	525.347	524.632	2.70	0.12	2.69	0.12

* value calculated taking evaporation and dissolution effects into account (cf. chapter 5.2)

5.6 UNCERTAINTIES IN BULK DENSITY DETERMINATION

Uncertainties in the determination of the bulk density of the large sized core samples include the exact determination of the wet and dry weight, and the volume of the samples. The artefacts with respect to the determination of the exact wet and dry weight of the core samples, and what can be done to minimize such artefacts, are described in detail in Section 5.3.

The volume of the cores is determined by measuring the diameter and length of the cores using a Vernier calliper. As the experience from multiple deep boreholes from several locations has shown, the diameter of the 10-12 cm cores is constant within a range of 0.05 cm (Eichinger et al. 2006, 2010, 2012, 2013). The measurement of the exact core length can be difficult if the surfaces of the upper and lower lids of the cores are uneven. Care is taken so that the top surfaces of the cylindrical core samples are cut straight. If the top surfaces are unevenly sawn or broken, the volume of the cores is determined by using the difference of the mass of core sample in air and in water (Archimedes principal, cf. Chapter 3).

5.7 BACKGROUND METHODOLOGY OF WATER-LOSS (CONNECTED) POROSITY DETERMINATION

Different types of porosity measurements characterize different parts of the pore space of a crystalline rock. For the indirect techniques of porewater characterization, appropriate porosities are needed for the recalculation of the in-situ solute concentrations and the determination of pore diffusion coefficients. In the low-permeability rock matrix of crystalline rocks, different types of porosity can be distinguished.

Physical or total porosity: the physical or total porosity of a rock describes the total pore space in a rock that is defined by the ratio of void volume to the total volume of the rock and can be calculated from the bulk density of a dry sample and its grain density (Norton & Knapp 1977). The physical porosity includes the volume not occupied by mineral grains, such as pore spaces between mineral grains, dead-end pores, microfractures, porous minerals (e.g., altered or secondary minerals) and fluid inclusions.

Connected porosity: the connected porosity of a rock describes the volume of connected pore space and is smaller than or equal to physical porosity. In crystalline rocks, it is commonly determined by the gravimetric water content measurement, by the diffusive isotope exchange technique (cf. Chapter 3), or by resin impregnation and quantitative visualization of the pore space (e.g., Hellmuth et al. 1993, Autio et al. 1998, Ota et al. 2003).

Geochemical porosity: the geochemical porosity, or tracer accessible porosity, describes the fraction of the connected porosity that is accessible to a certain ion. Depending on the rock composition, and its texture and grain size, previous work suggests that not all connected porosity is accessible for all dissolved solutes. In the absence of more detailed data, the Cl- and Br-accessible porosity of the investigated GAP04 samples is set equal to the connected porosity for the purposes of estimating diffusion coefficients. Potential effects, which lead to an exclusion or retardation of certain ions, should be investigated for each rock type.

5.8 WATER-LOSS POROSITY OF DH-GAP04 SAMPLES

The water-loss porosity of the intermediate gneiss samples varies slightly between 0.54±0.12 and 0.59±0.12 vol.% (Table 5.7). The water-loss porosity of the felsic gneiss sample is 0.37±0.08 vol.% (Table 5.7).

5.9 UNCERTAINTIES IN THE WATER-LOSS POROSITY DETERMINATION

The uncertainties in the determination of the connected porosity depend predominately on the artefacts and analytical errors induced in the determination of the water content and the bulk wet density, as described above.

Table 5.7: Water-loss Porosity of Core Samples from Borehole DH-GAP04

Lab Sample	Lithology	Water-loss porosity
		vol.%
GAP04-1	IGN	0.59±0.12
GAP04-2	IGN	0.54±0.12
GAP04-3	IGN	0.55±0.12
GAP04-4	FGN	0.37±0.08

5.10 CHARACTERIZATION OF PORE SPACE

Water-loss, or connected porosity, which is determined gravimetrically within this study, is the porosity accessible to water and, hence, the porosity relevant for solute transport. According to previous studies of crystalline rocks, the interconnected network of pores consists of inter- and intragranular pores. The intergranular pore space is equal to the grain boundary porosity between different mineral grains (mainly between feldspar and quartz). The intragranular pore space includes solution porosity associated with the alteration of mineral grains (e.g., the sericitization of alkali feldspars), porosity along cleavage and twinning planes, and microfractures in large mineral grains.

To visualise the connected porosity, all four samples obtained from borehole DH-GAP04 were impregnated by NHC-9 resin (cf. Chapter 3) and evaluated by UV microscopy. The resolution of the visualization of the impregnated pore space is limited to a few µm. Smaller, resin filled pores cannot be observed by this method. The visualization of pore space gives information about the shape, size and distribution of connected pores, which are important parameters with respect to the transport behaviour of solutes in the pore space. The impregnation by the resin is homogeneous throughout the drillcore in the inter- and the intragranular pore space. This provides evidence for an interconnected porosity in the samples. In all samples, porosity associated with grain boundaries was observed.

The grain boundaries between quartz and feldspar (Figures 5.4 to 5.7) are clearly visible, while biotite and amphibole grain boundaries are not well delineated by the resin (Figures 5.4 and 5.6). This indicates that the grain boundary pores associated with biotite and amphibole are smaller than the pores associated with the felsic minerals. Out of this observation, anisotropy, with respect to the solute transport can be assumed within the crystalline core samples.

Microfractures predominately occurring in amphiboles are penetrated by the impregnation resin (Figures 5.5 and 5.6). Commonly, these fractures show secondary infillings of sericite or

smectite, which gives evidence that they are not formed by sampling or preparation artefacts. Such filled microfractures are highly porous and connected to the intergranular porosity and, hence, accessible for resin and water. The pore space in the filled fractures is presumably very narrow. Solute transport may be influenced by the size of the pores and by surface charges of the secondary minerals, and this hypothesis requires verification by appropriate methods but is outside of the scope of the current study.

The moderately saussuritized plagioclases of sample GAP04-2 are penetrated by the impregnation resin (Figure 5.5). This indicates that the porosity depends on the alteration grade of the individual minerals, and that the intergranular pore space is connected to the intragranular pore space and filled with water under in-situ conditions. As described for the microfractures filled with secondary minerals, solute transport in the connected intergranular pore space of saussuritized plagioclase might also be affected by the narrow size and by charge effects. The visualization of the pore space using high magnification shows that resin can also penetrate cleavage planes in plagioclase (Figure 5.7).

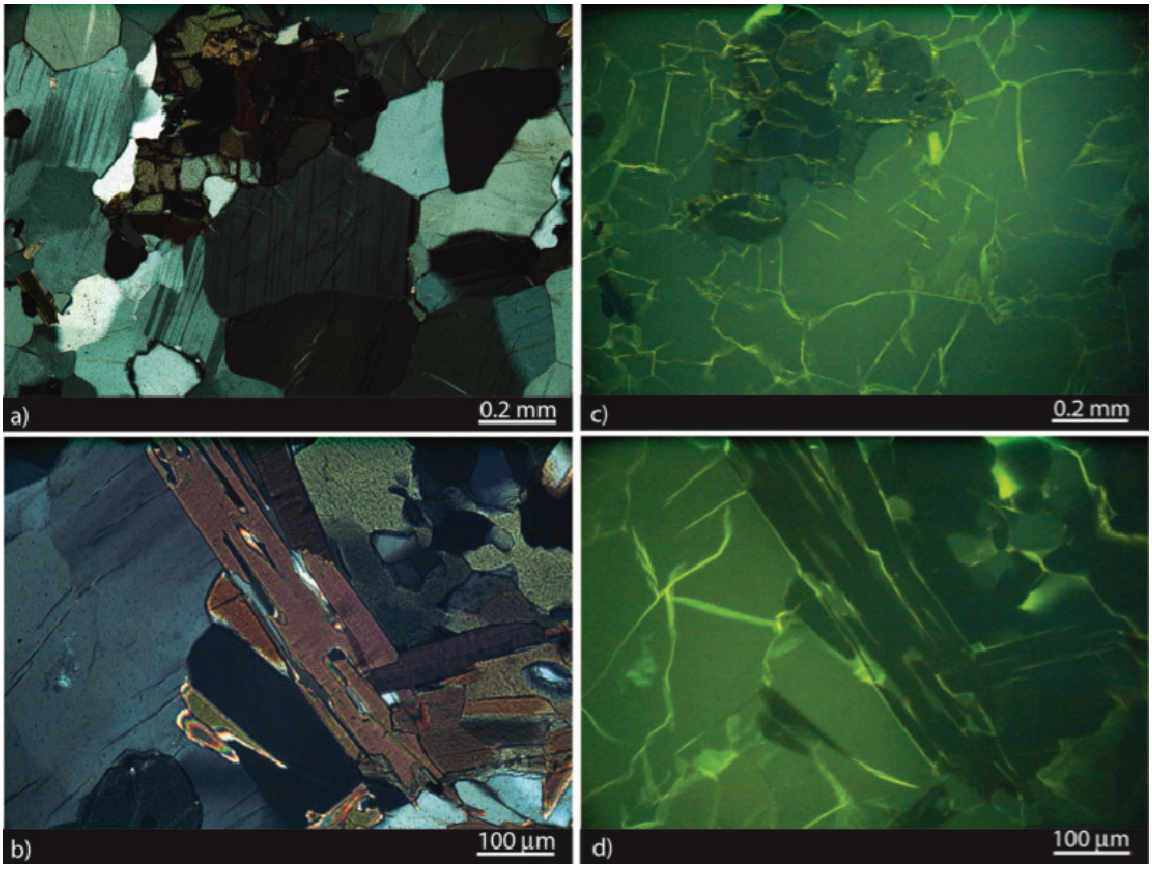

Figure 5.4: Intermediate Gneiss Sample GAP04-1; Visualization of the Connected Pore Space by Impregnation and UV-fluorescence Microscopy. (a), (c) Intergranular Connected Porosity Between Rock-forming Feldspar, Quartz and Amphibole Minerals Under UV and Transmitted Crossed-polarized Light; (b), (d) Intergranular Connected Porosity Between Biotite and Feldspar Minerals and Intragranular Porosity of Microfractures in Plagioclase Under UV and Transmitted Crossed-polarized Light

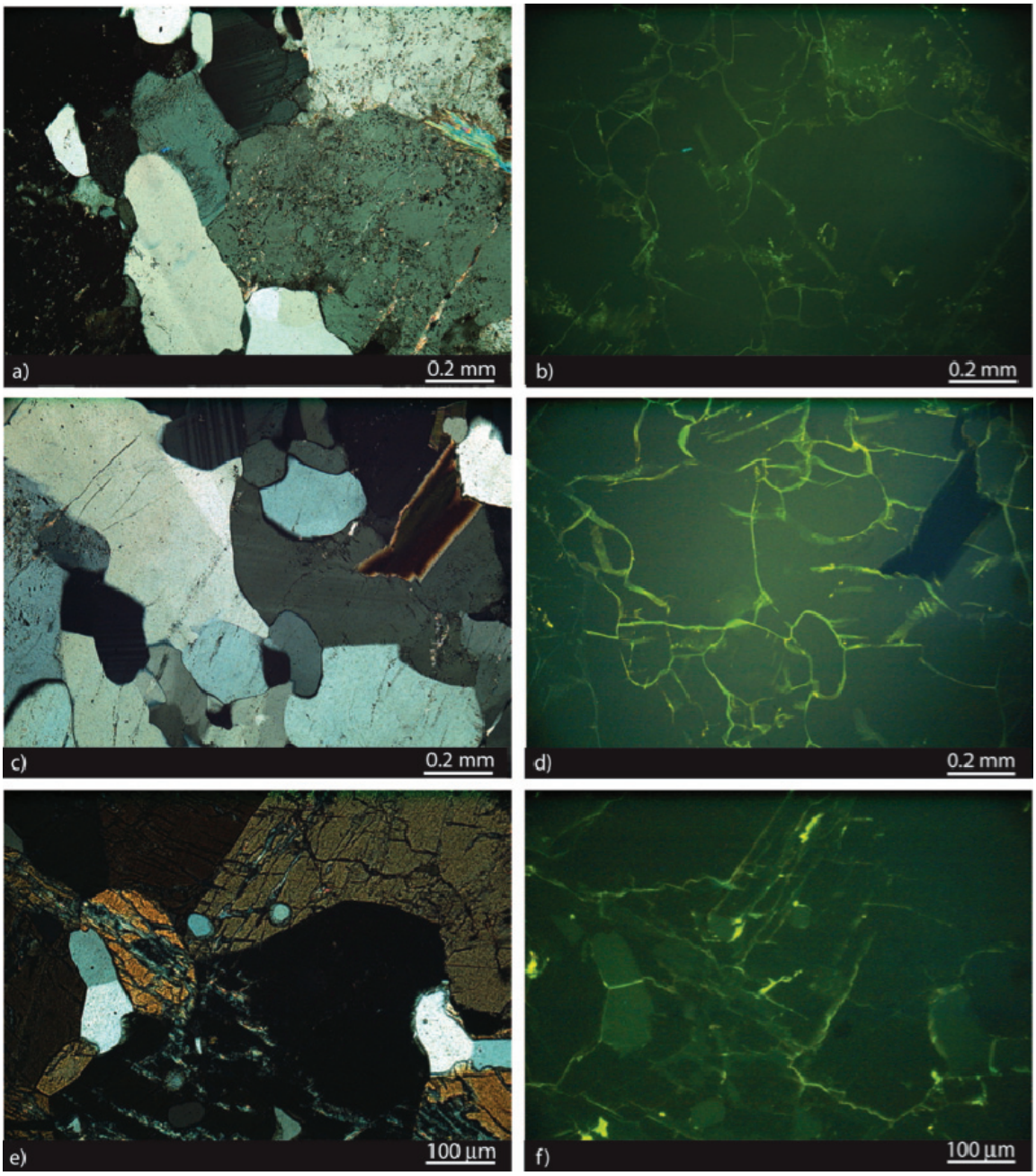

Figure 5.5: Intermediate Gneiss Sample GAP04-2; Visualization of the Connected Pore Space by Impregnation and UV-fluorescence Microscopy. (a), (b) Intergranular Connected Porosity Between Rock-forming Minerals and Intragranular Porosity in Moderately Altered Plagioclase Under UV and Transmitted Crossed-polarized Light; (c), (d) Intergranular Connected Porosity Between Feldspar and Quartz Minerals Under UV and Transmitted Crossed-polarized Light; (e), (f) Inter- and Intragranular Porosity in Amphibole Under UV and Transmitted Crossed-polarized Light

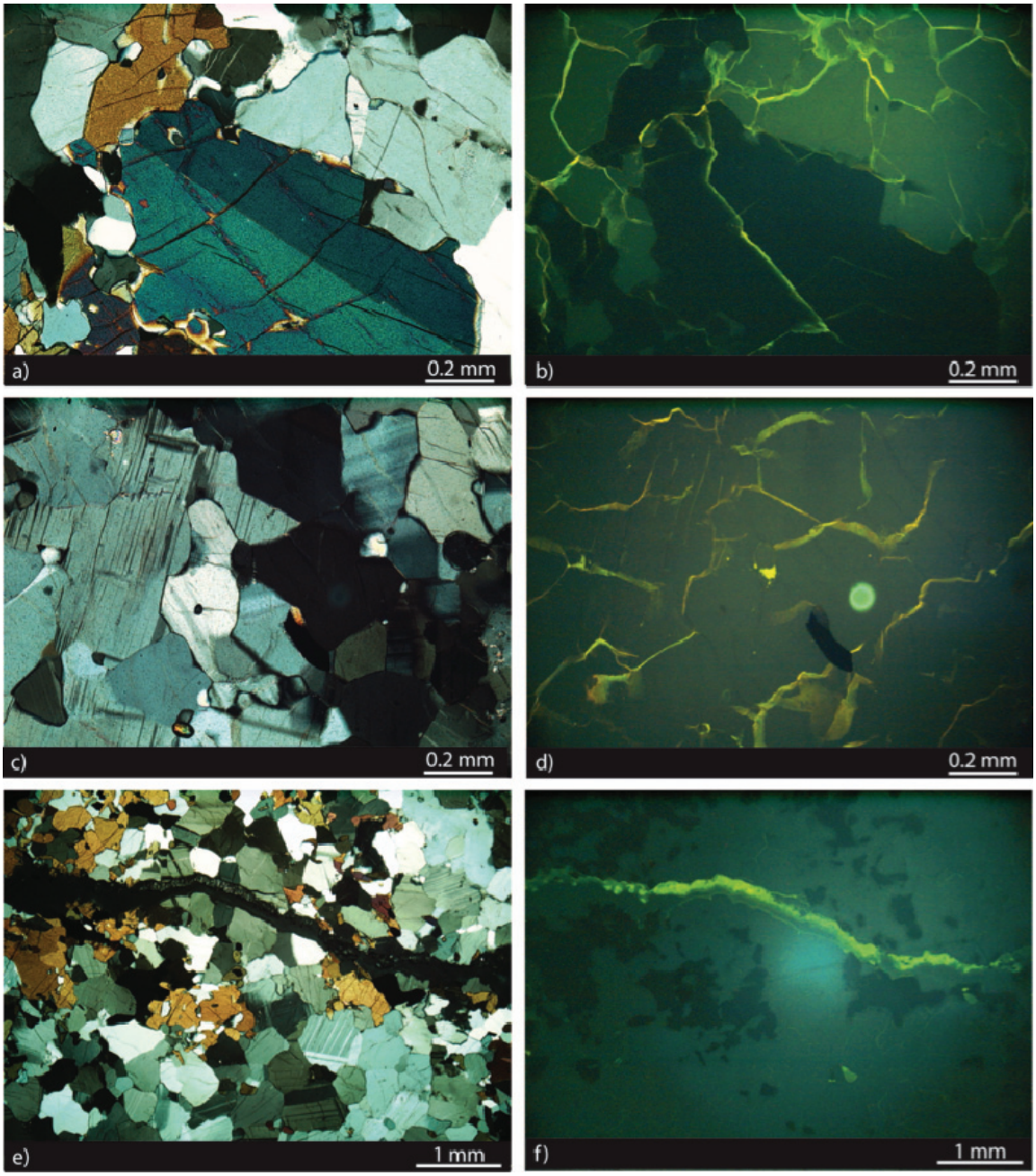

Figure 5.6: Intermediate Gneiss Sample GAP04-3; Visualization of the Connected Pore Space by Impregnation and UV-fluorescence Microscopy. (a), (b) Intergranular Connected Porosity Between Rock-forming Minerals and Intragranular Porosity in a Smectite-filled Microfissure in Amphibole Under UV and Transmitted Crossed-polarized Light; (c), (d) Intergranular Connected Porosity Between Feldspar and Quartz Minerals and Intragranular Connected Porosity Along Cleavages of Plagioclase Under UV and Transmitted Crossed-polarized Light; (e), (f) Impregnated Microfracture (originally gypsum-filled) Under UV and Transmitted Crossed-polarized Light

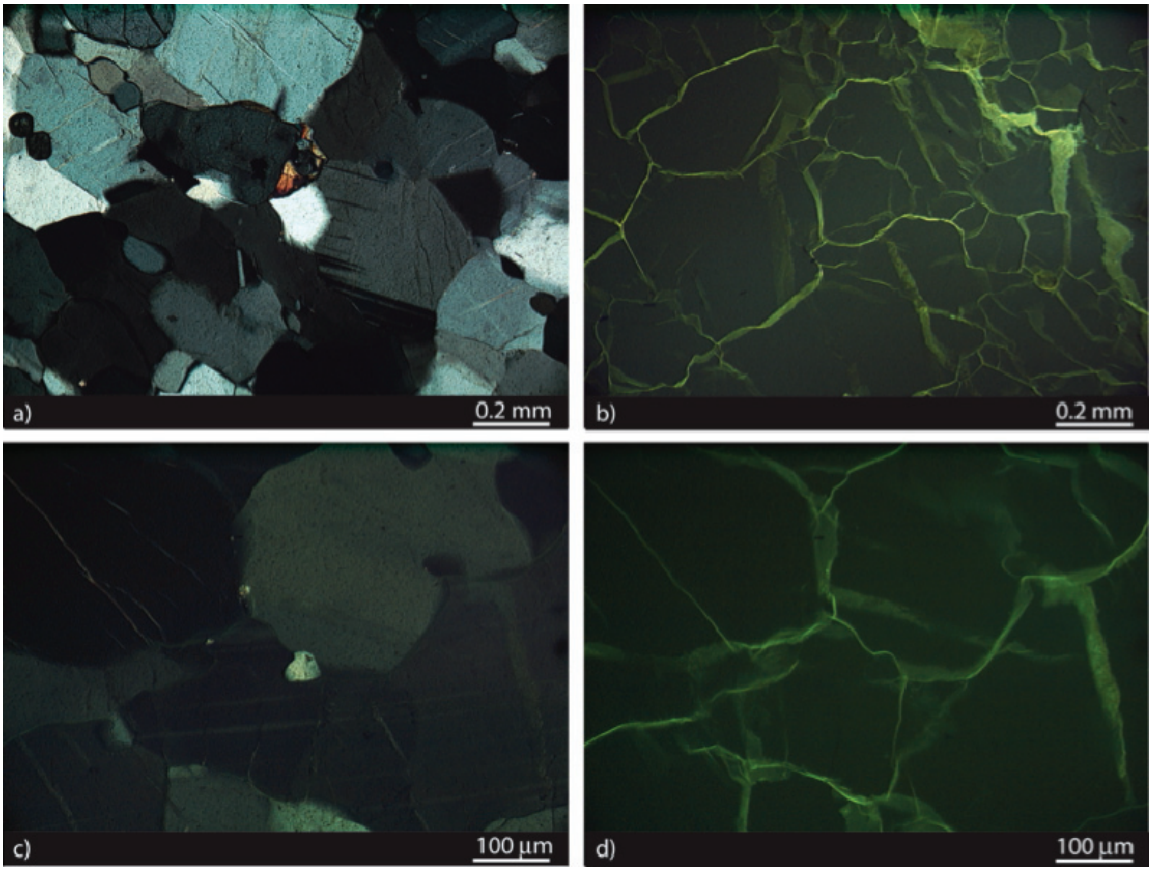

Figure 5.7: Felsic Gneiss Sample GAP04-4; Visualization of the Connected Pore Space by Impregnation and UV-fluorescence Microscopy. (a), (b) Intergranular Connected Porosity Between Rock-forming Minerals Under UV and Transmitted Crossed-polarized Light; (c), (d) Intergranular Connected Porosity Between Feldspar and Quartz Minerals and Intragranular Connected Porosity Along Cleavages of Plagioclase Under UV and Transmitted Crossed-polarized Light

Due to the fact that the degree of alteration can change significantly within the scale of few centimetres, the impregnation of the intragranular pore space confirms that porosity values cannot be extrapolated from one sample piece to another.

6. CHEMICAL TIME-SERIES FROM OUT-DIFFUSION EXPERIMENTS

Non-destructive out-diffusion experiments are performed based on the concept of chemical exchange between porewater residing in the rock matrix and a test solution of known composition surrounding the rock sample. The experimental setup is maintained until well-defined conditions between the two solution reservoirs are attained. Because of the closed-system character of out-diffusion experiments, the target conditions to be achieved between the two solution reservoirs are equilibrium for any solutes for which the porewater is the only source, and which are only subjected to transport processes. For those solutes understood to be involved in mineral reactions, steady-state conditions must be reached. A prerequisite for the successful quantification and interpretation of data obtained from out-diffusion experiments is the preservation of the original pore space during the entire experiment. Thus, disintegration of the original rock fabric due to swelling (e.g., clay-rich rocks) or extensive mineral dissolution (e.g., salt-bearing rocks) will greatly complicate, if not completely inhibit, a successful interpretation of out-diffusion experimental data. Swelling is commonly not an issue for crystalline rocks. Extensive mineral dissolution, which notably changes pore apertures and volume, seems restricted to special hydrogeological settings. Such settings include crystalline shield environments with brine groundwater compositions, or environments subjected to intense alteration processes (hydrothermal, weathering, permafrost) that produced substantial amounts of readily soluble secondary mineral phases in the rocks.

Accepting the above limitations, out-diffusion experiments also have advantages compared to other indirect porewater extraction techniques, especially if conducted on large-sized, originally saturated rock samples. Most importantly, out-diffusion experiments allow determination of the diluted porewater chemistry and the mass of porewater on the very same sample. This eliminates uncertainties related to porosity determinations in the back-calculation of test water concentrations to porewater concentrations. Conducting the experiments on large-sized samples further minimizes perturbations induced by sampling (e.g., drilling process) and sample handling (e.g., sawing, desaturation) due to the optimized ratio between the rock volume potentially affected by such processes and the undisturbed rock volume. The non-destructive nature of out-diffusion experiments inhibits leakage of mineral fluid inclusions that would perturb measured concentrations of chemically conservative compounds, such as Cl^- and Br^-. Such perturbation often is observed in crush-leach experiments with crystalline rocks (e.g., Smellie et al. 2003; Eichinger et al. 2006). For the present study, improved analytical techniques allowed continuous monitoring of all major solute concentrations in the eluate solutions during out-diffusion. This allows definition of mineral reactions and – at a later stage – possible determination of solute specific transport (e.g., ion-specific accessible porosity) in the matrix of crystalline rocks.
Disadvantages of out-diffusion experiments, as conducted in this study, are the high requirements of on-site sampling and sample handling, the long experiment time in the laboratory (several months), and the work-intensive nature of the experiments.

Out-diffusion experiments were performed on three intermediate gneiss and one felsic gneiss samples from borehole DH-GAP04 in order to derive the pore-water Cl^- and Br^- concentrations and $\delta^{37}Cl$ isotope signature. The intact core sections used in the experiments had diameters of 50.5-50.6 mm, lengths of 96.6-117.4 mm, and corresponding sample volumes of 193.5-236.1 cm^3. The saturated mass of the core sections ranged between 525.4-644.8 g. The water-rock ratio in the experiments ranged between 0.122 and 0.151. The chemical analytical data of the final eluate solutions are given in Table 6.1 (end of this Chapter) and those of the eluate time-series sub-samples in Appendix A.

6.1 MONITORING OF OUT-DIFFUSION EXPERIMENTS: SOLUTE TIME SERIES

6.1.1 Sampling and Analytical Strategy

To monitor the out-diffusion process, small volumes (0.5 mL) of eluate were removed from the out-diffusion solution in regular intervals – initially every few days, and later every few weeks. The collected solutions were stored in 1 mL sample holders for the IC auto-sampler. For samples GAP04-1 and GAP04-3, control analyses were performed on 1:10 dilutions of the 0.5 mL stock solution in May, August and September, 2012, to determine if equilibrium conditions were reached with respect to Cl^-. No significant change in Cl^- concentration was observed from June to September 2012, and the out-diffusion experiments were terminated for all samples on September 20th 2012 (i.e., after 283 days of equilibration).

After termination of the experiments, the supernatant final solutions were removed from the cylinders, filtered, and immediately analysed for pH and alkalinity. This was followed by a first analysis of the final solution to determine the accurate dilutions required for the subsamples – in order to match the machine calibration range for as many ions and sub-samples as possible. For most sub-samples, including the final solution, dilutions of 1:10 and 1:100 were sufficient for the quantification of most ions. The high SO_4^{-2} concentrations in sub-samples and final solutions of samples GAP04-1 to -3, however, required an additional dilution of 1:1000. The low concentrations observed in the final solution of sample GAP04-4 allowed the analyses of the undiluted sub-sample solutions without overloading the separation columns of the IC. Having produced this information, the time series sub-samples of all samples were analysed in one batch per sample, including the final solution. For samples GAP04-1 and GAP04-3, which were previously analysed in four batches, the second measurement resulted in a smoothing of the concentration curves as a function of time and a better match with the final solution. The concentration changes for individual samples, however, remained within a relative uncertainty of ±10% for all, and within ±5% for most samples. The complete chemical data of the eluate time series sub-samples are given in Appendix A.

6.1.2 Chemical Composition of Time-series Sub-samples

The eluates of intermediate gneiss samples GAP04-1 to -3 resemble each other in that they are highly concentrated Ca-SO_4 type solutions. The mainly positive charge imbalance of less than 2% of these solutions (cf. Appendix A) indicates that HCO_3^- is only a minor anion, although alkalinity could not be titrated on these small time-series subsamples. The chemistry contrasts with the more dilute eluate solutions of the felsic gneiss sample, GAP04-4, which display a positive charge imbalance of <20% and suggest HCO_3^- is a major anion in the fluid. Together with lower measured Ca^{+2} and SO_4^{-2} concentrations, the felsic gneiss eluate solutions are of a general Na-HCO_3-SO_4-Cl type fluid that evolves toward a Na-SO_4-HCO_3 type fluid by the end of the experiment. This difference in eluate solutions between the rock samples is interesting because the felsic gneiss sample was collected in the interval between the intermediate gneiss samples GAP04-2 and -3 (cf. Chapter 3).

Differences between eluate solution compositions (time series and end solution) of samples GAP04-1 to -3, and of sample GAP04-4, are indicated by lower molar Cl/SO_4 ratios (<0.06–0.40

compared to <0.40–1.06), lower molar Mg/SO_4 ratios (<0.02–0.1 compared to <0.06–0.15) and higher molar Ca/Sr ratios (<150–500 compared to <86–150). In contrast, the molar Ca/SO_4 ratio shows only minor variations in all solutions of the four samples (<0.63-0.90). Molar Na/Cl and Na/K ratios are rather constant in the eluate solution of the felsic gneiss sample, GAP04-4, but increase by about a factor of 2 in the eluate solutions of the intermediate gneiss samples.

Large changes in concentrations and ion-ion ratios for SO_4^{-2} and all cations within the time-series indicate that these ion concentrations are additionally influenced by mineral reactions during diffusive exchange. However, these mineral reactions are different in the intermediate gneiss samples GAP04-1 to -3 (which all show a similar behaviour) and the felsic sample GAP04-4. This is illustrated for samples GAP04-1 to -4 in Figures 6.1 and 6.2. In the intermediate gneiss sample, GAP04-01, SO_4^{-2}, Na^+ and K^+ show a linear relationship with Cl^-, the latter acting as a proxy for the out-diffusion time (Figure 6.1). In contrast, the same ions show an exponential relationship with Cl^- in the eluate solutions of the felsic gneiss sample GAP04-4. Calcium reaches constant concentrations after two time-series samples in intermediate gneiss sample GAP04-01 (corresponding to an out-diffusion time of 7 days, see below), whereas it exponentially increases as a function of Cl^- concentration until termination of the experiment in the felsic gneiss sample, GAP04-4 (Figure 6.1). Only Mg^{+2} and Sr^{+2} display a similar exponential increase in the two rock types, although to different degrees (Figure 6.1).

A different behaviour of the two samples is further observed when plotting the alkaline and earth alkaline cations versus SO_4^{-2} (Figure 6.2). For the intermediate gneiss sample, GAP04-1, all cations show a curved increase as a function of increasing SO_4^{-2}, and eventually result in rather constant concentrations towards the end of the experiment. The only exception is Ca^{+2}, which displays constant concentrations after the first two time-series samples. In contrast, all cations display a more linear relationship with SO_4^{-2} in the eluate solutions of the felsic gneiss sample GAP04-4, except for Mg^{+2}. The close match of Ca^{+2} and Sr^{+2} time-series data as a function of Cl^- and SO_4^{-2} further suggest a similar source for these two cations in the felsic gneiss sample.

The different evolution of eluate concentrations illustrated in Figures 6.1 and 6.2 demonstrate different mineral reactions during the out-diffusion experiments for the two rock types. On first inspection, a linear relationship between the conservative Cl^- and other ions could be interpreted as a similarly conservative behaviour during out-diffusion (i.e., diffusion controlled transport). However, fast reaction rates, where the concentrations become reaction controlled, will also result in a linear relationship with the truly conservative Cl^- (i.e., fast reaction rates mimic a diffusion-controlled system). In contrast, an exponential increase in ion concentration as a function of Cl^- suggests reaction-controlled transport (i.e., slow reaction rates). Further information about the type(s) of reaction(s) is obtained by exploring the eluate concentration behaviour as a function of time.

Figure 6.1: Behaviour of SO_4^{-2} and Alkaline and Earth-alkaline Cations as a Function of Cl^- Concentrations, Which Serve as a Proxy for the Elution Time, in Out-diffusion Experiments of the Intermediate Gneiss Sample GAP04-1 (left) and the Felsic Gneiss Sample GAP04-4 (right). Also Given are Correlation Coefficients of the Linear and Exponential Fits, Respectively. Note the Different Concentration Scales for the Two Samples. Error Bars Indicate the Analytical Error of ± 5%

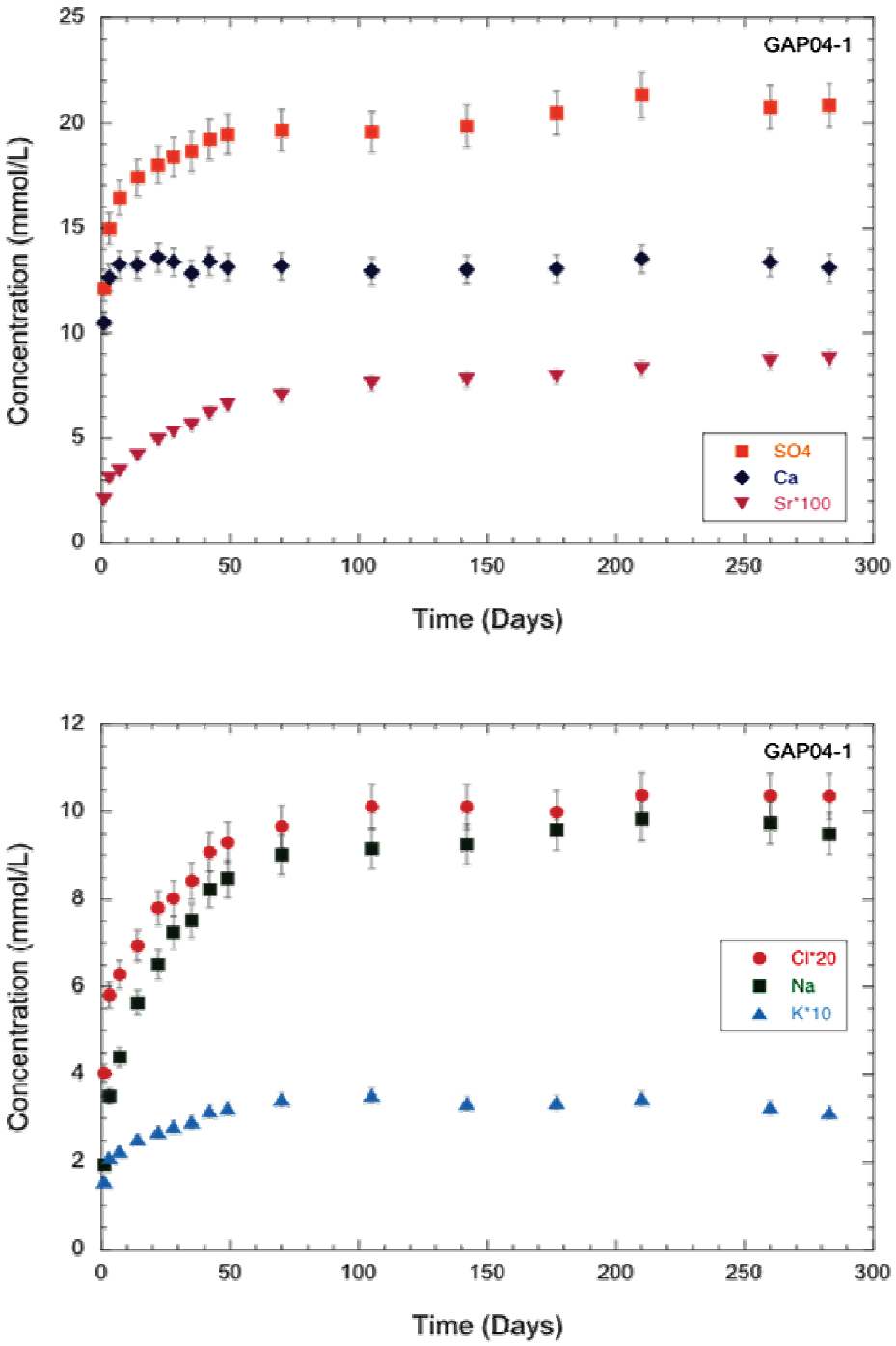

Figure 6.4: Intermediate Gneiss Sample GAP04-1; Concentrations of SO_4^{-2}, Ca^{+2} and Mg^{+2} (top) and Cl^-, Na^+ and K^+ (bottom) in Time-series Eluate Solutions as a Function of Out-diffusion Time. Note That the Sr^{+2}, Cl^- and K^+ Concentrations are Multiplied by Factors of 100, 20 and 10, Respectively. Error Bars Indicate the Analytical Error of ±5%

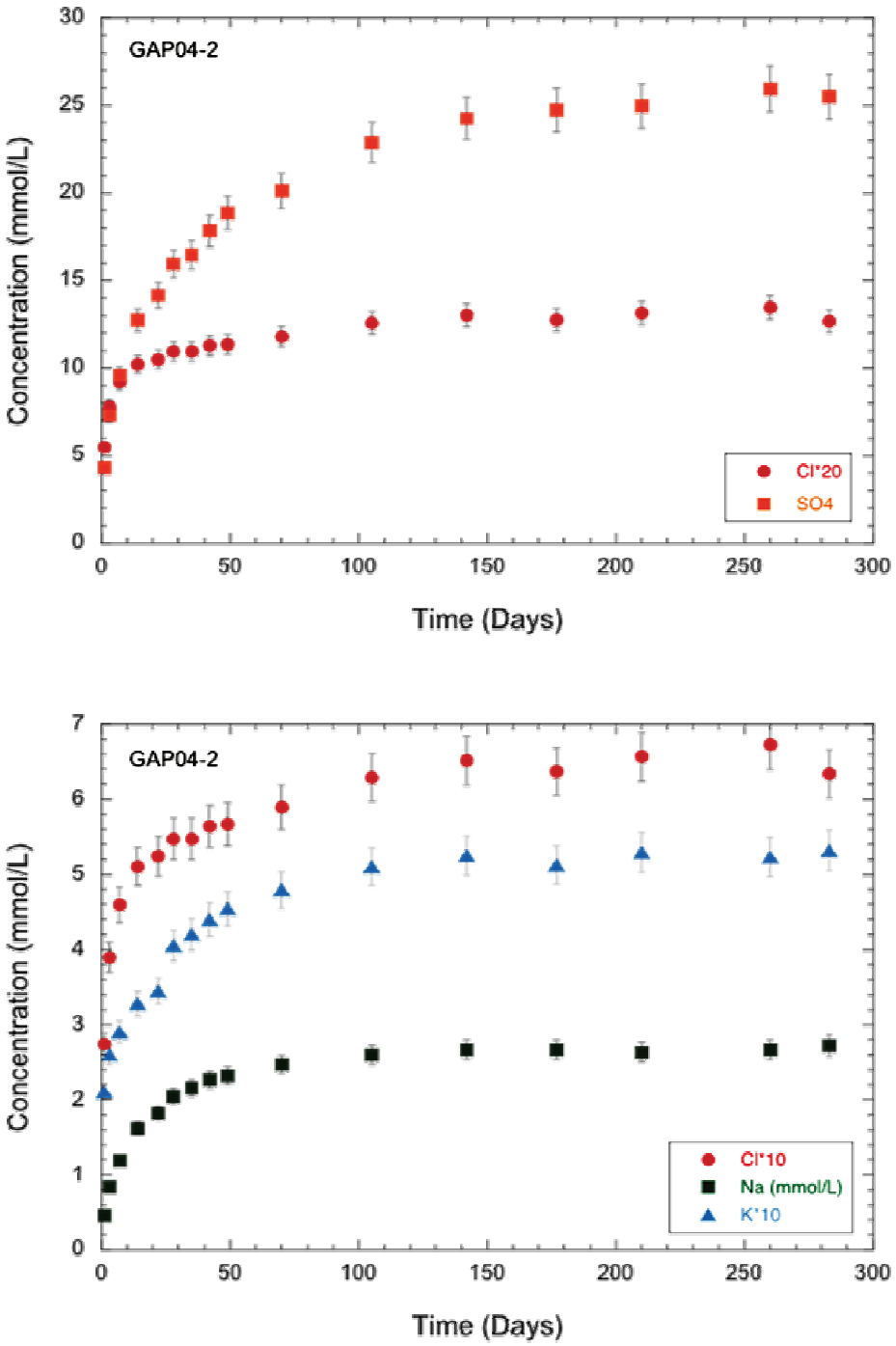

Figure 6.5: Intermediate Gneiss Sample GAP04-2; Concentrations of Cl^- and SO_4^{-2} (top) and Cl^-, Na^+ and K^+ (bottom) in Time-series Eluate Solutions as a Function of Out-diffusion Time. Note That the Cl^- Concentrations are Multiplied by Factors of 20 and 10, and K^+ by a Factor of 10. Arrows in the Lower Plot Indicate Sub-samples That Underwent Evaporation During Storage. Error Bars Indicate the Analytical Error of ±5%

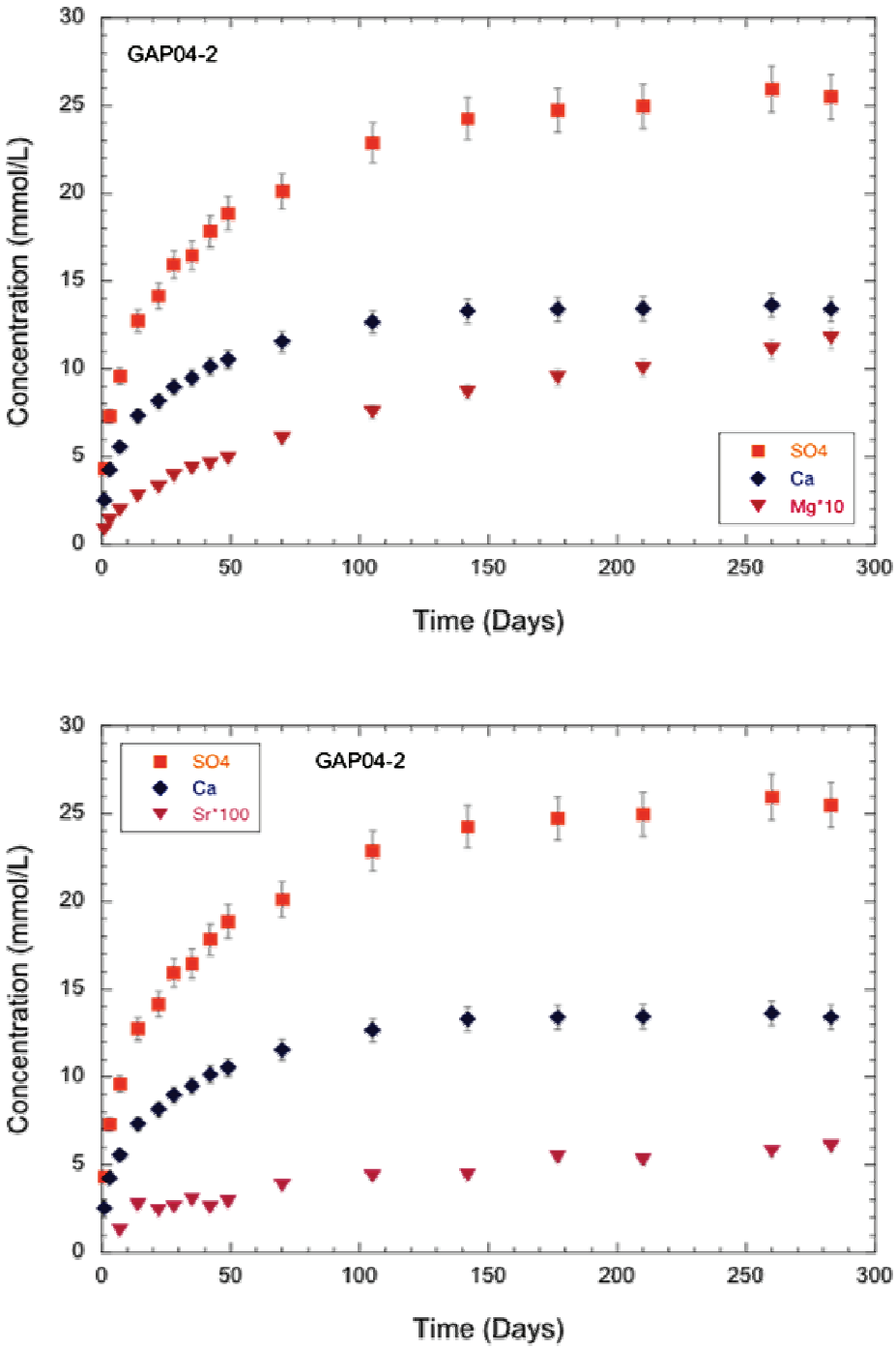

Figure 6.6: Intermediate Gneiss Sample GAP04-2; Concentrations of SO_4^{-2}, Ca^{+2} and Mg^{+2} (top) and SO_4^{-2}, Ca^{+2} and Sr^{+2} (bottom) in Time-series Eluate Solutions as a Function of Out-diffusion Time. Note That the Mg^{+2} and Sr^{+2} Concentrations are Multiplied by Factors of 10 and 100, Respectively. Error Bars Indicate the Analytical Error of ±5%

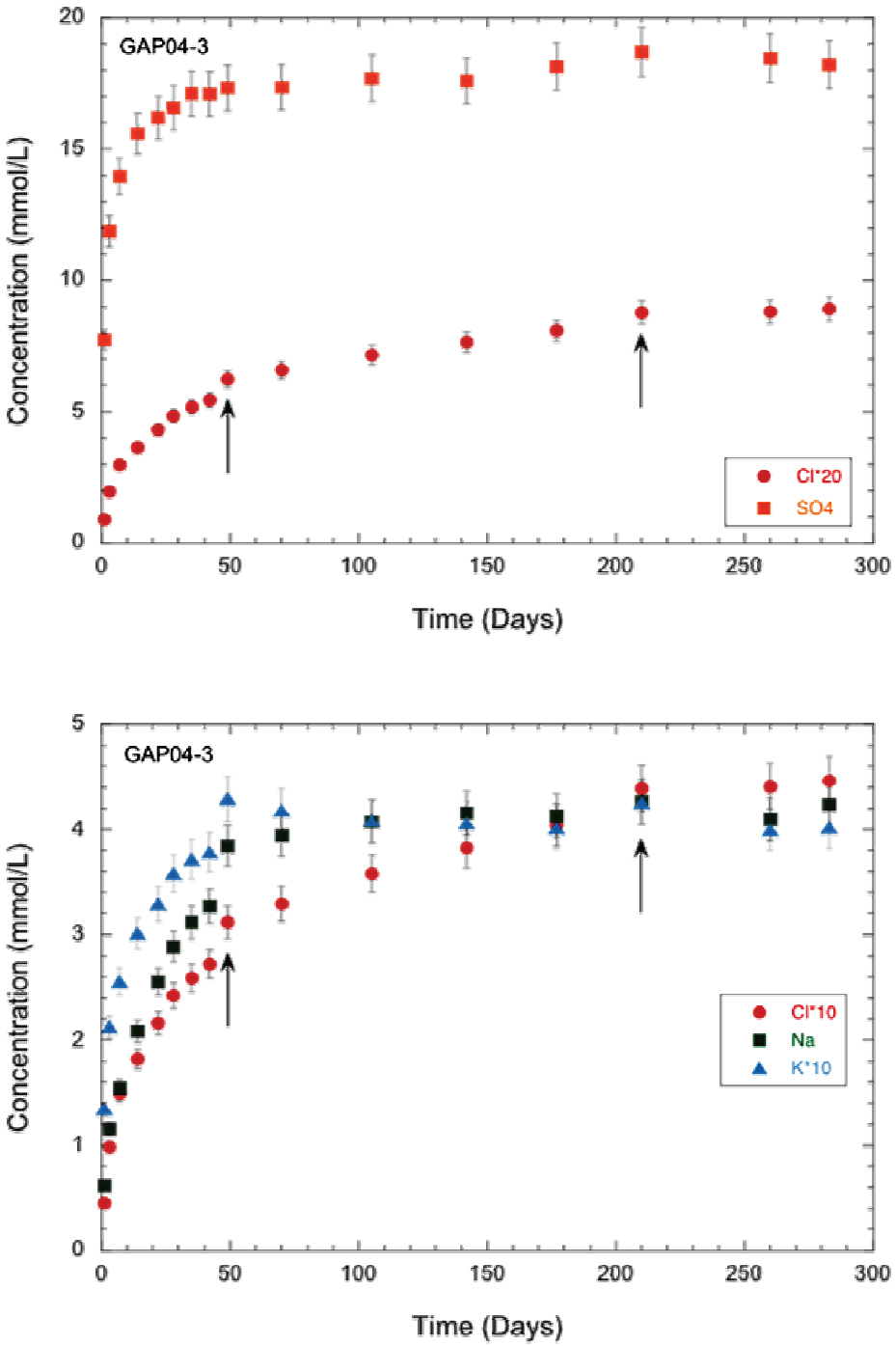

Figure 6.7: Intermediate Gneiss Sample GAP04-3; Concentrations of Cl^- and SO_4^{-2} (top) and Cl^-, Na^+ and K^+ (bottom) in Time-series Eluate Solutions as a Function of Out-diffusion Time. Note That the Cl^- Concentrations are Multiplied by Factors of 20 and 10, and K^+ by a Factor of 10. Arrows Indicate Sub-samples That Underwent Evaporation During Storage. Error Bars Indicate the Analytical Error of ±5%

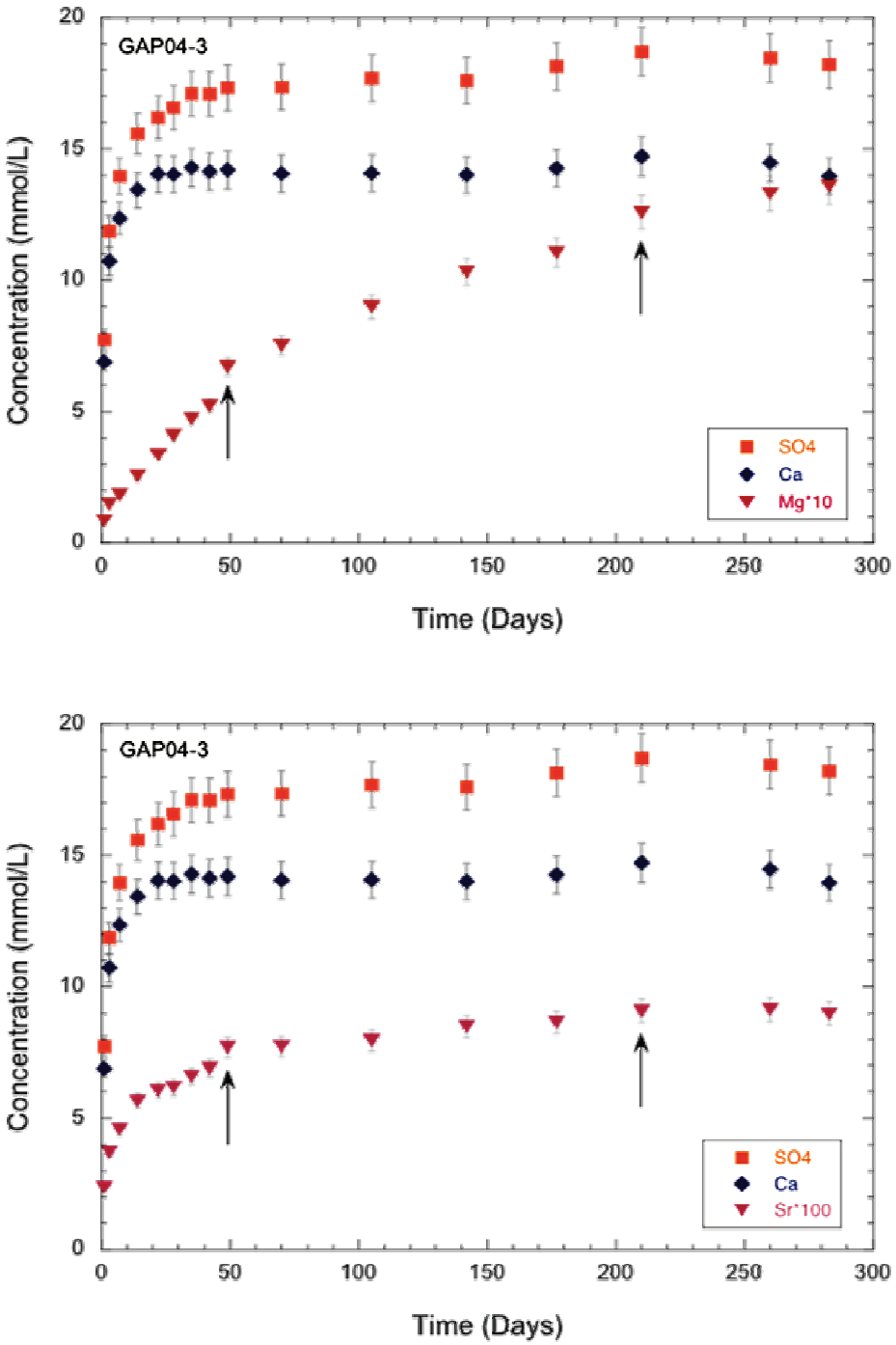

Figure 6.8: Intermediate Gneiss Sample GAP04-3; Concentrations of SO_4^{-2}, Ca^{+2} and Mg^{+2} (top) and SO_4^{-2}, Ca^{+2} and Sr^{+2} (bottom) in Time-series Eluate Solutions as a Function of Out-diffusion Time. Note That the Mg^{+2} and Sr^{+2} Concentrations are Multiplied by Factors of 10 and 100, Respectively. Arrows Indicate Sub-samples That Underwent Evaporation During Storage. Error Bars Indicate the Analytical Error of ±5%

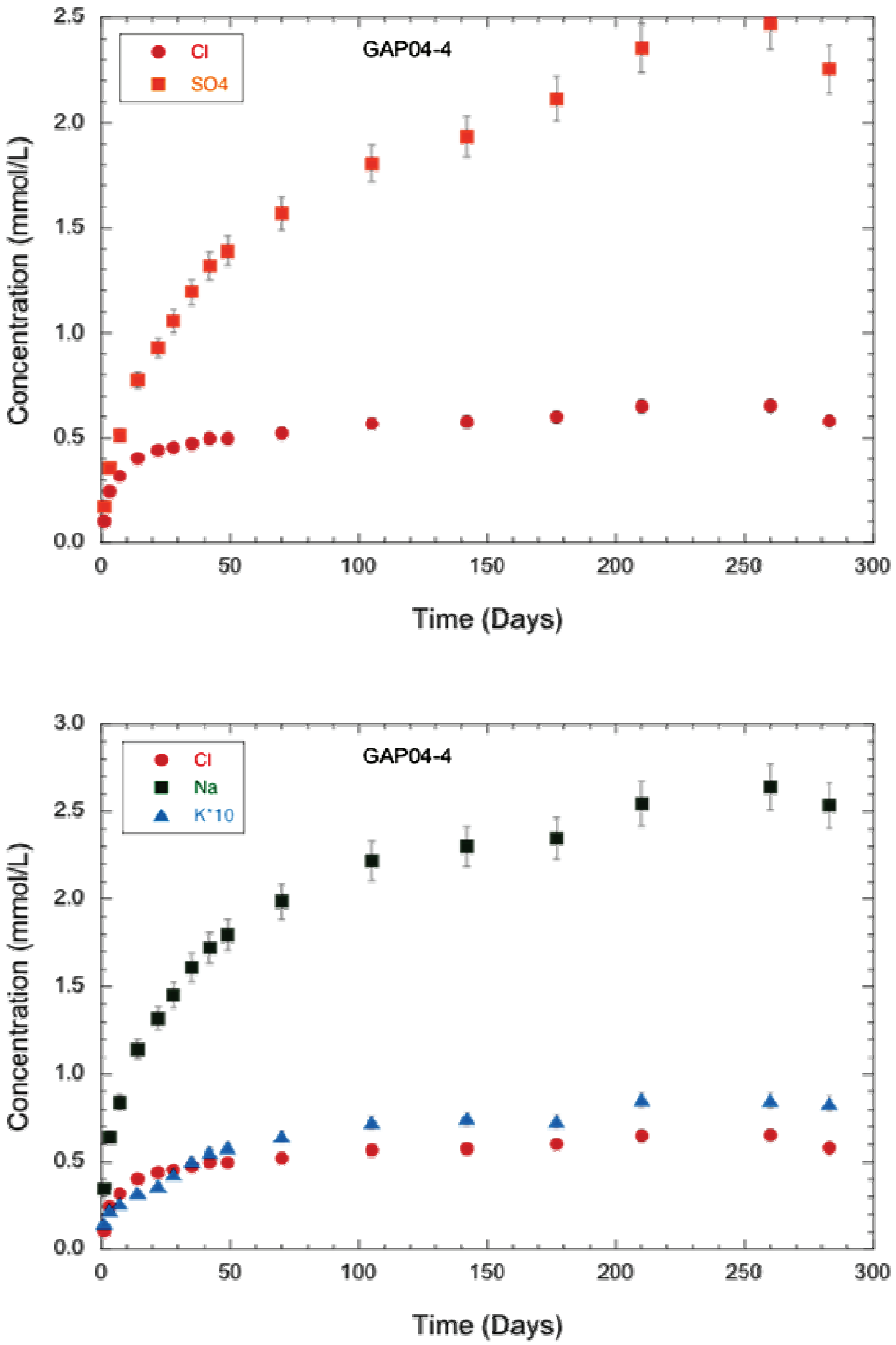

Figure 6.9: Felsic Gneiss Sample GAP04-4; Concentrations of Cl^-, Br^- and SO_4^{-2} (top) and Cl^-, Na^+ and K^+ (bottom) in Time-series Eluate Solutions as a Function of Out-diffusion Time. Note That the K^+ and Br^- Concentrations are Multiplied by Factors of 10 and 100, Respectively. Error Bars Indicate the Analytical Error of ±5%

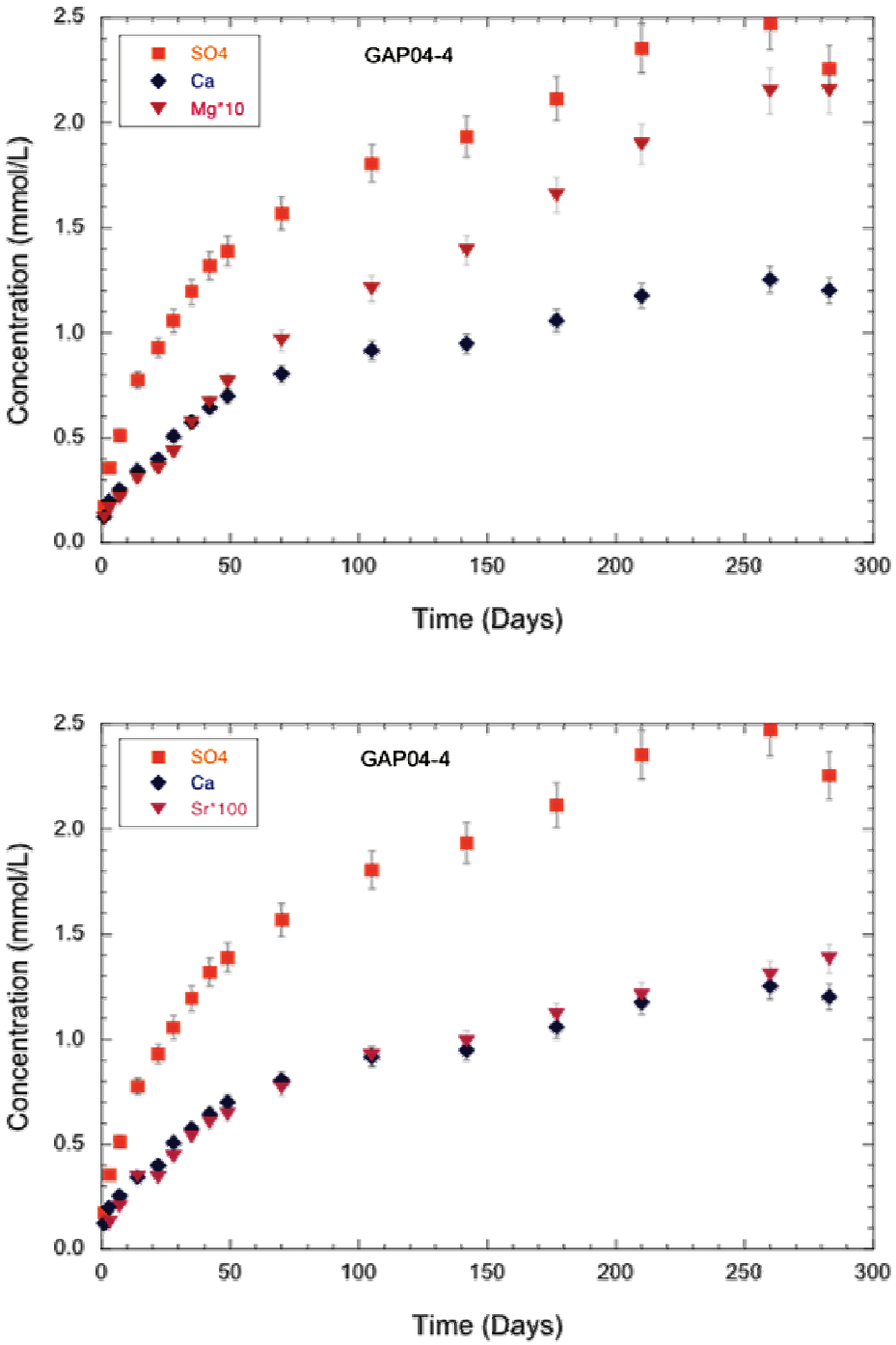

Figure 6.10: Felsic Gneiss Sample GAP04-4; Concentrations of SO_4^{-2}, Ca^{+2} and Mg^{+2} (top) and SO_4^{-2}, Ca^{+2} and Sr^{+2} (bottom) in Time-series Eluate Solutions as a Function of Out-diffusion Time. Note That the Mg^{+2} and Sr^{+2} Concentrations are Multiplied by Factors of 10 and 100, Respectively. Error Bars Indicate the Analytical Error of ±5%

6.2 CHEMICAL COMPOSITION OF FINAL OUT-DIFFUSION SOLUTION

The final eluate solutions of the out-diffusion experiments differ in composition and mineralization between the intermediate gneiss samples, GAP04-1 to -3, and the felsic gneiss sample, GAP04-4. Solutions of the intermediate gneiss samples are of a general Ca-Na-SO_4 chemical type, with Ca^{+2} comprising more than 60% and SO_4^{-2} comprising more than 90% of the total cations and anions, respectively. The total mineralization of these solutions ranges between 2347 mg/L and 2929 mg/L (Figure 6.11, Table 6.1). In contrast, the final eluate solution of the felsic gneiss sample is of a general Na-Ca-SO_4-HCO_3 type, with a total mineralization of only 403 mg/L.

As discussed in the previous sections, the chemical composition of the eluate solutions was greatly modified by water-rock reactions during out-diffusion of porewater into the surrounding test water. These modifications are especially pronounced in the intermediate gneiss samples and are less obvious in the felsic gneiss sample. Eluate solutions of the intermediate gneiss samples have pH values ranging from 7.13-7.39, at corresponding log pCO_2 of -2.28 to -2.44. The final eluate solution of the felsic gneiss sample is slightly higher at 7.63, with a corresponding log pCO_2 of -2.57 (Table 6.1). At the measured Ca^{+2} concentrations, the final eluate solutions are in equilibrium or slightly oversaturated with respect to calcite, whereas the solution of the felsic gneiss sample is slightly understaturated (Table 6.2). All final solutions are undersaturated with respect to dolomite. Because the initial test water was in equilibrium with atmospheric CO_2 (i.e., at a log pCO_2 of about -3.5), the increase in the partial pressure of CO_2 is attributed to carbonate dissolution and an unknown contribution of CO_2 from the porewater. This latter contribution appears higher, by an order of magnitude, in the felsic gneiss sample when compared to the intermediate gneiss samples. In the intermediate gneiss samples, the carbon inventory is lowered due to the precipitation of calcite to an unknown degree.

At the high Ca^{+2}, Sr^{+2} and SO_4^{-2} concentrations (525-559 mg/L, 5.29-7.86 mg/L and 1581-2001 mg/L, respectively) the final eluate solutions of the intermediate gneiss samples, GAP04-1 to -3, are in equilibrium with gypsum, but slightly understaturated with respect to celestite (Table 6.1). In contrast, the solution of the felsic gneiss sample is greatly undersaturated with gypsum (SI_{gypsum} = -1.8) and celestite ($SI_{celestite}$ = -1.5) at the low concentrations of Ca^{+2} (48 mg/L), Sr^{+2} (1.21 mg/L) and SO_4^{-2} (140 mg/L) measured.

Similarly, as for celestite, all solutions are undersaturated with respect to strontianite and other easily soluble secondary minerals of hydrothermal, or later, origin, such as brucite, epsomite or mirabillite (Table 6.2).

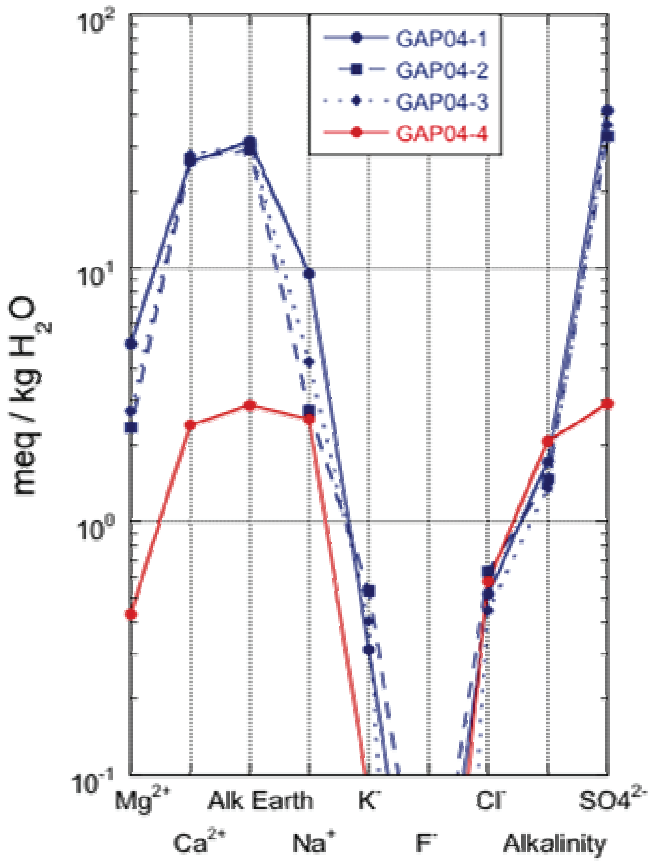

Figure 6.11: Schoeller Diagram of Final Eluate Solutions from Out-diffusion Experiments Conducted with Intermediate Gneiss (samples GAP04-1 to -3, blue) and Felsic Gneiss (sample GAP04-4, red) Drillcore Samples. Note the Large Differences in Composition and Chemical Type for the Solutions from Different Rock Types

Calculated mineral saturation states of the final eluate solutions indicate that the solutions experienced dissolution and precipitation reactions during the experiment. Under closed system conditions, precipitation of calcite will occur in solutions in contact with gypsum until gypsum equilibrium is attained. The (as of yet) incomplete equilibration with celestite may be attributed to lower dissolution kinetics and different occurrence of celestite when compared to gypsum. All of these findings are corroborated by the observed occurrence of gypsum in the intergranular pore space and microfractures, whereas celestite and calcite tend to be restricted to inter- and intragranular pore space, respectively (cf. Chapter 4). The identification of these phases in the rock matrix indicates, however, that the in-situ porewater is at equilibrium with these mineral phases.

Table 6.1: Chemical Composition of Final Eluate Solutions from Out-diffusion Experiments

Sample		GAP-1	GAP-2	GAP-3	GAP-4
Borehole Meter	m a.b.	501.5	651.9	557.7	606.7
Depth Below Surface	m b.s.	473.4	572.8	526.5	615.5
Rock Type		IGN	IGN	IGN	FGN
Start Experiment		12.12.11	12.12.11	12.12.11	12.12.11
End Experiment		20.09.12	20.09.12	20.09.12	20.09.12
Time	days	283	283	283	283
Experiment Temperature	ºC	45	45	45	45
Initial Water Mass	ml	78.4	80.6	87.9	77
Final water mass	ml	63	61.4	70.9	66.1
Time Series Water Mass	ml	7.5	7.5	7.5	7.5
Initial Rock Mass	g	642.592	532.859	644.359	525.067
Ratio Exp.Water : Rock		0.120	0.150	0.140	0.150
MISCELLANEOUS PROPERTIES					
Date Analysis		28.12.12	20.09.12	28.12.12	20.09.12
Sample Temperature	ºC	20	20	20	20
pH	-log(H+)	7.39	7.13	7.23	7.63
CATIONS					
Sodium (Na+)	mg/l	218.1	62.6	97.4	58.3
Potassium (K+)	mg/l	12.2	20.8	15.7	3.3
Calcium (Ca+2)	mg/l	524.8	537.3	559.2	48.2
Magnesium (Mg+2)	mg/l	61.0	28.5	33.0	5.2
Strontium (Sr+2)	mg/l	7.7	5.3	7.9	1.2
ANIONS					
Fluoride (F-)	mg/l	0.18	0.34	<0.16	0.07
Chloride (Cl-)	mg/l	18.4	22.5	15.8	20.5
Bromide (Br-)	mg/l	<0.16	<0.16	<0.16	0.12
Nitrate (NO3-)	mg/l	<0.16	<0.16	<0.16	<0.016
Sulfate (SO4-2)	mg/l	2002	1581	1750	139.8
Total Alkalinity	meq/l	1.72	1.46	1.35	2.07
Total Alkalinity as HCO3	mg/l	104.9	89.1	82.4	126.3
PARAMETERS CALCULATED FROM ANALYTICAL DATA					
Sum of Analysed Constituents	mg/l	2949	2347	2561	403
Sum Cations	meq/l	4.119E+01	3.253E+01	3.544E+01	5.481E+00
Sum Anions	meq/l	-4.393E+01	-3.503E+01	-3.823E+01	-5.564E+00
Charge Balance:	%	-3.22%	-3.70%	-3.78%	-0.76%
ION-ION RATIOS					
Cl/SO4	mol/mol	0.025	0.039	0.025	0.398
Br*1000/Cl	mol/mol		3.4		2.505
Na/Cl	mol/mol	18.32	4.29	9.49	4.37
Na/K	mol/mol	30.34	5.12	10.54	30.36
Ca/SO4	mol/mol	0.63	0.81	0.77	0.83
Mg/SO4	mol/mol	0.12	0.07	0.07	0.15
Ca/Sr	mol/mol	149.5	222.2	155.5	87.0

Table 6.2: Mineral Saturation Indices of Final Eluate Solutions from Out-diffusion Experiments

Sample		GAP-1	GAP-2	GAP-3	GAP-4
Borehole Meter	m a.b.	501.5	651.9	557.7	606.7
Depth Below Surface	m b.s.	473.4	572.8	526.5	615.5
Rock Type		IGN	IGN	IGN	FGN
CARBONATE SYSTEM					
Temperature	ºC	45	45	45	45
pH	-log(H+)	7.39	7.13	7.23	7.63
Total Alkalinity	meq/L	1.72	1.46	1.35	2.07
Total Carbon	mol/L	1.855E-03	1.661E-03	1.494E-03	2.166E-03
Log pCO2		-2.4378	-2.2811	-2.4186	-2.5726
MINERAL SATURATION INDICES					
Anhydrite		-0.25	-0.28	-0.24	-1.83
Brucite		-5.62	-6.35	-6.10	-5.72
Calcite		0.13	-0.09	-0.03	-0.15
Celestite		-0.14	-0.34	-0.15	-1.50
Dolomite (disordered)		-0.96	-1.76	-1.59	-1.49
Dolomite (ordered)		-0.39	-1.19	-1.02	-0.92
Epsomite		-3.14	-3.51	-3.43	-4.68
Fluorite		-0.04	-1.52		-3.43
Gypsum		-0.01	-0.04	-0.01	-1.60
Magnesite		-1.09	-1.66	-1.55	-1.33
Mirabillite		-5.07	-6.22	-5.81	-6.97
Strontianite		-1.22	-1.62	-1.40	-1.28

7. CHLORINE, BROMINE AND CHLORINE ISOTOPES IN POREWATERS

7.1 BACKGROUND – CONSERVATIVE TRACER INVESTIGATIONS

The conservative behaviour of chloride and bromide, the absence of Cl- and Br-bearing minerals in the rock, and the non-destructive character of the out-diffusion method, make the porewater the only source for dissolved Cl and Br in the experimental solution. This allows calculation of the Cl and Br concentration in the porewater using mass balance calculations, according to Equation 13, given that equilibrium in the out-diffusion experiment is achieved. A further requirement for the mass balance calculations is knowledge of the Cl- and Br-accessible porosity in the different rocks. Here, the Cl- and Br-accessible porosity is set equal to the water-loss porosity determined on the large sized out-diffusion core samples.

Chloride and bromide are good indicators for the composition of porewater. In combination with the chemistry of recent and palaeo groundwaters, interpretations regarding the preservation of different groundwater types (saline vs. fresh water) can be made. In addition to Cl and Br, stable chlorine isotopes and Br/Cl elemental ratios serve as tracers that provide information about the source and the origin of chloride in porewater and groundwater.

Bromide occurs in aqueous systems predominately as Br^- and behaves similarly to chloride. In inorganic systems, Br is geochemically conservative. Bromide is a good indicator for seawater salinity because it is difficult to decrease the Br/Cl ratio from a seawater precursor (Br*1000/Cl mass ratio of seawater = 0.34, Davis et al. 1998). The Br/Cl ratio of water can be changed due to evaporation of seawater until halite saturation is reached (Br/Cl > seawater), or by dissolution of halite by meteoric water (Br/Cl < seawater).

The stable isotopes of chlorine are also geochemically conservative. The isotopic ratio of dissolved chlorine can only be affected by physical processes such as ion filtration, diffusion, geothermal boiling, brine evaporation, salt deposit formation and freezing of saline water (Kaufmann et al. 1984, Philips and Bentley 1987, Eggenkamp 1994, Frape et al. 2000, Ziegler et al. 2001, Stewart and Spivak 2004, Zhang et al. 2006).

Estimates of the time scales involved in the exchange of porewater and fracture groundwater can be obtained by comparing the tracer concentrations of porewater with those of adjacent fracture groundwaters. The degree of interaction depends on: (a) the constancy of the boundary conditions in the adjacent fracture(s), i.e., the time of constant groundwater composition in these fractures; (b) the distance between the investigated porewater samples and the next water-conducting fracture; and (c) the petrophysical properties (pore diffusion coefficient and porosity) of the bedrock. Knowing these parameters, the interaction of the both reservoirs can be quantified as a function of time and space by comparing the signatures of chemically conservative elements and their isotopes.

7.2 CHLORINE, BROMINE AND CHLORINE ISOTOPES IN POREWATER FROM DH-GAP04

Porewater chlorine concentrations, as well as stable chlorine isotope signatures, were determined on all four samples from borehole DH-GAP04. Porewater bromine concentrations could only be determined for the sample GAP04-4 (cf. Section 6.1.1).

For all samples, equilibrium was achieved with respect to chloride (and bromide), as shown by their chloride and bromide elution curves (cf. Chapter 6, Figures 6.3, 6.5, 6.7, 6.9). In all experiments, there was no significant influence of test water evaporation or removal observable. The porewater masses of the used core pieces were determined according to the procedure described in Section 5.2. Based on experience from work on crystalline core samples from Scandinavian sites, it is assumed that the influence of drilling fluid on the porewater Cl- and Br concentrations is <10% and, hence, within the range of analytical error.

Porewater chloride concentrations vary between 960±220 and 2200±480 mg/kgH_2O and show an increasing trend with increasing depth (Table 7.1). The porewater bromide concentration and Br*1000/Cl ratio of sample GAP04-4 is 12.8±2.8 mg/kg H_2O and 5.8±1.8, respectively (Table 7.1). Stable chlorine isotope signatures vary between -6.04±0.08 and -2.89±0.05‰ SMOC (Table 7.1).

Interpretations about the exchange with adjacent fracture groundwater cannot be made due to a lack of reliable groundwater data at the time this report was prepared.

Table 7.1: Chloride and Bromide Concentrations, Br*1000/Cl Mass Ratios and δ37Cl Signatures of Porewater Extracted from Core Samples of Borehole DH-GAP04

Lab Sample	Depth	$Dist_{PW-GW}$	Cl_{PW}	Br_{PW}	Br*1000/Cl	$\delta^{37}Cl_{PW}$
	(m b.s.)	(M)	(mg/kg_{H_2O})	(mg/kg_{H_2O})	(mg/mg)	(‰ SMOC)
GAP04-1	473.4	24.1	980±200	b.d.	-	-2.89±0.05
GAP04-2	572.8	5.7	1740±420	b.d.	-	-4.03±0.07
GAP04-3	526.5	2.6	960±220	b.d.	-	-6.04±0.08
GAP04-4	615.5	12.7	2200±480	12.8±2.8	5.8±1.8	-5.49±0.07

7.3 UNCERTAINTIES IN THE POREWATER Cl, Br AND CHLORINE ISOTOPE DETERMINATION AND THEIR CONTROL

Chlorine and bromine concentrations are calculated by mass balance equations based on the determined test water Cl and Br concentrations, the mass of test water, and the mass of porewater.

The δ^{37}Cl ratio measured for the experimental solutions directly corresponds to the porewater Cl isotope signature. This is because the attained equilibrium in the out-diffusion experiment, with respect to total Cl, is expected to result in equilibrium with respect to the Cl isotopes (Gimmi and Waber 2004).

A prerequisite for the exact determination of the Br and Cl concentrations, as well as the chlorine isotope signatures, in porewater is the achievement of equilibrium with respect to Cl and Br during the out-diffusion experiments. The state of equilibration between porewater and the surrounding test water is controlled by periodically taking sub-samples that are analysed for Cl and Br concentrations. Equilibrium is achieved when the Cl and Br concentrations are constant within analytical uncertainty (±5%) for at least 20 days. The calculated Cl and Br concentrations are corrected for the mass and the concentration of removed solution (cf. Equation 13). Experience from multiple porewater studies in crystalline environments indicates

that, for naturally saturated core samples with diameters of 5 cm, equilibrium with respect to Cl and Br is reached after a half a year to a year at a temperature of 45°C (Eichinger et al. 2006, 2010, 2013; Waber et al. 2005, 2009a, b).

For the calculation of the porewater Cl and Br concentrations, an exact determination of the mass of porewater is required (see Chapter 5).

Another factor that has some influence on the calculation of the porewater tracer concentrations is the volume of test water, which can be influenced by evaporation or by leakage during sub-sampling. To evaluate these disturbing effects, the weights of the cylinders and the test water are determined exactly at the beginning and end of the out-diffusion experiments. Additionally, the masses of the removed sub-sample solution is monitored and taken into account.

The ingress of drilling fluid as a result of stress release, and the formation of a drilling disturbed zone, both of which lead to the creation of pore space, can lead to a dilution of the Cl and Br concentrations of porewater. The proportion of drilling fluid in porewater can be evaluated by using NaI traced drilling fluid, as described in Section 5.3.2. Knowing the Cl, Br and I concentrations of the drilling fluid, the porewater Cl and Br concentrations can be corrected using mass balance equations. The dilution of the porewater chemistry is almost exclusively caused by the ingress of dilute drilling fluid in newly created pore space. The contact time between the drilling fluid and the core samples is generally too short to have a detectable influence as a result of diffusive exchange. Porewater studies in crystalline rocks from the Forsmark and Olkiluoto sites show that the influence of infiltrated drilling fluid on the porewater Cl and Br concentrations is below 10%, which is within the error range of reported values (Waber et al. 2011, Meier 2012, Eichinger et al. 2013).

8. DETERMINATION OF $\delta^{18}O$ AND $\delta^{2}H$ OF POREWATER

8.1 BACKGROUND AND AIM OF $\delta^{18}O$ AND $\delta^{2}H$ DETERMINATION IN POREWATER

The stable isotopes of water ($\delta^{18}O$, $\delta^{2}H$) provide information about the origin, conditions of infiltration, and water-rock interactions within the system. The water isotope composition of porewater is modified as a function of time by exchange with the various fluids percolating in conductive structures. As for dissolved constituents in the porewaters, such exchange mainly occurs by diffusion into the low-permeability rock matrix of crystalline rocks (e.g., de Paolo 2006, Waber et al. 2012). The generation and preservation of fracture fluid signatures in the porewater depends on the interaction time with fluids in conductive structures, the distance between the sampled porewater and the conductive structure, and the rock diffusivity.

Porewater stable isotope ratios of crystalline rocks can be assessed by the diffusive isotope exchange technique (cf. Section 3.3.5.1). The porewater is allowed to equilibrate with test water of known isotopic composition over the vapour phase in a closed system. Two such experiments are required per sample in order to obtain the necessary mass balance equations, allowing for the calculation of porewater $\delta^{18}O$ and $\delta^{2}H$ signatures and the mass of the porewater (cf. Equations 9 and 10).

8.2 $\delta^{18}O$ AND $\delta^{2}H$ OF POREWATER OF DH-GAP04 CORE SAMPLES

Isotope diffusive exchange experiments have been carried out on 3 core samples (6 individual experiments) from borehole DH-GAP04. For the fourth sample, too little core material was available to conduct the experiment.

In the absence of other knowledge, and based on the permafrost origin of the rock samples, 0.6 mol NaCl was added to the test waters for the porewater-test water exchange in order to adjust the test water vapour pressure approximately to that of the porewater, and to minimize mass transfer from test water to porewater. Actual equilibration times between the two reservoirs were 13-18 days, as calculated according to Equations 6 and 7. To assure full equilibration, the two reservoirs were allowed to equilibrate over a period of 60 days.

Over the entire equilibration time, the change in total mass (i.e., container + rock + crystallization dish + test water) was below 0.06%, indicating that the containers were tight during the entire experiment and no evaporation occurred (Table 8.1). However, a substantial loss of test water from the crystallization dish (7-27%) was observed for the various experiments (Table 8.1). In turn, the masses of the rock material increased only by <0.01% in the various experiments. The change in rock mass before and after the experiment can, thus, not account for the total amount of test water lost from the crystallization dish.

A small transfer of test water to the surface of the rock chips is commonly observed in the diffusive isotope exchange technique (e.g., Rübel et al. 2002, Pearson et al. 2003, Waber and Smellie 2005, Eichinger 2009). Such transfer might occur because of a non-saturated state of the rock samples, and/or large differences in the salinity or water activity, respectively, between porewater and test water. As long as this transfer is limited in its amount, and limited to the rock and the test water (i.e., as long as the total transfer of test water is less than 10% and total mass of rock and test water remains constant during the experiment), this will not impact the

derivation of the porewater isotope composition. For the investigated GAP samples, this last condition is, however, not fulfilled (Table 8.1).

The control weight measurements shown in Table 8.1 indicate that a substantial amount of test water must have condensed on the wall of the large glass container during the experiments. For such a three-reservoir system, involving evaporation and condensation steps, the isotope composition of the test waters cannot be corrected for in the determination of porewater isotopic composition.

The isotope compositions of the initial and reacted test water solutions of each experiment are given in Table 8.2. As a first control, these data are compared to the Global Meteoric Water Line (GMWL). The initial isotope composition should plot on the GMWL and this is the case for most of the reacted test water solutions. It is assumed that test water solutions equilibrated with the same rock sample (i.e., the same porewater) should show the same relative deviation from the GMWL. As shown in Figure 8.1, this is not the case for the three GAP samples. Inspection of the measured isotope compositions reveals that these data cannot be explained by a simple evaporation process, as already concluded above from the control weight measurements. A second process, such as the precipitation of gypsum – caused by evaporation prior to the experiments – might be involved. Such an effect is evident in the strongly enriched $\delta^{18}O$ and $\delta^{2}H$ values of the test water solutions from sample GAP04-4 LAB (-1.26‰ and -55.0‰ V-SMOW, respectively), whereas the values of the GAP04-4 N-GRIP test solutions are comparable to those of the other samples (Table 8.2). Similarly, the $\delta^{18}O$ and $\delta^{2}H$ values of the test water solution, GAP04-2 N-GRIP, appear too enriched compared to the other samples.

Table 8.1: Chloride Control Weight Measurements on Isotope Diffusive Exchange Experiments Conducted with LAB and N-GRIP Test Water Solutions

		Masse before experiment			Masses after experiment		
Lab Sample	**Test solution**	$m_{exp,tot}$	m_{rock}	$m_{test\ water}$	$m_{exp,tot}$	m_{rock}	$m_{test\ water}$
		(g)	(g)	(g)	(g)	(g)	(g)
GAP04-1	LAB	831.265	227.629	2.070	830.916	227.656	1.680
GAP04-1	N-GRIP	828.243	218.865	2.064	828.082	218.894	1.866
GAP04-2	LAB	803.817	183.104	1.554	803.656	183.126	1.353
GAP04-2	N-GRIP	801.113	193.276	1.551	800.820	193.291	1.227
GAP04-3	No experiments conducted due to too little rock material						
GAP04-3							
GAP04-4	LAB	761.640	150.886	1.576	761.218	150.885	1.146
GAP04-4	N-GRIP	757.083	148.277	1.574	756.985	148.274	1.460

A further test of the reliability of isotope composite ions analysed on diffusive exchange test water solutions involves determination of the water content calculated by isotope mass balance relationships (Table 8.3). For samples GAP04-1 and GAP04-4, negative water contents are calculated, indicating that the experiments failed. The water content derived by isotope mass balance for sample GAP04-2 is about three times higher for the LAB experiment and about

twice as high for the N-GRIP experiment when compared to the corresponding gravimetric water content determined by drying the rock material after the exchange experiment (Table 8.3). Such high differences are not acceptable and reliable porewater isotope values cannot be derived.

Table 8.2: Chloride – Measured Isotope Ratios ($\delta^{18}O$, $\delta^{2}H$) on Initial (standard) and Reacted Test Water Solutions (LAB and N-GRIP)

Lab Sample		$\delta^{18}O$ (‰ V-SMOW)	$\delta^{2}H$ (‰ V-SMOW)
Initial test water solution			
LAB		-11.99	-87.3
N-GRIP		-26.80	-207.7
Reacted test water solution			
GAP04-1	LAB	-6.50	-72.9
GAP04-1	N-GRIP	-23.26	-192.1
GAP04-2	LAB	-8.77	-76.2
GAP04-2	N-GRIP	-20.03	-185.5
GAP04-3	No experiments conducted due to too little rock material		
GAP04-3			
GAP04-4	LAB	-1.26	-55.0
GAP04-4	N-GRIP	-23.88	-191.1

Table 8.3: Hypothetical Water Contents of the Sample Subjected to Isotope Diffusive Exchange as Calculated from the Isotope Composition of the Reacted Test Water Solutions (LAB and N-GRIP) in Comparison with the Gravimetric Water Content Determined by Drying of the Rock Material after the Experiment

	Water content determined by diffusive isotope exchange technique		Gravimetric water content		
Lab Sample	$WC_{IsoEx},\delta^{18}O$	$WC_{IsoEx},\delta^{2}H$	$WC_{WL,IsoEx,LAB}$	$WC_{WL,IsoEx,N\text{-}GRIP}$	$WC_{WL,\ IsoEx,\ ave}$
	(wt.%)	(wt.%)	(wt.%)	(wt.%)	(wt.%)
GAP04-1	-0.10	0.01	0.23	0.26	0.25±0.01
GAP04-2	0.24	0.08	0.12	0.09	0.11±0.02
GAP04-3	No experiments conducted due to too little rock material				
GAP04-4	-0.36	-0.12	0.06	0.21	0.13±0.07

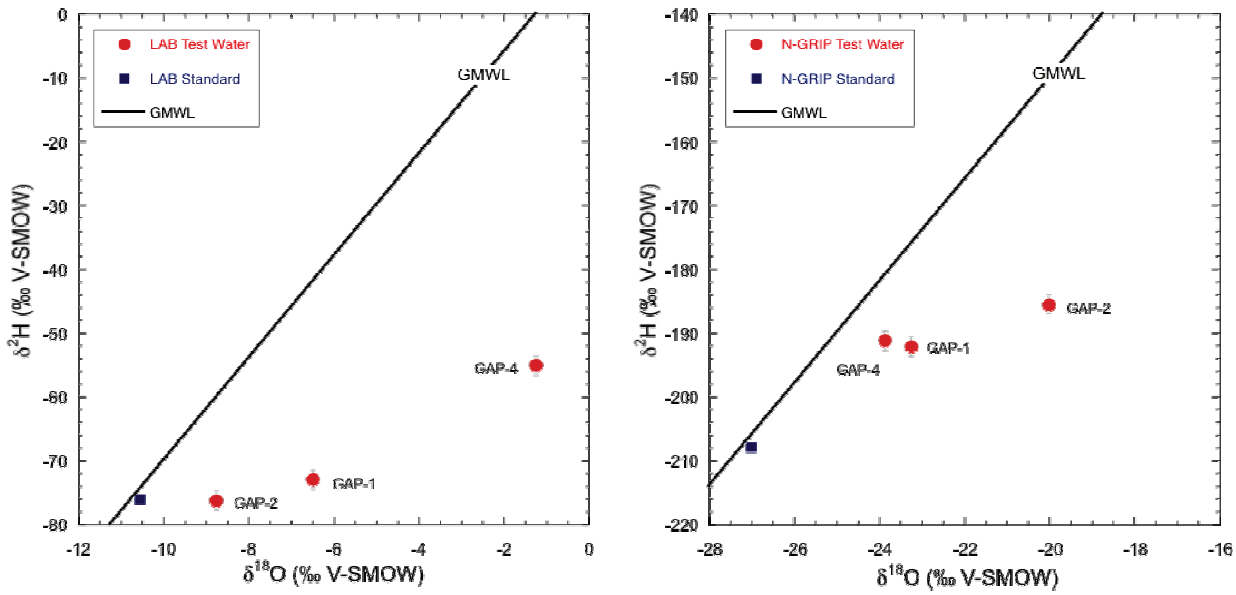

Figure 8.1: Measured Isotope Ratios ($\delta^{18}O$, $\delta^{2}H$) of Initial (Standard) and Reacted Test Water Solutions (LAB and N-GRIP). Note the Different Deviations from the Global Meteoric Water Line (GMWL; Craig 1961) for the Isotope Composition of Reacted Test Water Solutions from the Same Sample; Analytical Uncertainties are ±0.25‰ for $\delta^{18}O$ and 1.5‰ for $\delta^{2}H$

To conclude, no reliable porewater isotope composition could be obtained for any of the GAP samples. The various reasons for the failure of the isotope diffusive exchange experiments are listed in decreasing order of importance below.

<u>Evaporation of core samples in the interim between sample recovery and receipt at the laboratory</u>:

As discussed in Chapter 5, only 55-70% of the original porewaters were present in the core samples upon arrival in the laboratory. Such significant evaporation will lead to precipitation of various hydrated secondary salt minerals, with unknown fractionation effects on the remaining porewater isotope composition. Such precipitation is enhanced by the apparently high SO_4 concentrations in the porewaters (cf. Chapter 7) and the much lower solubility of secondary sulphate salts compared to the chloride salts.

<u>Low mass of core material available for the experiments</u>:

The mass of the three samples available for the isotope diffusive exchange experiments was only 147-227 g when compared to the suggested minimum mass of at least 400 g for rocks with water contents <0.5 wt.% (e.g., Eichinger 2009). For one sample, no material was available. The low rock masses and the low volumes of porewater support the interpretation of perturbing effects.

Condensation of porewater during the experiment:

This is indicated by the control weight measurements, though condensation was visually difficult to detect on the glass containers.

8.3 UNCERTAINTIES IN THE DETERMIATION OF POREWATER STABLE ISOTOPE COMPOSITIONS AND THEIR CONTROL

The low water content of crystalline rocks makes the diffusive isotope exchange technique very sensitive to artefacts induced during sampling, experiment and analyses. In addition, accurate determination of the stable isotope composition of porewaters requires knowledge about the salinity of porewater in order to adjust the water activity between porewaters and test waters in these experiments. Whereas some of the important parameters and processes can be controlled by strictly following a well-established sampling protocol (e.g., Waber & Smellie 2008), others, such as salinity and porewater chemistry, are commonly unknown and have to be estimated based on experience.

As shown by Rogge (1997) and Rübel (2000), the error of the calculated porewater isotope composition depends predominately on the mass ratio between porewater and test water. The smallest error is obtained if this ratio remains close to unity. To allow duplicate isotope measurements on the test water solutions, a volume of about 2.5 mL is required. For crystalline rocks with a water content of ~0.5 wt.%, this corresponds to a total rock mass of 800-1000 g for two exchange experiments in order to determine the $\delta^{18}O$ and $\delta^{2}H$ isotope signatures and the mass of porewater after isotope equilibration between porewater and test water.

In the following section, the most common artefacts resulting in deviations of the calculated isotope composition and water mass from that of the porewater isotope composition are briefly described.

Influence of evaporation during sampling, preparation and experiment time

Evaporation of porewater during sampling, preparation and experimentation leads to higher $\delta^{18}O$ and $\delta^{2}H$ signatures following Rayleigh fractionation. Significant evaporation of porewater can result in the precipitation of hydrated secondary salts, which can modify the isotope ratios of the residual porewater. Evaporation occurring between the recovery of the cores and the preparation of the samples can be controlled according to the procedure described in Section 3.1. Evaporation of porewater during the experiments is controlled by taking the weights of the rocks before and after the diffusive isotope exchange experiments. Theoretically, the isotope ratios of porewater could be corrected according to Rayleigh fractionation in the case of evaporation. However, the formation of secondary hydrated salt minerals and the resulting isotopic fractionation cannot be controlled, which hinders a thorough correction of the values.

Evaporation of test water during the experiments leads also to higher isotopic signatures, but not to the precipitation of solid salt phases. The evaporation of test solution and porewater during the experiments, as well as any water transfers within the closed experiments, are controlled by taking the exact weights (±0.001 g) of the rock, test water and the entire closed experiment, both before and after equilibration.

Influence of incomplete equilibration between porewater and test water

To assure isotope equilibration between the two reservoirs, and to account for the initially unknown diffusivity of the rock, the applied equilibration time should be chosen about three to four times as long as that calculated by Equation 6 and 7 (cf. Section 3.3.5.1). It should be noted that evaporation from the glass container (i.e., open system) always describes a non-equilibrium (i.e., transient) state that cannot be quantified with respect to the water isotopes.

Artefacts induced by the salinity of porewater

The isotope exchange between porewater in a rock sample and the test water over the vapour phase depends on the water activity in these reservoirs and – in certain cases – the porewater composition. Differences in water activity will result in an unacceptable mass transfer of either test water to rock sample or vice versa. In case of Cl-rich porewater, its chemistry should be matched in the test water in terms of the most abundant cation because of the differences in the hydration shells of Cl-complexes (e.g., NaCl vs. $CaCl_2$) and related effects on the isotope composition of the free water molecules. For Cl-dominated porewater environments, de Haller et al. (2014, *in preparation*) investigated this latter effect for a series of salinity and compositional ranges of natural and re-saturated porewater in argillaceous rocks. Whereas the type of Cl-dominated porewater composition poses a major problem in the isotope analyses using conventional isotope ion ratio mass spectrometry, this problem appears to be, at least partly, overcome using the more recent cavity ring down spectroscopy (e.g., Mazurek et al. 2013). While progress has been made in recent years for Cl-dominated, saline porewater environments in argillaceous rocks, little is known about similar effects in SO_4-dominated, saline environments. For a successful conduction of the isotope diffusive exchange technique in highly saline porewater environments in crystalline rocks with very low water contents, an adaption of this method is still required.

In this context, it should be mentioned that in the Scandinavian crystalline rocks subjected to porewater investigations, Cl^- or HCO_3^- are commonly the major anions and the total salinity surpassed that of seawater in only a few samples (Waber et al. 2008, 2011; Eichinger et al. 2006, 2009, 2013).

Artefacts induced by the ingress of drilling fluid

Similar to the Cl and Br concentrations (cf. Chapter 7), the porewater isotope composition can be modified by the ingress of drilling fluid into the drillcore during the drilling process. Such influence depends on the stress release of the drillcore and the drilling disturbed zone (DDZ) created during the contact time of drillcore and drilling fluid. It can be evaluated using drilling fluid with known $\delta^{18}O$ and $\delta^{2}H$ signatures and additionally traced with an artificial tracer. This was evaluated for porewaters from crystalline rocks from the Olkiluoto investigation site (Meier 2012, Eichinger et al. 2013). For these rocks, it could be shown that a drilling fluid ingress of <10% of the total amount of porewater only leads to a very small shift of about 0.02‰ in the $\delta^{18}O$ and $\delta^{2}H$ porewater signatures obtained by isotope diffusive exchange experiments. Such small deviation is within the error range of the porewater values calculated from exchange experiments.

Artefacts induced by the analyses of isotope signatures

Under optimal conditions, rather large masses of rock material are used for the exchange to allow test water volumes of at least 3 mL in the experiments. These volumes are not sufficient for repeat analyses of $\delta^{18}O$ and $\delta^{2}H$ in the applied test water using conventional mass spectrometry. Newer techniques, such as cavity ring down spectroscopy, as applied in this study, allow replicate measurements for $\delta^{18}O$ and $\delta^{2}H$ on such small volumes. More recently, these methods have also been tested for the exact determination of $\delta^{18}O$ and $\delta^{2}H$ in test water of salinity of >4 M and of different composition (NaCl, $CaCl_2$; cf. Mazurek et al. 2013). Although certain problems, such as memory effects, remain with this technique (in the case that not enough replicate analyses can be performed due to limitations in sample material), the analytical part commonly contributes the smallest portion, if any at all, to the artefacts inhibiting the derivation of the porewater isotope composition by the diffusive exchange technique.

9. SUMMARY AND CONCLUSIONS

The chemical and isotopic characterization of porewater residing in the inter- and intragranular pore space of the low-permeability rock matrix is an important component with respect to the site characterization and safety assessment of potential host rocks for radioactive waste disposal.

Porewater in crystalline rocks can be extracted by indirect methods, based on naturally saturated core samples. Those methods, which were developed and improved during several porewater investigations on different investigation sites, were applied on four core samples from the deep borehole DH-GAP04, located in the Kangerlussuaq area (West Greenland).

Porewater extraction methods and the subsequent calculation of the porewater tracer concentrations, as well as the stable isotope signatures, are sensitive for artefacts induced by stress release, the drilling process, sample preparation and experimental artefacts. These artefacts can be controlled and evaluated using an advanced sampling, sample packing and experimental protocol.

Aims of this study were to describe: 1) the necessary methods for porewater characterization in crystalline rocks; and 2) potential disturbing artefacts – control, prevention and evaluation, all of which are summarized in Table 9.1.

Table 9.1: Summary of Artefacts Influencing Porewater Characterization Methods and Their Possible Control, Prevention and Evaluation

Determination of:	Potential disturbing effects	Evaluation, control and prevention of disturbing effects
Water content and water-loss porosity	- Evaporation during packing and transport	- Instruction on the on-site packing – staff to guarantee a fast and proper packing - Weighing the core samples immediately after recovery from the borehole and after unwrapping in the lab
	- Creation of artificial pore space and entrance of water during the preparation of core pieces	- Use of large sized (~ 5 cm diameter, > 8 cm length) core samples
	- Overestimation of the amount of porewater due to the dehydration of hydrated minerals	- Investigation of the mineralogy and petrography of the rock samples - Sequential drying of samples at 45°C and 105°C
	- Incomplete drying of the core pieces	- Frequent monitoring of the weight loss during drying
	- Overestimation of the mass of porewater due to on core surfaces sorbed water	- Controlled drying of the core surfaces and monitoring of the weights during drying

Determination of:	Potential disturbing effects	Evaluation, control and prevention of disturbing effects
	- Overestimation of the amount of porewater due to the ingress of drilling fluid in new pore space created by stress release and the drilling process (DDZ)	- Drilling with traced (e.g., NaI) drilling fluid and quantification of the volume of drilling fluid in the pore space by out-diffusion experiments and mass balance calculations with respect to iodine
Pore diffusion coefficient	- Modification of porosity during the out-diffusion experiments due to dissolution or precipitation of minerals - Modification of the Cl- and Br- elution curves due to evaporation effects	- Evaluation of the rock petrography and test water chemistry - Control of weights of test water during the experiment and of the bottles during storage
Chlorine, bromine and chlorine isotopes of porewater	- Artefacts of the determination of the in-situ water content	- See above
	- Incomplete equilibration between porewater and test water during the out-diffusion experiments	- Frequent sampling of sub-samples and control of the equilibration state with respect to Cl and Br
	- Dilution of porewater due to ingress of drilling fluid	- Drilling with traced (e.g., NaI) drilling fluid
$\delta^{18}O$ and $\delta^{2}H$ values of porewater	- Evaporation during sampling, preparation and experiment time	- Application of the specially developed sampling and preparation protocol - Control of the weights right after recovery and after unwrapping in the lab - Use of large sample sizes (> 300 g) - Weight control of the rocks, test water and glasses before and after the diffusive isotope exchange experiments
	- Salinity differences between porewater and test water and influence of hydrated mineral	- Investigation of the mineralogy and petrography of the used core samples - Assimilation of the test water chemistry on the porewater chemistry
	- Deterioration of the isotope signature of porewater by the ingress of drilling fluid	- Drilling with traced (e.g., NaI) drilling fluid

Another goal of this study was to apply the porewater characterization methods on four crystalline rock samples from borehole DH-GAP04 and to evaluate the obtained results with respect to the potential disturbing effects.

Therefore, four core samples were taken between 473 and 615 m b.s. from borehole DH-GAP04 consisting of slightly foliated to foliated, isogranular, macroscopically unaltered intermediate gneiss and felsic gneiss.

A prerequisite for porewater studies in low permeability crystalline rock is the preservation of the naturally saturated state of the core samples, which can be achieved by the described sampling and packing procedure.

A loss of vacuum in the sample bags, observed upon arrival at the lab, and dry core surfaces, provided evidence of evaporation of porewater from the GAP04 samples during the long transport time. Weight comparison of the cores before and after emerging them into test water during the long-term out-diffusion experiments indicated that 30-45% of the originally present porewater was evaporated. Significant evaporation has an impact on the determination of the pore diffusion coefficient and the stable isotope signatures of the porewater.

The analyses of the test solutions for the out-diffusion experiments showed, for three samples, sulphate concentrations between 1.6 and 2.0 g/kgH_2O, which indicate dissolution of sulphate minerals. PhreeqC modelling of the test water chemistry showed that the solutions of three samples are saturated with respect to gypsum. Mineralogical and petrographical investigations gave further evidence for the presence of gypsum dispersed in the rock matrix and present in microfractures, which were not visible macroscopically. The presence of gypsum in the rock matrix and in microfractures, and its dissolution during the out-diffusion experiments, has an influence on the determination of water content, the water-loss porosity and the pore diffusion coefficient of the individual core samples.

Taking all artefacts into account, the gravimetric water contents are between 0.19 and 0.21 wt.% for intermediate gneiss (n=3) and 0.14 wt.% for felsic gneiss (n=1) samples, resulting in water-loss porosities of 0.54 to 0.59 vol.% for intermediate gneiss and 0.37 vol.% for felsic gneiss. The large errors determined by Gaussian error propagation, which range between 0.03 and 0.04 wt.% (21-24%), and between 0.08 and 0.12 vol.% (20-24% of the values), respectively for intermediate gneiss and felsic gneiss, are predominately caused by the uncertainty in the determination of the initial wet weight, which is influenced by evaporation during sampling and transport.

Impregnation and visualization of the connected pore space shows that porewater is present and interconnected in the intergranular pore space between the single rock forming grains, and the intragranular pore space along cleavages, altered sections and filled microfractures.

The different shapes of the Cl elution curves of the four investigated samples indicate variations in the transport properties, which can be attributed to the different texture and structure of the core samples. Nevertheless, all samples were in equilibrium with respect to Cl at the end of the experiments, which allowed a correlation of the test water Cl concentration to the porewater concentration.

The anion and cation elution curves gave information about potential mineral reactions during the experiments. The chloride concentrations of porewater of the individual core samples varied between 960 and 2200 mg/kgH_2O. The bromide concentration of the sample taken at 615.5 m b.s. is 12.8 mg/kgH_2O, resulting in a Br*1000/Cl ratio of 5.8. The errors for the porewater Cl and Br concentrations, which are in the range of 21 to 25%, result mainly from the uncertainties in the determination of water contents.

The results obtained for the stable isotope composition of porewater of core samples from borehole DH-GAP04 determined by the diffusive isotope exchange technique are not reliable. The reasons for the failing of the experiments are: 1) the low mass of core sample available for the experiments; 2) the significant evaporation of porewater before the arrival in the lab; and, 3) the presence of gypsum in the cores and the salinity of the porewater, both of which were unknown beforehand. These effects allow for neither an evaluation of the influence of the individual processes nor a potential correction.

Recommendations for an analytical programme for future porewater studies in crystalline environments are summarized in Table 9.2.

Table 9.2: Recommendation for Porewater Investigations in Crystalline Rocks

Parame-ter	Recommended activities and analytical programme	Purpose
Drilling and sampling	- Detailed planning of sampling depths and intervals with respect to the hydro-geological and hydraulic environment of the sampling sites But: Short-term flexible on site determination and change of sampling positions of core samples for pw investigations based on the by the individual drillings encountered hydrogeological systems	- Achievement of the best output with respect to the characterization of an hydrogeological environment of an investigation site
	- Instruction of on-site sampling staff; responsible people for the potential artefacts induced by a wrong sampling and packing procedure	- Avoidance of evaporation of porewater from the cores during the time between recovery from the borehole and arrival in the lab - Avoidance of a too long contact time of the core samples with drilling fluid →Preservation of the naturally saturated state of the core samples
	- Drilling with traced (e.g., NaI) drilling fluid	- Quantification of the influence of drilling fluid ingressed in the core on the water content, connected porosity and porewater tracer-concentrations and isotope signatures
	- Logging of water-conducting fractures and their transmissivities	- Determination of the distance between fractures and porewater samples - Differences in water flow →Necessary information for the interpretation of the porewater - fracture groundwater interaction and the hydro-geological system of a site
	- Sampling of fracture groundwater and analyses of dissolved constituents and stable isotopes	- Comparison of chemical and isotopical composition of porewater and fracture groundwater →Necessary information for the interpretation of the porewater - fracture groundwater interaction and the hydro-geological system of a site

Petrography and Mineralogy	- Detailed macroscopic description, comparison and documentation of the obtained core samples - Determination of the bulk mineral composition of selected samples from encountered lithologies by transmitted light thin section petrography and scanning electron microscopy - Visualization of pore space by resin impregnation and UV-microscopy	- Information about differences of the obtained samples and potential relation to further data - Information about occurrence of minerals, which can have influence on the test water chemistry and isotopes - Information about potential dissolvable and/or hydrated minerals, which can have influence on the test water chemistry and water content determination - Information about alteration grades of individual samples, which can have influence on the porosity of rock samples - Correlation of the experimentally determined petrophysical properties with the petrography of the rocks - Information about structure and texture of the rocks, which are important in context of diffusion paths along grain boundaries - Information about the grain sizes of rock forming minerals, which can be perturbed by the drilling process - Direct information about the type of pore space, where porewater resides (intergranular vs intragranular) - Information about the extent of drilling disturbed zone
Water content and water-loss porosity	- Determination of the gravimetric water content by drying at various temperatures on every single used core section - Frequent monitoring and documentation of the drying - Determination of the water content by the diffusive isotope exchange technique - Determination of the bulk, wet and bulk dry density by Vernier calliper or buoyancy in a liquid medium	- Achievement of the porewater mass, which is the basis for the calculation of the pw tracer concentrations - Warranty of a full drying and hints about the porewater transportation system - Comparison of water content results and evaluation of the diffusive isotope exchange data - Necessary data for the calculation of the water-loss porosity
Pore diffusion coefficient	Out-diffusion experiments: - Frequent taking of subsamples during the out-diffusion experiments and analysing them for Cl, Br and main anions and cations - 1 dimensional modelling of the Cl- and Br-elution curves - 2 dimensional modelling of the Cl- and Br-elution curves - In case of drilling with NaI traced drilling fluid: 2-3 zone 2 dimensional modelling of the Cl- Br- and I-elution curves	- Set-up of Cl and Br elution curves, which serve as basis for the modelling - Set-up of ion elution curves to see potential dissolution of rock forming minerals - First information about the pore diffusion coefficient - detailed information about the pore diffusion coefficient →Necessary information for the interpretation of the porewater - fracture groundwater interaction and the hydro-geological system of a site - Information about the extension of a drilling disturbed zone in the investigated cores

Test water chemistry	Out-diffusion experiments: - Determination of the chemistry, pH and alkalinity of out-diffusion solutions	- Information about the water type of porewater - Information about dissolution of rock forming minerals and potentially occurring salts like gypsum
Cl, Br and δ^{37}Cl in porewater	Out-diffusion experiments: - Control of equilibration state between porewater and test water with respect to Cl and Br by taking sub-samples and analysing them for their Cl- and Br-concentrations - Determination of the Cl- and Br-concentrations and δ^{37}Cl values in out-diffusion test solutions and calculations of the porewater Cl- and Br-concentrations using the gravimetrically determined water content	- Control of full equilibration between the two reservoirs with respect to Cl and Br - Information about different water components, e.g. hydrothermal brine components, seawater, meteoric water, preserved in porewater - Information about the exchange of present-day fracture groundwater with porewater of individual samples
δ^{18}O and δ^{2}H porewater	Diffusive isotope exchange technique: - Determination of the δ^{18}O and δ^{2}H values of test waters used in the diffusive isotope exchange experiments and calculation of the isotope signature of porewater	- Information about the climatic infiltration conditions of in porewater preserved water component(s) - Information of potential in-situ water-rock or water-gas interactions - Information about the exchange of present-day fracture groundwater with porewater of individual samples

ACKNOWLEDGEMENTS

Much appreciation is given to the GAP drilling sampling team for the on-site selection and packaging and rapid dispatching of the drillcore samples to the University of Bern. The support of Sarah Hirschorn, Monique Hobbs and Laura Kennell throughout the study was much appreciated. We are grateful for the analytical support by Priska Baehler and Stephan Weissen (solution chemistry) at the Institute of Geological Sciences, University of Bern.

REFERENCES

Aaltonen I., B. Douglas, S. Frape, E. Henkemans, M. Hobbs, K.E. Klint, A. Lehtinen, L. Claesson Liljedahl, P. Lintinen, T. Ruskeeniemi. 2010. The Greenland Analogue Project, Sub-Project C; 2008 Field and Data Report. Posiva Working report 2010-62, Posiva Oy, Eurajoki, Finland.

Autio, J., M. Siitari-Kauppi, J. Timonen, K. Hartikainen, J. Hartikainen. 1998. Determination of the porosity, permeability and diffusivity of rock in the excavation-disturbed zone around full-scale deposition holes using the 14C-PMMA and He-gas methods. Journal of Contaminant Hydrology, 35, 19-29.

Bennike, O., S. Björk. 2002. Chronology of the last recession of the Greenland Ice Sheet. Journal of Quaternary Science, 17, 211-219.

Christiansen, H.H., O. Humlum. 2000. Permafrost. *In*: Jakobsen, B.H., J. Böcher, N. Nielsen, R. Guttesen, O. Humlum, E. Jensen (eds.). Topografisk Atlas Grönland. Det Kongelige DanskeGeografiske Selskab og Kort & Matrikelstyrelsen.

Craig, H. 1961. Standard for reporting concentrations of deuterium and oxygen-18 in natural water. Science, 133, 1833-1834.

Davis, S.N., D.O. Whittemore, J. Fabryka-Martin. 1998. Uses of Chloride/Bromide Ratios in Studies of Potable Water. Ground Water, 36(2), 338-350.

De Haller, A., M. Hobbs, Spangenberg, J., Meier, D. 2014. Benchmarking of the Isotope Diffusive Exchange Method Using Opalinus Clay and Queenston Shale Rocks Equilibrated with Synthetic Saline Solution. NWMO TR-2014-14 (*in preparation*). Toronto, Canada.

Eggenkamp, H.G.M. 1994. δ^{37}Cl: The geochemistry of chlorine isotopes. PhD-thesis, University of Utrecht, Utrecht, Netherlands.

Eichinger, F., H.N. Waber and J.A.T. Smellie. 2006. Characterization of Matrix Pore Water at the Olkiluoto Investigation Site, Finland. Posiva Working Report 2006-103, Posiva Oy, Olkiluoto Finland. (Available at http://www.posiva.fi)

Eichinger, F., J. Rüedi, H.N. Waber and R. Möri. 2008. Characterization of matrix pore water - Diffusion profile in GTS rock matrix. Nagra Project Report NPB 08-16, Nagra, Wettingen, Switzerland.

Eichinger, F. 2009. Matrix pore water – fracture groundwater interaction in crystalline bedrock based on natural tracers: An archive of long-term hydrogeological evolution. PhD Thesis, Institute of Geological Sciences, University of Bern, Bern, Switzerland.

Eichinger, F., J. Hämmerli, H.N. Waber, L.W. Diamond, J.A.T. Smellie. 2010. Characterization of Matrix Pore Water and Fluid Inclusions in Olkliuoto Bedrock from Drilling OL-KR47. Posiva Working Report 2010-58, Posiva Oy, Olkiluoto, Finland. (Available at http://www.posiva.fi)

Eichinger, F., Hämmerli, J., Waber, H.N., Diamond, L.W. and Smellie, J.A.T. 2013. Chemistry and dissolved gases of matrix pore water and fluid inclusions in Olkiluoto bedrock from drillhole ONK-PH9. Posiva Working Report 2011-63, Posiva Oy, Olkiluoto, Finland. (Available at http://www.posiva.fi)

Eichinger, F., D. Meier and H.N. Waber. 2013. Matrix pore water in Olkiluoto bedrock from drilling OL-KR54 and OL-KR55 - Chemical and isotopic characterization and evaluation of contamination by drilling fluid. Posiva Working Report 2013-xx, Posiva Oy, Olkiluoto, Finland (*in print*).

Engels, S., Helmens, K. 2010. Holocene environmental changes and climate development in Greenland. SKB R-Report R-10-65, SKB, Stockholm, Sweden. (Available at http://www.skb.se)

Forman, S.L, L. Marin, C. van der Veen, C. Tremper, B. Csatho. 2007. Little Ice Age and neoglacial landforms at the inland ice margin, Isunguata Sermia, Kangerlussuaq, west Greenland. Boreas, Vol.36, pp.341-351.

Frape, S.K., G. Bryant, R. Blomqvist, T. Ruskeeniemi. 2000. Evidence from stable chlorine isotopes for multiple sources of chloride in groundwaters from crystalline shield environments. IAEA-SM-336/24, 19-30.

Frieg, B., W.R. Alexander, H. Dollinger, C. Bühler, P. Haag, A. Möri, K. Ota. 1998. In situ resin impregnation for investigating radionuclide retardation in fractured repository host rocks. Journal of Contaminant Hydrology, 35, 115-130.

Gimmi, T., N.N. Waber. 2004. Modelling of Tracer Profiles in Pore Water of Argillaceous Rocks in the Benken Borehole: Stable Water Isotopes, Chloride, and Chlorine Isotopes; Nagra Tech. Rep. 2004-05, Nagra, Wettingen, Switzerland.

Gorbatsevich, F.F. 2003. Decompaction mechanism of deep crystalline rocks under stress relief. Tectonophysics, 370, 121 – 128.

Harper, J., A. Hubbart, T. Ruskeeniemi et al. 2012. The Greenland Analogue Project. Posiva Working Report 2012-16, Poyiva Oy, Eurajoki, Finland.

Hellmuth, K.H., M. Siitari-Kauppi, A. Lindgerg. 1993. Study of porosity and migration pathways in crystalline rock by impregnation with 14C- polymethylmethacrylate. Journal of Contaminant Hydrology, 13, 403-418.

ISRM. 1979. Suggested methods for determining water content, porosity, density, absorption and related properties and swelling and slake-durability index properties. Int. J. Rock Mech. Min. Sci. & Geomech. Abstr., 16, p141-156.

Jacobsson, L., M. Flansbje, R. Christiansson, T. Jansson. 2007. Measurement of micro crack volume in low porosity crystalline rock. *In*: Proceedings 11th Congress of the International Society for Rock Mechanics, Lisbon 1. Taylor & Francis Group, London, 55 - 58.

Jörgensen, A.S., F. Andreasen. 2007. Mapping of permafrost surface using ground penetrating radar at Kangerlussuaq Airport, western Greenland. Cold Regions Science and Technology, 48, 64-72.

Kaufmann, R., A. Long, H. Bentley, S. Davis. 1984. Natural chlorine isotope variations. Nature, 309, 338-340.

Kowallis, B.J., H.F. Wang. 1983. Microcrack study of granitic cores from Illinois deep borehole UPH 3. Journal of Geophysical Research, 88(B9), 737 – 7380.

Mazurek, M., T. Oyama, F. Eichinger, A. de Haller. 2013. Squeezing of pore water from core samples of DGR boreholes: Feasibility study. NWMO technical report NWMO TR-2013-19. Toronto, Canada.

Meglis, I.L., T. Engelder, E.K. Graham. 1991. The effect of stress-relief on ambient microcrack porosity in core samples from the Kent Cliffs (New York) and Moodus (Connecticut) scientific research boreholes. Tectonophysics, 186, 163 – 173.

Meier, D. 2012. Matrix pore water in crystalline rocks at Olkiluoto, Finland: Chemical and transport properties and artefacts induced by drill core sampling. Masters thesis University of Bern, Bern, Switzerland.

Möri, A. 2009. In situ matrix diffusion in crystalline rocks: An experimental approach. PhD Thesis, Institute of Geological Sciences, University of Bern, Bern, Switzerland.

Morrow, C.A., D.A. Lockner. 1994. Permeability differences between surface-derived and deep drillhole core samples. Geophysical Research Letters, 21(19), 2151 – 2154.

Norton, D., R. Knapp. 1977. Transport Phenomena in Hydrothermal Systems: The Nature of Porosity. American Journal of Science, 277, 913-936.

Ota, K., A. Möri, W.R. Alexander, B. Frieg, M. Schild. 2003. Influence of the mode of matrix porosity determination on matrix diffusion calculations. Journal of Contaminant Hydrology, 61, 131-145.

Pearson, F.J., D. Arcos, A. Bath, J.-Y Boisson, A.M. Fernánde, H.E. Gäbler, E. Gaucher, A. Gautschi, L. Griffault, P. Hernán, H.N. Waber. 2003. Mont Terri Project – Geochemistry of Water in the Opalinus Clay Formation at the Mont Terri Laboratory; Reports of the Federal Office of Water and Geology (FOWG); Geology Series No. 5; Bern, Switzerland.

Philips, F.M., H.W. Bentley. 1987. Isotopic fractionation during ion filtration: I. Theory. Geochimica et Cosmochimica Acta, 51, 583-695.

Pöllänen, J., P. Heikkinen and A. Lehtinen. 2012. Difference Flow Measurements in Greenland, Drillhole DH-GAP04 in July 2011. Posiva Working Report 2012-13, Posiva Oy, Olkiluoto, Finland.

Rogge, T. 1997. Eine molekular-diffusive Methode zur Bestimmung des Porenwassergehaltes und der Zusammensetzung von stabilen Isotopen im Porenwasser von Gestein. Unpubl. Diploma Thesis, Institut für Umweltphysik, Unversity of Heidelberg.

Rübel A.P., Ch. Sonntag, J. Lippmann, F.J. Pearson and A. Gautschi. 2002. Solute transport in formations of very low permeability: Profiles of stable isotope and dissolved noble gas

contents of pore water in the Opalinus Clay, Mont Terri, Switzerland. Geochim. Cosmochim. Acta, 1311–1321.

Schild, M., S. Siegesmund, A. Vollbrecht, M. Mazurek. 2001. Characterization of granite matrix porosity and pore-space geometry by in situ and laboratory methods. Geophysical Journal International, 146(1), 111-126.

Smellie, J.A.T., H.N. Waber, S.K. Frape. 2003. Matrix fluid chemistry experiment – Final report June 1998 – March 2003. SKB Technical Report, TR-03-18, SKB, Stockholm, Sweden.

Stewart, M.A., A.J. Spivack. 2004. The Stable-Chlorine Isotope Compositions of Natural and Anthropogenic Materials. Reviews in Mineralogy and Geochemistry, 55, 231-254.

Tullborg, E.-L. and S.Å. Larson. 2006. Porosity in crystalline rocks – a matter of scale. Eng. Geol. 84, 75–83.

van Gool J A M, L.N. Connelly, M. Marker, F.C. Mengel. 2002. The Nagssugtoqidian orogen of West Greenland: tectonic evolution and regional correlation from a West Greenland perspective. Can. J. Earth Sci., 39, 665–686.

Waber, H. N. and Smellie, J.A.T. 2005. Forsmark site investigation. Borehole KFM06A: Characterization of pore water. Part I: Diffusion experiments. SKB P-05-196, Svensk Kärnbränslehantering AB, Stockholm, Sweden. (Available at http://www.skb.se).

Waber, H.N. and J.A.T. Smellie. 2008. Characterization of pore water in crystalline rocks. App. Geochem., 23, 1834–1861.

Waber, H.N., T. Gimmi and J.A.T. Smellie. 2009a. Porewater in the rock matrix. Site descriptive modelling. SDM-Site Forsmark. SKB R-08-105, Svensk Kärnbränslehantering AB, Stockholm, Sweden. (Available at http://www.skb.se).

Waber, H.N., T. Gimmi, A. deHaller, and J.A.T. Smellie. 2009b. Porewater in the rock matrix. Site descriptive modelling SDM Site Laxemar. SKB R-08-112, Svensk Kärnbränslehantering AB, Stockholm, Sweden. (Available at http://www.skb.se).

Waber, H.N., T. Gimmi and J.A.T. Smellie. 2011. Effects of drilling and stress release on transport properties and porewater chemistry of crystalline rocks. J. Hydrol., 405, 316-332.

Waber, H.N., T. Gimmi, and J.A.T. Smellie. 2012. Reconstruction of palaeoinfiltration during the Holocene using porewater data (Laxemar, Sweden). Geochim. Cosmochim. Acta, 94, 109-127.

Wallroth, T., H. Lokrantz, A. Rimsa. 2010. The Greenland Analogue Project; Literature review of hydrogeology/hydrogeochemistry. SKB R-10-34, Svensk Kärnbränslehantering AB, Stockholm, Sweden. (Available at http://www.skb.se).

Weidick, A., O. Bennike. 2007. Quaternary geological history and geology of Jakobshavn I Isbræand the Disko Bugt region, West Greenland: a review. Geological Survey of Denmark and Greenland Bulletin 14.

Zhang, M., S.K. Frape, M.Y. Hobbs, M.R. Jensen, R. Blomqvist, T. Ruskeeniemi. 2006. Fractionation of chlorine isotopes between ice and groundwater: Identification of freezing processes. Geochimica et Cosmochimica Acta, 70(18), A736.

Ziegler, K., M.L. Coleman, R.J. Howarth. 2001. Palaeohydrodynamics of fluids in the Brent Group (Oseberg Field, Norwegian North Sea) from chemical and isotopic compositions of formation waters. Applied Geochemistry, 16, 609-632.

APPENDIX A: TABULAR PRESENTATION OF ION CONCENTRATIONS OF ELUATE TIME SERIES

TABLUAR PRESENTATION OF ION CONCENTRATIONS OF ELUATE TIME SERIES

Table A1: Ion Concentrations of Eluate Time Series of Sample GAP04-1 (in mg/L)

Sample	Days	Na	K	Ca	Mg	Sr	F	Cl	Br	NO3	SO4
		mg/L	mg/L	mg/L	mg/L	mg/L	mg/L	mg/L	mg/L	mg/L	mg/L
GAP-1-A	1	44.4	6.1	419.5	5.3	1.8	<0.16	7.1	<0.16	1.3	1163
GAP-1-B	3	80.4	8.2	506.4	9.0	2.7	<0.16	10.3	<0.16	1.5	1438
GAP-1-C	7	101.0	8.8	531.0	12.1	3.0	<0.16	11.1	<0.16	1.5	1579
GAP-1-D	14	129.6	9.8	530.5	16.4	3.7	<0.16	12.3	<0.16	1.5	1671
GAP-1-E	22	149.7	10.5	544.3	20.4	4.3	<0.16	13.8	<0.16	1.6	1729
GAP-1-F	28	166.5	11.0	536.0	22.6	4.6	<0.16	14.2	<0.16	1.6	1765
GAP-1-G	35	172.7	11.4	514.1	24.4	4.9	0.16	14.9	<0.16	1.8	1792
GAP-1-H	42	189.2	12.3	537.5	26.7	5.4	0.16	16.1	<0.16	1.7	1847
GAP-1-I	49	194.7	12.6	526.1	29.1	5.8	<0.16	16.5	<0.16	1.5	1869
GAP-1-K	70	207.4	13.4	528.6	37.3	6.1	0.17	17.1	<0.16	<0.16	1887
GAP-1-L	105	210.4	13.7	518.6	43.4	6.7	0.21	17.9	<0.16	<0.16	1879
GAP-1-M	142	212.8	13.0	521.4	47.2	6.8	0.20	17.9	<0.16	<0.16	1908
GAP-1-N	177	220.6	13.1	522.8	51.1	6.9	0.19	17.7	<0.16	<0.16	1968
GAP-1-O	210	226.0	13.5	542.2	55.8	7.3	0.17	18.4	<0.16	<0.16	2050
GAP-1-P	260	224.0	12.7	535.3	60.3	7.6	<0.16	18.4	<0.16	<0.16	1994
GAP-1-FINAL	283	218.1	12.2	524.8	61.0	7.7	0.18	18.4	<0.16	<0.16	2002

Table A2: Ion Concentrations of Eluate Time Series of Sample GAP04-1 (in mmol/L)

Sample	Days	Na	K	Ca	Mg	Sr	F	Cl	Br	NO3	SO4
		mmol/L	mmol/L	mmol/L	mmol/L	mmol/L	mmol/L	mmol/L	mmol/L	mmol/L	mmol/L
GAP-1-A	1	1.9	0.16	10.5	0.22	0.02		0.20		0.022	12.1
GAP-1-B	3	3.5	0.21	12.6	0.37	0.03		0.29		0.025	15.0
GAP-1-C	7	4.4	0.22	13.2	0.50	0.03		0.31		0.024	16.4
GAP-1-D	14	5.6	0.25	13.2	0.67	0.04		0.35		0.024	17.4
GAP-1-E	22	6.5	0.27	13.6	0.84	0.05		0.39		0.026	18.0
GAP-1-F	28	7.2	0.28	13.4	0.93	0.05		0.40		0.025	18.4
GAP-1-G	35	7.5	0.29	12.8	1.00	0.06	0.008	0.42		0.029	18.7
GAP-1-H	42	8.2	0.32	13.4	1.10	0.06	0.008	0.45		0.027	19.2
GAP-1-I	49	8.5	0.32	13.1	1.20	0.07		0.46		0.025	19.5
GAP-1-K	70	9.0	0.34	13.2	1.53	0.07	0.009	0.48			19.6
GAP-1-L	105	9.2	0.35	12.9	1.78	0.08	0.011	0.51			19.6
GAP-1-M	142	9.3	0.33	13.0	1.94	0.08	0.010	0.51			19.9
GAP-1-N	177	9.6	0.34	13.0	2.10	0.08	0.010	0.50			20.5
GAP-1-O	210	9.8	0.34	13.5	2.29	0.08	0.009	0.52			21.3
GAP-1-P	260	9.7	0.32	13.4	2.48	0.09		0.52			20.8
GAP-1-FINAL	283	9.5	0.31	13.1	2.51	0.09	0.009	0.52			20.8

Table A3: Molar Ion Ratios of Eluate Time Series of Sample GAP04-1

		Na/Cl	Na/K	Ca/SO4	Mg/SO4	Ca/Sr	Cl/SO4
GAP-1-A	1	9.6	12.4	0.86	0.02	508.2	0.017
GAP-1-B	3	12.0	16.7	0.84	0.02	408.5	0.019
GAP-1-C	7	14.0	19.6	0.81	0.03	385.8	0.019
GAP-1-D	14	16.2	22.5	0.76	0.04	317.3	0.020
GAP-1-E	22	16.7	24.3	0.75	0.05	276.7	0.022
GAP-1-F	28	18.1	25.8	0.73	0.05	252.2	0.022
GAP-1-G	35	17.8	25.8	0.69	0.05	228.8	0.023
GAP-1-H	42	18.1	26.1	0.70	0.06	216.5	0.024
GAP-1-I	49	18.2	26.3	0.67	0.06	199.4	0.024
GAP-1-K	70	18.7	26.4	0.67	0.08	188.1	0.025
GAP-1-L	105	18.1	26.1	0.66	0.09	170.3	0.026
GAP-1-M	142	18.3	27.8	0.65	0.10	167.5	0.025
GAP-1-N	177	19.2	28.6	0.64	0.10	164.9	0.024
GAP-1-O	210	19.0	28.6	0.63	0.11	163.2	0.024
GAP-1-P	260	18.8	30.0	0.64	0.12	154.4	0.025
GAP-1-FINAL	283	18.3	30.3	0.63	0.12	149.5	0.025

Table A4: Ion Concentrations of Eluate Time Series of Sample GAP04-2 (in mg/L)

Sample	Days	Na	K	Ca	Mg	Sr	F	Cl	Br	NO3	SO4
		mg/L	mg/L	mg/L	mg/L	mg/L	mg/L	mg/L	mg/L	mg/L	mg/L
GAP-2-A	1	10.5	8.2	101.0	2.0	<1.0	<0.16	9.7	<0.16	0.67	266
GAP-2-B	3	19.2	10.2	170.0	3.3	<1.0	<0.16	13.8	<0.16	0.64	454
GAP-2-C	7	27.3	11.3	223.0	4.7	1.1	<0.16	16.3	<0.16	0.64	595
GAP-2-D	14	37.1	12.8	294.0	6.7	2.4	0.20	18.1	<0.16	0.72	790
GAP-2-E	22	41.8	13.5	327.0	7.9	2.1	0.23	18.6	<0.16	0.66	878
GAP-2-F	28	47.0	15.8	360.0	9.5	2.3	0.22	19.4	<0.16	0.62	988
GAP-2-G	35	49.5	16.4	380.0	10.5	2.6	0.25	19.4	<0.16	0.64	1021
GAP-2-H	42	52.1	17.2	406.0	11.1	2.2	0.24	20.0	<0.16	0.61	1106
GAP-2-I	49	53.3	17.8	422.0	11.9	2.5	0.24	20.1	<0.16	0.52	1170
GAP-2-K	70	56.8	18.7	463.0	14.7	3.4	0.31	20.9	0.16	0.44	1247
GAP-2-L	105	59.7	19.9	508.0	18.3	3.8	0.34	22.3	0.17	0.06	1418
GAP-2-M	142	61.3	20.5	533.0	21.1	3.9	0.37	23.1	0.17	0.05	1504
GAP-2-N	177	61.3	20.0	537.0	23.1	4.8	0.36	22.6	0.17	0.05	1534
GAP-2-O	210	60.5	20.7	538.0	24.4	4.6	0.35	23.3	0.17	0.04	1549
GAP-2-P	260	61.3	20.5	546.3	27.0	5.0	0.37	23.9	<0.16	<0.16	1608
GAP-2-FINAL	283	62.6	20.8	537.3	28.5	5.3	0.34	22.5	<0.16	<0.16	1581

Table A5: Ion Concentrations of Eluate Time Series of Sample GAP04-2 (in mmol/L)

Sample	Days	Na	K	Ca	Mg	Sr	F	Cl	Br	NO3	SO4
		mmol/L	mmol/L	mmol/L	mmol/L	mmol/L	mmol/L	mmol/L	mmol/L	mmol/L	mmol/L
GAP-2-A	1	0.46	0.21	2.52	0.08			0.27		0.011	2.8
GAP-2-B	3	0.84	0.26	4.24	0.14			0.39		0.010	4.7
GAP-2-C	7	1.19	0.29	5.56	0.19	0.013		0.46		0.010	6.2
GAP-2-D	14	1.61	0.33	7.34	0.28	0.027	0.011	0.51		0.012	8.2
GAP-2-E	22	1.82	0.34	8.16	0.33	0.024	0.012	0.52		0.011	9.1
GAP-2-F	28	2.04	0.41	8.98	0.39	0.026	0.012	0.55		0.010	10.3
GAP-2-G	35	2.15	0.42	9.48	0.43	0.030	0.013	0.55		0.010	10.6
GAP-2-H	42	2.27	0.44	10.13	0.46	0.026	0.013	0.56		0.010	11.5
GAP-2-I	49	2.32	0.45	10.53	0.49	0.029	0.013	0.57		0.008	12.2
GAP-2-K	70	2.47	0.48	11.55	0.60	0.038	0.016	0.59	0.002	0.007	13.0
GAP-2-L	105	2.60	0.51	12.67	0.75	0.043	0.018	0.63	0.002	0.001	14.8
GAP-2-M	142	2.67	0.53	13.30	0.87	0.044	0.020	0.65	0.002	0.001	15.7
GAP-2-N	177	2.67	0.51	13.40	0.95	0.054	0.019	0.64	0.002	0.001	16.0
GAP-2-O	210	2.63	0.53	13.42	1.00	0.053	0.018	0.66	0.002	0.001	16.1
GAP-2-P	260	2.67	0.52	13.63	1.11	0.058	0.020	0.67			16.7
GAP-2-FINAL	283	2.72	0.53	13.40	1.17	0.060	0.018	0.63			16.5

Table A6: Molar Ion Ratios of Eluate Time Series of Sample GAP04-2

		Na/Cl	Na/K	Ca/SO4	Mg/SO4	Ca/Sr	Cl/SO4
Sample	Days						
GAP-2-A	1	1.7	2.2	0.91	0.03		0.099
GAP-2-B	3	2.1	3.2	0.90	0.03		0.082
GAP-2-C	7	2.6	4.1	0.90	0.03	440.4	0.074
GAP-2-D	14	3.2	4.9	0.89	0.03	271.2	0.062
GAP-2-E	22	3.5	5.3	0.89	0.04	340.4	0.057
GAP-2-F	28	3.7	5.0	0.87	0.04	347.5	0.053
GAP-2-G	35	3.9	5.1	0.89	0.04	316.8	0.051
GAP-2-H	42	4.0	5.2	0.88	0.04	395.4	0.049
GAP-2-I	49	4.1	5.1	0.86	0.04	365.7	0.047
GAP-2-K	70	4.2	5.2	0.89	0.05	302.0	0.045
GAP-2-L	105	4.1	5.1	0.86	0.05	291.4	0.043
GAP-2-M	142	4.1	5.1	0.85	0.06	300.9	0.042
GAP-2-N	177	4.2	5.2	0.84	0.06	246.2	0.040
GAP-2-O	210	4.0	5.0	0.83	0.06	254.9	0.041
GAP-2-P	260	4.0	5.1	0.81	0.07	237.0	0.040
GAP-2-FINAL	283	4.3	5.1	0.81	0.07	222.2	0.039

Table A7: Ion Concentrations of Eluate Time Series of Sample GAP04-3 (in mg/L)

Sample	Days	Na	K	Ca	Mg	Sr	F	Cl	Br	NO3	SO4
		mg/L	mg/L	mg/L	mg/L	mg/L	mg/L	mg/L	mg/L	mg/L	mg/L
GAP-3-A	1	14.2	5.3	275.9	2.1	2.1	<0.16	1.6	<0.16	0.71	743
GAP-3-B	3	26.6	8.3	429.5	3.6	3.2	<0.16	3.5	<0.16	0.27	1140
GAP-3-C	6	35.5	10.0	495.0	4.4	4.0	<0.16	5.3	<0.16	0.89	1340
GAP-3-D	13	47.9	11.8	538.3	6.2	4.9	<0.16	6.4	<0.16	0.90	1498
GAP-3-E	21	58.7	12.9	562.6	8.2	5.3	<0.16	7.7	<0.16	0.69	1556
GAP-3-F	27	66.3	14.0	561.9	9.9	5.4	<0.16	8.6	<0.16	0.68	1593
GAP-3-G	34	71.7	14.5	572.5	11.5	5.8	<0.16	9.2	<0.16	0.63	1644
GAP-3-H	41	75.2	14.8	566.3	12.7	6.0	<0.16	9.6	<0.16	0.37	1643
GAP-3-I	48	88.3	16.8	568.8	16.3	6.7	<0.16	11.0	<0.16	<0.16	1665
GAP-3-K	69	90.7	16.3	563.6	18.3	6.8	<0.16	11.7	<0.16	<0.16	1666
GAP-3-L	104	93.6	16.0	563.9	21.8	7.0	<0.16	12.7	<0.16	<0.16	1700
GAP-3-M	141	95.6	15.9	561.2	25.1	7.4	<0.16	13.6	<0.16	<0.16	1690
GAP-3-N	176	95.0	15.7	571.6	26.8	7.6	<0.16	14.3	<0.16	<0.16	1743
GAP-3-O	209	98.1	16.6	589.9	30.6	8.0	0.17	15.6	<0.16	0.20	1796
GAP-3-P	259	94.2	15.6	580.0	32.3	8.0	<0.16	15.6	<0.16	0.73	1773
GAP-3-FINAL	282	97.4	15.7	559.2	33.0	7.9	<0.16	15.8	<0.16	<0.16	1750

Table A8: Ion Concentrations of Eluate Time Series of Sample GAP04-3 (in mmol/L)

Sample	Days	Na	K	Ca	Mg	Sr	F	Cl	Br	NO3	SO4
		mmol/L	mmol/L	mmol/L	mmol/L	mmol/L	mmol/L	mmol/L	mmol/L	mmol/L	mmol/L
GAP-3-A	1	0.62	0.13	6.88	0.08	0.024	<0.16	0.04	<0.16	0.011	7.7
GAP-3-B	3	1.16	0.21	10.72	0.15	0.037	<0.16	0.10	<0.16	0.004	11.9
GAP-3-C	6	1.54	0.26	12.35	0.18	0.046	<0.16	0.15	<0.16	0.014	14.0
GAP-3-D	13	2.08	0.30	13.43	0.26	0.056	<0.16	0.18	<0.16	0.014	15.6
GAP-3-E	21	2.56	0.33	14.04	0.34	0.061	<0.16	0.22	<0.16	0.011	16.2
GAP-3-F	27	2.89	0.36	14.02	0.41	0.062	<0.16	0.24	<0.16	0.011	16.6
GAP-3-G	34	3.12	0.37	14.29	0.47	0.066	<0.16	0.26	<0.16	0.010	17.1
GAP-3-H	41	3.27	0.38	14.13	0.52	0.069	<0.16	0.27	<0.16	0.006	17.1
GAP-3-I	48	3.84	0.43	14.19	0.67	0.077	<0.16	0.31	<0.16	<0.16	17.3
GAP-3-K	69	3.94	0.42	14.06	0.75	0.077	<0.16	0.33	<0.16	<0.16	17.3
GAP-3-L	104	4.07	0.41	14.07	0.90	0.080	<0.16	0.36	<0.16	<0.16	17.7
GAP-3-M	141	4.16	0.41	14.00	1.03	0.085	<0.16	0.38	<0.16	<0.16	17.6
GAP-3-N	176	4.13	0.40	14.26	1.10	0.086	<0.16	0.40	<0.16	<0.16	18.1
GAP-3-O	209	4.27	0.43	14.72	1.26	0.091	<0.16	0.44	<0.16	0.003	18.7
GAP-3-P	259	4.10	0.40	14.47	1.33	0.091	<0.16	0.44	<0.16	0.012	18.5
GAP-3-FINAL	282	4.24	0.40	13.95	1.36	0.090	<0.16	0.45	<0.16	<0.16	18.2

Table A9: Molar Ion Ratios of Eluate Time Series of Sample GAP04-3

		Na/Cl	Na/K	Ca/SO4	Mg/SO4	Ca/Sr	Cl/SO4
Sample	Days						
GAP-3-A	1	13.7	4.6	0.89	0.01	291.3	0.006
GAP-3-B	3	11.8	5.4	0.90	0.01	289.5	0.008
GAP-3-C	6	10.4	6.0	0.89	0.01	270.0	0.011
GAP-3-D	13	11.5	6.9	0.86	0.02	237.8	0.012
GAP-3-E	21	11.8	7.8	0.87	0.02	231.9	0.013
GAP-3-F	27	11.9	8.1	0.85	0.02	227.6	0.015
GAP-3-G	34	12.0	8.4	0.83	0.03	216.9	0.015
GAP-3-H	41	12.0	8.7	0.83	0.03	204.9	0.016
GAP-3-I	48	12.3	9.0	0.82	0.04	184.3	0.018
GAP-3-K	69	12.0	9.4	0.81	0.04	182.1	0.019
GAP-3-L	104	11.4	10.0	0.80	0.05	176.9	0.020
GAP-3-M	141	10.9	10.2	0.80	0.06	165.0	0.022
GAP-3-N	176	10.2	10.3	0.79	0.06	164.9	0.022
GAP-3-O	209	9.7	10.0	0.79	0.07	162.0	0.023
GAP-3-P	259	9.3	10.2	0.78	0.07	158.4	0.024
GAP-3-FINAL	282	9.5	10.5	0.77	0.07	155.5	0.025

Table A10: Ion Concentrations of Eluate Time Series of Sample GAP04-4 (in mg/L)

Sample	Days	Na	K	Ca	Mg	Sr	F	Cl	Br	NO3	SO4
		mg/L	mg/L	mg/L	mg/L	mg/L	mg/L	mg/L	mg/L	mg/L	mg/L
GAP-4-A	1	8.0	0.6	4.9	0.3	<0.10	0.04	3.7	0.03	1.26	10.7
GAP-4-B	3	14.7	0.9	8.0	0.4	0.11	0.05	8.7	0.06	1.37	22.1
GAP-4-C	6	19.3	1.0	10.1	0.5	0.18	0.05	11.3	0.07	1.42	31.7
GAP-4-D	13	26.3	1.3	13.8	0.7	0.30	0.06	14.3	0.08	1.35	48.0
GAP-4-E	21	30.3	1.4	16.0	0.9	0.30	0.06	15.6	0.09	1.27	57.6
GAP-4-F	27	33.4	1.7	20.3	1.1	0.39	0.06	16.1	0.09	1.04	65.5
GAP-4-G	34	37.0	2.0	23.0	1.4	0.47	0.07	16.8	0.09	0.578	74.1
GAP-4-H	41	39.6	2.2	25.8	1.6	0.53	0.06	17.6	0.09	0.033	81.8
GAP-4-I	48	41.3	2.3	28.0	1.9	0.56	0.07	17.6	0.09	0.039	86.1
GAP-4-K	69	45.7	2.5	32.2	2.3	0.67	0.07	18.5	0.10	0.035	97.2
GAP-4-L	104	51.0	2.8	36.7	2.9	0.81	0.07	20.1	0.11	0.044	112.0
GAP-4-M	141	52.9	2.9	38.0	3.4	0.87	0.08	20.4	0.11	0.043	120.0
GAP-4-N	176	54.0	2.9	42.4	4.0	0.98	0.08	21.3	0.11	0.038	131.0
GAP-4-O	209	58.5	3.3	47.1	4.6	1.06	0.09	23.0	0.13	0.046	146.0
GAP-4-P	259	60.7	3.3	50.2	5.2	1.14	0.07	23.1	0.13	0.042	153.3
GAP-4-FINAL	282	58.3	3.3	48.2	5.2	1.21	0.07	20.5	0.12	<0.016	139.8

Table A11: Ion Concentrations of Eluate Time Series of Sample GAP04-4 (in mmol/L)

Sample	Days	Na	K	Ca	Mg	Sr	F	Cl	Br	NO3	SO4
		mmol/L	mmol/L	mmol/L	mmol/L	mmol/L	mmol/L	mmol/L	mmol/L	mmol/L	mmol/L
GAP-4-A	1	0.35	0.01	0.12	0.01		0.002	0.10	0.000	0.020	0.11
GAP-4-B	3	0.64	0.02	0.20	0.02	0.001	0.003	0.24	0.001	0.022	0.23
GAP-4-C	6	0.84	0.03	0.25	0.02	0.002	0.003	0.32	0.001	0.023	0.33
GAP-4-D	13	1.14	0.03	0.34	0.03	0.003	0.003	0.40	0.001	0.022	0.50
GAP-4-E	21	1.32	0.04	0.40	0.04	0.003	0.003	0.44	0.001	0.020	0.60
GAP-4-F	27	1.45	0.04	0.51	0.04	0.004	0.003	0.45	0.001	0.017	0.68
GAP-4-G	34	1.61	0.05	0.57	0.06	0.005	0.004	0.47	0.001	0.009	0.77
GAP-4-H	41	1.72	0.06	0.64	0.07	0.006	0.003	0.50	0.001	0.001	0.85
GAP-4-I	48	1.80	0.06	0.70	0.08	0.006	0.004	0.50	0.001	0.001	0.90
GAP-4-K	69	1.99	0.06	0.80	0.10	0.008	0.004	0.52	0.001	0.001	1.01
GAP-4-L	104	2.22	0.07	0.92	0.12	0.009	0.004	0.57	0.001	0.001	1.17
GAP-4-M	141	2.30	0.07	0.95	0.14	0.010	0.004	0.58	0.001	0.001	1.25
GAP-4-N	176	2.35	0.07	1.06	0.17	0.011	0.004	0.60	0.001	0.001	1.36
GAP-4-O	209	2.54	0.09	1.18	0.19	0.012	0.004	0.65	0.002	0.001	1.52
GAP-4-P	259	2.64	0.09	1.25	0.21	0.013	0.004	0.65	0.002	0.001	1.60
GAP-4-FINAL	282	2.53	0.08	1.20	0.22	0.014	0.003	0.58	0.001		1.46

Table A12: Molar Ion Ratios of Eluate Time Series of Sample GAP04-4

		Na/Cl	Na/K	Ca/SO4	Mg/SO4	Ca/Sr	Cl/SO4
Sample	Days						
GAP-4-A	1	3.35	23.5	1.10	0.11		0.93
GAP-4-B	3	2.61	28.5	0.86	0.07	154.0	1.06
GAP-4-C	6	2.63	32.2	0.76	0.06	124.0	0.97
GAP-4-D	13	2.84	35.5	0.69	0.06	99.6	0.81
GAP-4-E	21	3.00	36.5	0.67	0.06	116.2	0.73
GAP-4-F	27	3.20	33.8	0.74	0.06	115.0	0.67
GAP-4-G	34	3.40	32.1	0.74	0.07	107.0	0.61
GAP-4-H	41	3.47	31.2	0.76	0.08	106.4	0.58
GAP-4-I	48	3.62	30.9	0.78	0.09	108.5	0.55
GAP-4-K	69	3.81	30.8	0.79	0.10	104.6	0.52
GAP-4-L	104	3.91	30.6	0.79	0.10	99.4	0.49
GAP-4-M	141	4.00	30.8	0.76	0.11	95.9	0.46
GAP-4-N	176	3.91	32.1	0.78	0.12	94.8	0.44
GAP-4-O	209	3.92	29.8	0.77	0.12	97.1	0.43
GAP-4-P	259	4.05	31.1	0.79	0.13	96.0	0.41
GAP-4-FINAL	282	4.37	30.4	0.83	0.15	87.0	0.40